目　次

3. 参考論文

(1) 鳥巣式石灰岩の Sr 同位体による堆積年代と炭素同位体層序から推定されるジュラ紀後期～白亜紀前期の古海洋循環.

柿崎喜宏，石川剛志，永石一弥，谷水雅治，川越寛子，狩野彰宏

平成 19 年度深田地質研究助成報告書 (2008) 25-46.

(2) Age constraints on the origin and growth history of a deep-water coral mound in NE Atlantic drilled in IODP Expedition 307.

Kano, A., Ferdelman, T.G., Williams, T., Henriet, J.-P., Ishikawa, T., Kawagoe, N., Takashima, C., Kakizaki, Y., Abe, K., Sakai, S., Browning, E.L., Li, X. and The IODP Expedition 307 Scientists

Geology, **35** (2007) 1051-1054.

(3) Uppermost Jurassic limestone mounds and the recent tufa deposits in southern Shikoku Province.

Kano, A., Kakizaki, Y., Shiraishi, F., Kawai, T. and Matsuoka, J.

International Sedimentological Congress 2006 Excursion guidebook, B08. (2006) pp.13.

主論文

Chemostratigraphy of the Torinosu-type Limestone and its implication to the global oceanographic processes from late Jurassic to early Cretaceous

鳥巣式石灰岩の化学層序と そのジュラ紀後期から白亜紀前期の汎世界的海洋学的プロセスへの意義

2009

Department of Earth and Planetary Systems Science

Graduate School of Science

Hiroshima Univerisity

Yoshihiro KAKIZAKI

Chemostratigraphy of the Torinosu-type Limestone and its implication to the global oceanographic processes from late Jurassic to early Cretaceous

鳥巣式石灰岩の化学層序と
そのジュラ紀後期から白亜紀前期の汎世界的海洋学的プロセスへの意義

Yoshihiro Kakizaki

Abstract The Late Jurassic and the Early Cretaceous were peculiar periods in terms of the accelerated global carbon cycle. The breakup of the supercontinent Pangea generated new seaways, expanded coastal settings and humid climates, and intensified weathering, which increased the continental flux of inorganic nutrients and carbonate alkalinity to seawater. In the eutrophied ocean, flourished calcareous planktons and reef-builders contributed to fix both organic and inorganic carbons under the circumstance of a relatively high CO_2 concentration. These pictures have been drawn mostly with geologic and geochemical informaton collected from the Tethyan areas that roughly correspond to present-day Europe. However, the Tethys only covered less than 20% of the oceanic surface, and the rest was another ocean, Palaeo-Pacific that was even much larger than the present-day Pacific. The accomplished picture of the mid-Mesozoic global oceanography therefore requires improvement of the information from this huge ocean. Here I present the chemostratigraphic study of Late Jurassic to Early Cretaceous, which is first done for marine sediments in the Palaeo-Pacific, and revise the global oceanographic picture.

The study object is so-called “the Torinosu-type limestones” that was deposited in the western Palaeo-Pacific from Late Jurassic to Early Cretaceous and is now distributed nearly all through the Japanese Islands. In prior to applying the chemostratigraphy, I first studied sedimentology of the limestone by microfacies analysis and interpreted the depositional environments. The spatical and temporal distribution of microfacies of the Koike Limestone Member allows reconstruction of a carbonate platform generally dipping from south to north. I observed reefal frameworks consisting of corals, stromatoporoids, and microencrusters in the southernmost section. The coral fragments were transported

to the north and deposited with fine-grained carbonates in a deeper setting. The northward deepening trend is also supported by the texture of the oncoidal facies, which changes from grainstone in the south to pack–wackestone in the north. I recognized cyclic facies changes in most sections; these are best illustrated by quantitative analysis performed for one of the sections. Here, recurring upward-fining cycles consisting of coral floatstone, oncoidal facies, and peloidal wacke–grainstone probably formed in response to decreasing water-energy.

Secondly, I evaluated the ages of the Torinosu-type limestones by Sr isotopic stratigraphy. The $^{87}Sr/^{86}Sr$ ratios of 22 brachiopods collected from five sections revealed consistent ages with the previous biostratigraphy. The age of the upper horizon of the Koike Limestone Member ranges from 150 Ma to 149 Ma (late Kimmeridgian to early Tithonian). The two limestone sections corresponding to the lower and upper horizons of the Nankai Group (Shikoku Island of SW Japan) are assigned the ages of 143 to 142 Ma (Berriasian), and 136 to 132 Ma (early to late Hauterivian), respectively. From the other two sections in Shikoku Island of SW Japan, the age was evaluated from several horizons, which can be used for calculating the rate of deposition. Based on the assumption of a constant rate of deposition, a limestone section of the Torinosu Group was deposited during the period 151 Ma (late Kimmeridgian) to 140 Ma (late Berriasian), and a section of the Imaidani Group is assigned the age of 151 Ma (late Kimmeridgian) to 143 Ma (early Berriasian). These results show that intensive deposition of carbonate occurred in the shallow fore-arc platform in SW Japan from the Tithonian to the Berriasian, when the biocalcification was globally intensified. The deposition of carbonate was very likely interrupted by sea level fall during early Valanginian.

Thirdly, I measured carbon isotopic composition of 189 limestone samples collected in ~1-m-interval from the study sections. The $\delta^{13}C$ values of each section range; from -2.5 to +1.9‰ in the Koike section, -1.9 to +2.2‰ in the Nakanosawa sections, from -8.3 to +1.3‰ in the North Naradani section, from -0.8 to +2.2‰ in the South Furuichi, from +0.7 to +1.6‰ in the Kubukawa, and from -2.3 to +1.6‰ in the Shiraishi section. Considering Mn/Sr ratio, $\delta^{18}O$ values, and limestone texture, diagenetic alternation to the $\delta^{13}C$ values was recognized for many of the spamples, especially ones in the North Naradani and the Shiraishi sections. After rejecting these altered values, I could succeed to construct a composite carbon isotopic profile in the western Palaeo-Pacific Ocean during a 12-m.y. period from Kimmeridgian (late Jurassic) to Berriasian (earliest Cretaceous), in which the

$\delta^{13}C$ values appear a relatively narrow range from +0.5‰ to +2.2‰. This profile shows a distinct difference from the well-established Tethyan profile in terms of the Kimmeridgian records that are > 1.0‰ lower than the Tethyan values. The higher Tethyan values likely reflected on vigorous production and burial of organic carbon that is consistent to ubiquitous occurrence of petroleum source rocks in the Tethys but not in Palaeo-Pacific. Seawater exchange between the two oceans was reduced in degree to leave the difference in $\delta^{13}C$ of dissolved inorganic carbon. This interregional difference declined during Tithonian and disappeared in Berriasian as suggested by the Torinosu profile. The isotopic homogenization likely resulted from the increased seawater exchange in response to the development of the Hispanic and Mozambique corridors in Tithonian.

My Palaeo-Pacific data provide new insight to mid-Mesozoic ocean models that are mainly based on Tethyan records. However, the picture is not accomplished, yet. The mid-Mesozoic information from the Palaeo-Pacific marine carbonates is still fragmentary and needs more attention in order to improve our understanding on carbon cycle and ocean circulation during this greenhouse epoch and before the onset of Oceanic Anoxic Events (OAEs).

CONTENTS

Chapter #1. INTRODUCTION

Break-up of the Supercontinent Pangea from the Late Jurassic to the Early Cretaceous brought a substantial influence to the global carbon circulation. Expanded seaways in the gaps between the broken continents induced a humid climate along the coastal areas (Weissert and Mohr, 1996), which intensified chemical weathering. Vigorous weathering supplied inorganic nutrients (e.g., PO_4^{3-}) to seawater, and enhanced marine organic mass productivity in the eutrophied sea (Weissert and Mohr, 1996). Carbonate alkalinity and cations, such as Ca^{2+}, were also increased, and this resulted in diversification of reef communities and carbonate deposition on the expanded continental shelves (e.g. Kiessling, 2001; Leinfelder et al., 2002; Philip, 2003; Kano et al., 2007b). Such carbonate platforms were broadly developed in low latitudes of the Tethys Ocean as seen typically in the huge reef complexes exposed in Western Europe and the Mexican Gulf Coast. Degree of the suppersaturation of calcite was probably high because the semi-inorganic components such as ooids were developed in a wide range of palaeolatitudes (Opdyke and Wilkinson, 1990). The explosive expansion of planktonic foraminifer and calcareous nannoplankton (e.g. Roth, 1987; Erba, 2006) further enhanced the carbonate deposition (e.g. Leinfelder et al., 2002; Philip, 2003). Transition from Jurassic to Cretaceous was certainly a period of active carbonate deposition (Opdyke and Wilkinson, 1988). The activated carbon cycle left fingerprints on the carbon isotopic stratigraphy. The $\delta^{13}C$ profile established in the Tethyan province indicates high values (+2 to +3‰) in the Late Jurassic, which have been considered to result from the high production and burial rates of organic carbon (e.g. Weisssert and Mohr, 1996; Padden et al., 2002; Weisssert and Erba 2004). The $\delta^{13}C$ values decreased to ca. 1.2 ‰ in Berriasian, and followed to a positive excursion called Weissert OAE in Valanginian (Channel et al., 1993; Weissert et al., 1998; Erba et al, 2004; Weissert and Erba, 2004).

However, these trends in carbonate deposition and isotopic stratigraphy were based on the records from the Tethyan province, mostly in Western Europe and the Mexican Gulf Coast, which have been studied by palaeontologists and sedimentologists since the 19th century. The Late Jurassic Tethys Ocean was located in the low latitudes surrounded by North America, Gondwana, and European landmasses (Fig. 1A) and were thalassic in comparing with the Palaeo-Pacific Ocean that occupied about 80% of the global ocean. The two oceans were different in terms of close/openness, latitudinal distribution, water

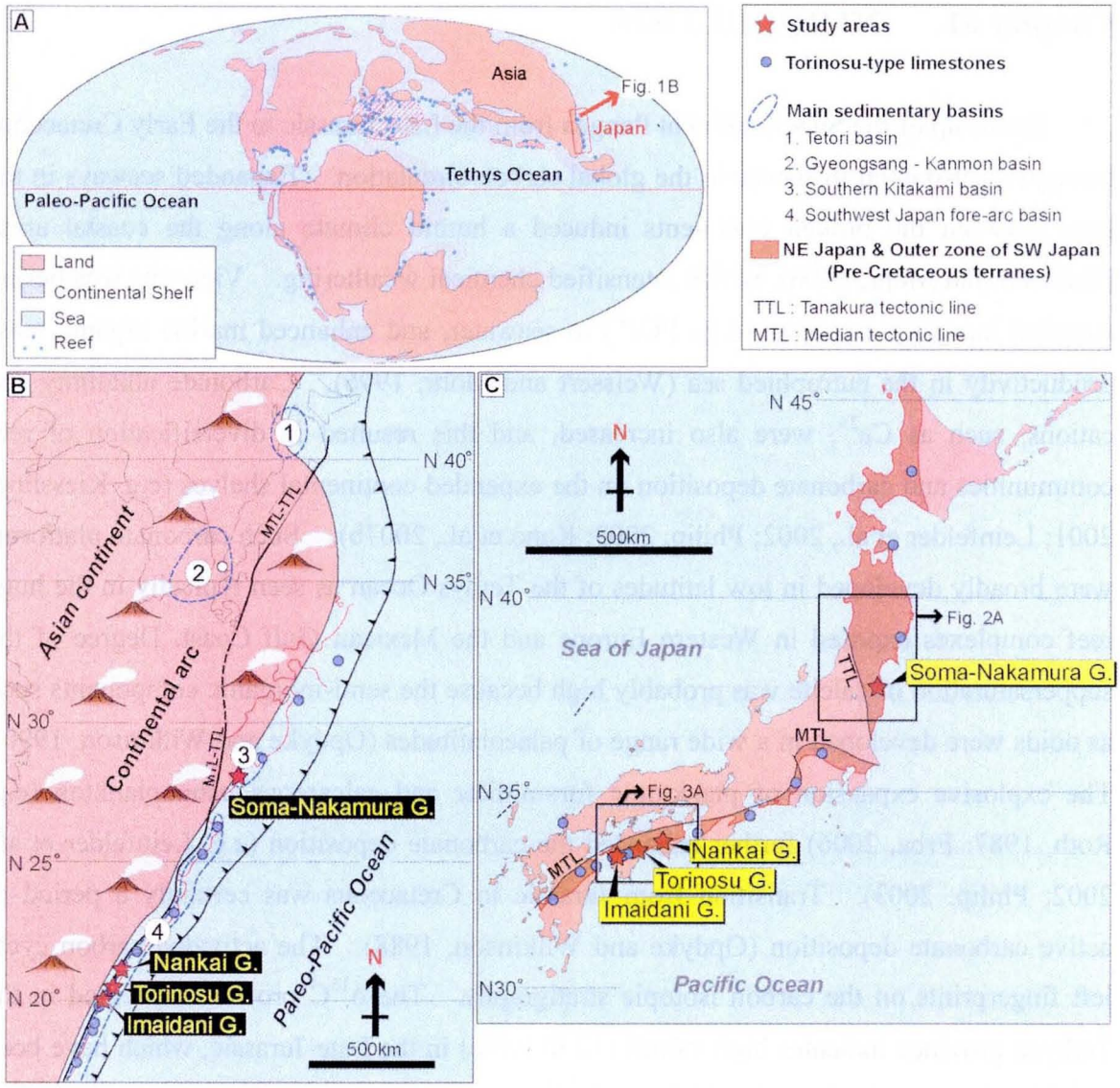

Figure 1. **(A)** Palaeogeography of the Late Jurassic world. The area, where carbon isotopic stratigraphy was well studied, is shown by shaded pattern. Distribution of reefs was modified after Leinfelder et al (2002). **(B)** Palaeogeography of Japan and the adjacent areas in late Jurassic. Alignment and outline of Japanese Islands are based on Maruyama and Seno (1986), and Tazawa (1993, 2004). The palaeo-latitudes are from palaeomagnetological data of Ren et al. (2002) and Metelkin et al. (2007). **(C)** Tectonic divisions of the modern Japanese Islands. The Torinosu-type limestone mainly occurs in the Northeast Japan and the outer zone of the Southwest Japan (Tamura, 1961b; Shiraishi and Yoshidomi, 2005).

depth, and potentially in carbon cycle. Therefore, we need to notice the versatility of the Tethyan records that have represented the global trends of the mid-Mesozoic oceanography. The problem is the limited development of shallow marine carbonates in Palaeo-Pacific Province (Leinfelder et al., 2002). Despite of requirement to reconstruct the global carbon

cycle and ocean circulation of this period, the Palaeo-Pacific data have been demonstrated fragmentary from limited areas (e.g. Aguirre-Urreta, 2008; Kakizaki and Kano, 2009).

Potential material to solve the problem is the limestones in the Japanese Islands, which were located at the northwestern margin of Palaeo-Pacific Ocean in this period. They are called "The Torinosu-type limestone" following to the German geologist, Heinrich Edmund Naumann, who first recognized the limestone in a village in Sakawa Town (Kochi Prefecture) and named after the locality (Harada, 1890). Since then, the limestone was subjected first to palaeontological studies (e.g., Yabe and Toyoma, 1928; Yabe and Sugiyama, 1935; Eguchi, 1951) that recognized a wide distribution of a similar fauna broadly correlated to the Tethyan-type fauna of the relevant age (e.g., Tamura, 1961a). In fact, the Torinosu-type limestone is distributed in all of the four main Japanese Islands (from Hokkaido to Kyushu). The subsequent studies further found that these limestones share lithological features, such as shallow marine lithofacies, siliciclastic at least in a part, and high organic contents (Kimura, 1956; Tamura, 1960b; Mori, 1963; Eguchi and Shoji, 1965) and followed by sedimentological studies that dealed with more detailed features of a specific limestone body (e.g. Kano, 1988; Morino et al., 1989; Morino, 1993; Kano and Jiju, 1995; Kiyama and Iryu, 1998; Shiraishi and Kano, 2004; Kakizaki and Kano, 2009).

The development of the Torinosu-type limestones is most prominent in the fore-arc basins of the Jurassic accretionary complexes (the Chichibu Terrane) of southwestern Japan (Matsuoka, 1992). They represent unique configuration and stratigraphic occurrence, as generally in lenticular bodies of a relatively small size (typically several tens of meters thick, and several hundred meters wide). The limestone bodies are often developed in several horizons in a mudstone-dominating section, such as seen in Shikoku Island, where the Torinosu-type limestone is best developed (e.g. Morino et al., 1989; Kano and Jiju, 1995).

The Torinosu-type limestone probably provides an opportunity to study carbon isotopic stratigraphy of the Palaeo-Pacific province, if the depositional age is determined in detail. But, lack of lateral extension and poor occurrence of age-diagnostic fossils make the establishment of detailed interregional correlation of the limestone bodies difficult. Hence, based only on rare occurrence of ammonites and radiolarians, the age of the limestone was vaguely believed to belong to the Late Jurassic to the Early Cretaceous (e.g. Matsuoka, 1992; Kashiwagi et al., 2002; Takei and Matsuoka, 2004; Sato and Taketani, 2008).

In order to evaluate the age, I attempted to apply Sr isotope stratigraphy for the Torinosu-type limestone in four stratigraphic units namely; the Soma-Nakamura Group in Fukushima Prefecture, the Imaidani Group in Ehime Prefecture, the Nankai Group and the Torinosu Group in Kochi Prefecture (Fig. 1B). A continuously increasing trend of the $^{87}Sr/^{86}Sr$ ratio from the Oxfordian to the Barremian insures its credibility to provide the constraint for the age to the Torinosu-type limestone. Based on the age assignment, I show a carbon isotopic profile for each section, and compile the data into the standard profile during ca. 12-m.y.-period (from Late Kimmeridgian to Berriasian), as the first record from the Palaeo-Pacific Ocean.

Following this introductory chapter, I describe the details on the study sections of the Torinosu-type limestone in Chapter #2, and the methods in Chapter #3. Then, Chapter #4 represents the results on three topics; sedimentology of limestone, age estimation based on Sr-isotopic ratio, and carbon isotopic profiles, which broadly corresponding to the contents of the following three papers published in or submitted to peer-review journals, respectively.

(1) Kakizaki, Y. and Kano A., 2009. Architecture and chemostratigraphy of the latest Jurassic shallow marine carbonate in NE Japan, western Palaeo-Pacific. Sedimentary Geology, 214, 49-61.

(2) Kakizaki, Y., Ishikawa, T., Nagaishi, K., Tanimizu, M., and Kano, A., Strontium isotopic ages of the Torinosu-type limestones (Late Jurassic to Early Cretaceous, Japan), as an implication for palaeocanography. Submitted to Journal of Asian Earth Science.

(3) A Late Jurassic to Early Cretaceous carbon isotopic profile from the Paleo-Pacific: New insight into oceanographic changes with the continental drift. Submitted to Geology.

Based on these data, I synthesize the discussions in Chapter #5, which include platform architecture, depositional cycle, sedimentation rate of the Torinosu-type limestone, palaeoceanography in the Palaeo-Pacific Ocean, the global marine carbon cycle, and ocean-circulation from the Late Jurassic to the earliest Cretaceous. Finally, my thesis is closed with important outcomes form my five-year research in the Department of Earth and

Planetary Systems Science, Hiroshima University, in Chapter #6.

Chapter #2. GEOLOGICAL SETTINGS

2.1. Torinosu-type limestones

"The Torinosu-type limestone" that was first used by Naumann, is now the term that denotes shallow marine limestones of the late Jurassic to the early Cretaceous age, developed in Japanese Islands (Tamura, 1960, 1961a, 1961b). During this period, Japan was located at the eastern margin of the Asian Continent that faced the northwestern area of the Palaeo-Pacific Ocean (Fig.1A), where the Izanagi Plate subducted (Maruyama and Seno, 1986). Along the continental arc, accretion of pelagic sediments, seamounts, and microcontinents formed tectonic complexes, on which shallow marine environments developed for carbonate sedimentation (Matsuoka, 1992). However, carbonate sedimentation was interrupted temporally and spatially possibly by active tectonics and siliciclastic influx.

The Mesozoic accretionary complexes were displaced by a large transform fault (Tanakura and Median tectonic lines; Fig. 1B and C) after the late Cretaceous. The relative dislocation by the fault could have reached about 1,500 km, evident from the strike-slip model on the formation of the Japanese Islands (Tazawa, 1993, 2004). The Torinosu-type limestone is currently distributed in the Northwest Japan and the outer zone of the Southwest Japan (Fig. 1C). These two terranes were largely displaced northward since the late Cretaceous, from their original location in lower latitudes ranging from 20 to 28 degree in the north (Fig. 1B).

Only the Soma-Nakamura Group, out of the four studied units, is located in the Northeast Japan (Fig. 2A). The other three limestone-bearing units, the Nankai Group, the Torinosu Group, and the Imaidani Group (Fig. 3), are situated in Shikoku Island where the upper Jurassic to the lower Cretaceous shallow marine deposits are distributed in the South belt of the Chichibu Terrane extending in the east-west direction.

2.2. The Soma-Nakamura Group

In the Southern Kitakami Terrane of northeastern Japan, the Torinosu-type limestones were formed in a continental shelf setting (Minoura, 1985). One of these limestone bodies, the Koike Limestone Member of the Nakanosawa Formation in the

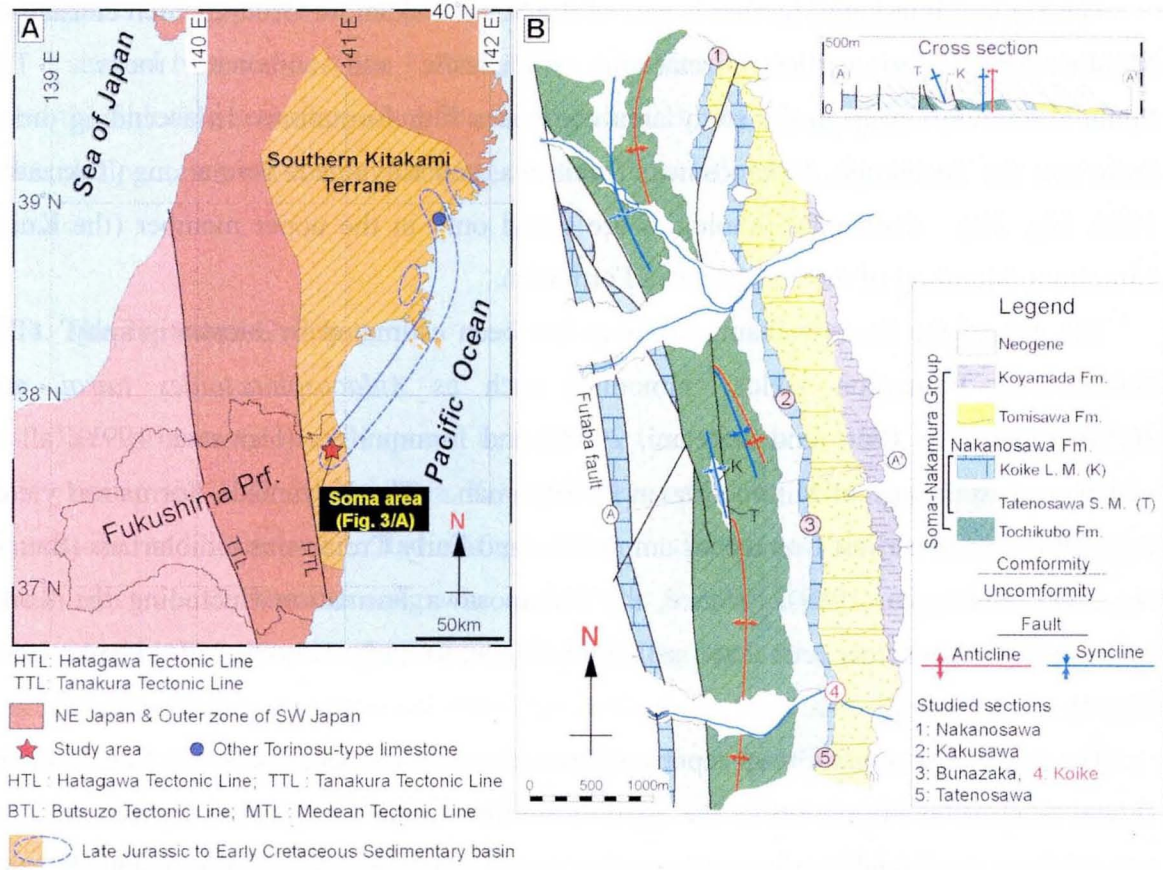

Figure 2. The geological setting of the study sections of the Koike Limestone Member. **(A)** Map of northern Honshu Island showing the location of the Southern Kitakami Terrane. Soma-Nakamura Group is located in the southernmost of the Jurassic-Cretaceous sedimentary basin. **(B)** Geological map and cross section of the Soma-Nakamura Group in the study area. Localities of the five study sections (1-5) are shown.

Soma-Nakamura Group in northeastern Fukushima Prefecture, is larger than its counterparts in southwestern Japan (Fig. 2B). There have been many palaeontological (Eguchi, 1951; Tamura, 1961b; Mori, 1963; Imaizumi, 1965; Shikama and Yui, 1973), sedimentological (Eguchi and Shoji, 1965; Morino, 1992; Uematsu, 1997; Kiyama and Iryu, 1998), and geochemical studies (Kimura, 1953; Igarashi and Fujinuki, 1972) in the region, which provide a standard stratigraphic framework for the Torinosu-type limestone.

The Soma-Nakamura Group in the study area forms an anticlinorium on a north trending axis. The Koike Limestone Member appears on both the eastern and western flank of the anticlinorium and extends over a strike length of about 8 km (Fig. 2B). The limestone of the western flank is strongly deformed and recrystallized owing to the activity of the Futaba Fault, and original sedimentary structures are not preserved. The limestone of the eastern flank, however, preserves a variety of sedimentary facies and fossils.

The Koike Limestone Member is part of the Soma-Nakamura Group, which consists of Middle Jurassic to earliest Cretaceous siliciclastic and carbonate rocks. The Soma-Nakamura Group in the study area comprises four formations. In ascending order, these are: the Tochikubo, Nakanosawa, Tomisawa, and Koyamada formations (Takizawa, 1996, Fig. 2B). Carbonate lithologies are found only in the upper member (the Koike Limestone Member) of the Nakanosawa Formation.

The age of the Soma-Nakamura Group has been estimated by biostratigraphy. The Nakanosawa Formation yields ammonites such as *Aulacosphinctoides tairai*, and *Hybonotyceras* sp. (Sato and Taketani, 2008), and foraminifers (Uematsu, 1997), all of which suggest an age of Kimmeridgian to Tithonian. The Koyamada Formation yields Late Tithonian to earliest Cretaceous ammonites and Early Cretaceous radiolarians (Sato et al., 2005; Matsuoka, 1989). Hence, the Nakanosawa Formation (including the Koike Limestone Member) has been dated as Kimmeridgian to Early Tithonian (Takizawa, 1996, Fig. 4).

The Soma-Nakamura Group represents two transgressive sequences; the first from the fluvial Tochikubo Formation to the shallow marine Koike Limestone Member, and the second from the fluvial Tomisawa Formation to the marine Koyamada Formation (Kiyama and Iryu, 1998). Hence, the top of the limestone member corresponds to the boundary between the two transgressive sequences. The exact boundary was not exposed in accessible outcrops, but likely abrupt as seen at Kakusawa (Fig. 2B), where oncoidal packstone is exposed just 2 m below coarse fluvial sandstone of the Tomisawa Formation.

2.3. The Nankai Group

The Nankai Group in eastern Kochi Prefecture is exposed in a 2 km wide area extending 10 km from east to west. The lithologies mainly consist of alternation of mudstone and sandstone, which contains lenticular limestone bodies that are less than 20 m thick and have a lateral extension of several hundred meters. Morino et al. (1989) suggested that radiolarians and bivalves assigned this group to the Early Cretaceous (Valanginian to Barremian), judged by. This age is youngest among the Torinosu-type limestones distributed in SW Japan. On the other hand, Kozai et al (2004) suggested an older age ranging from the Oxfordian to the Berriasian (Fig. 4). Morino (1993) studied the limestone exposed in the Nishinokawa section (Fig. 3B) and interpreted that it

represents transgressive facies because it overlies sandstone yielding brackish bivalves.

I studied two sections; the Kubokawa section located 3km southeast of Birafu village, and the Shiraishi section located 5km northeast of Birafu village (Fig. 3B). According to the geologic structure, the Shiraishi section is stratigraphically above the Kubokawa section.

2.4. The Torinosu Group

The Torinosu Group is exposed in a narrow (ca. 1 km wide) belt extending more than 60 km in the E-W direction in Kochi Prefecture. The lithofacies mainly consist of mudstone and limestone. Radiolarians from mudstone and calcareous nannoplankton from calcareous mudstone assign the ages of the Kimmeridgian to the Valanginian (Aita and Okada, 1986; Kano, 1988; Matsuoka, 1992, Fig. 4). The limestone normally occurs as lenticular bodies accompanied with marlstone at the base, and contains shallow marine components, such as ooids and reef-builders (stromatoporoids and corals). Sedimentological studies of Kano (1988) and Kano and Jiju (1995) have demonstrated that the limestone bodies were carbonate mounds formed a topographic high.

I studied the 150 m thick limestone section exposed in the north of Naradani of Sakawa Town (North Naradani section; Fig. 3C).

2.5. The Imaidani Group

The Imaidani Group is the lateral extension of the Torinosu Group, and is exposed in Seiyo City of Ehime Prefecture. The lithofacies mainly consist of shale-rich alternation and lenticular bodies of shallow marine limestone, which have been described by Shiraishi and Kano (2004) as a reefal framework constructed by corals, stromatoporoids, and microencrusters. Presence of radiolarians and ammonites in the mudstone of the lower part of the group suggests an age ranging from the Kimmeridgian to the Tithonian (Yao et al., 1982; Takei and Matsuoka, 2004, Fig. 4).

I studied the south Furuichi section located 500 m northwest of Furuichi, where the largest limestone body of the group is exposed (Nakatsugawa limestone body; Fig. 3D).

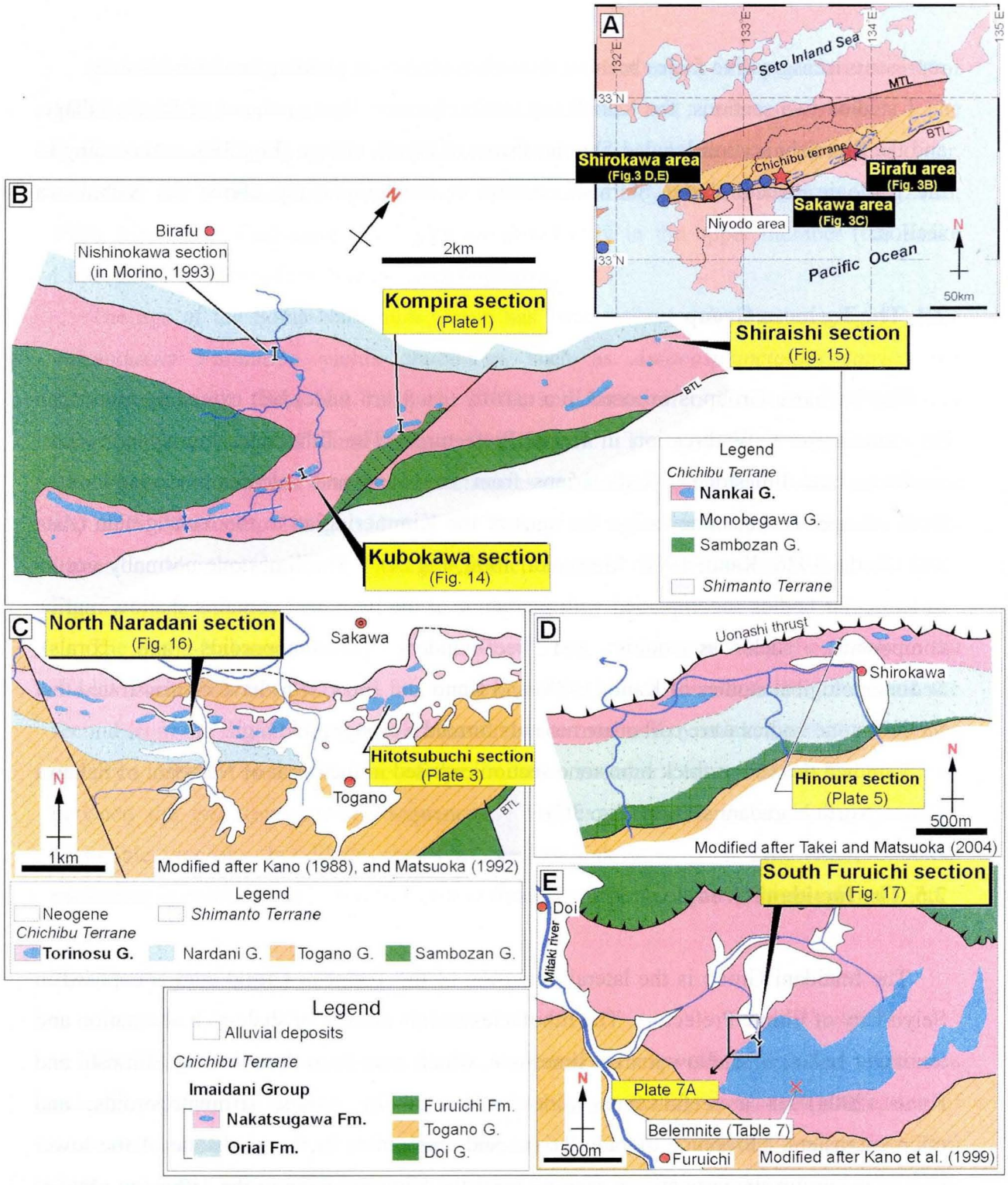

Figure 3. The geological setting of the study sections on the Shikoku Island. **(A)** The late Jurassic to early Cretaceous basins in the outer zone of the Southwest Japan in Shikoku Island (Tashiro, 1985; Matsuoka et al., 1998). **(B)** Geological map of the Nankai Group around Birafu, showing locations of the Kubokawa, Shiraishi, and Kompira sections. **(C)** The North Naradani and Hitotsubuchi sections of the Torinosu Group in Sakawa area (modified after Kano, 1988; Matsuoka, 1992). **(E)** and **(D)** The Hinoura (Fig. 3D: modified after Takei and Matsuoka, 2005) and the South Furuichi sections (Fig. 3E: modified after Kano et al., 1999) of the Imaidani Group in Shirokawa area.

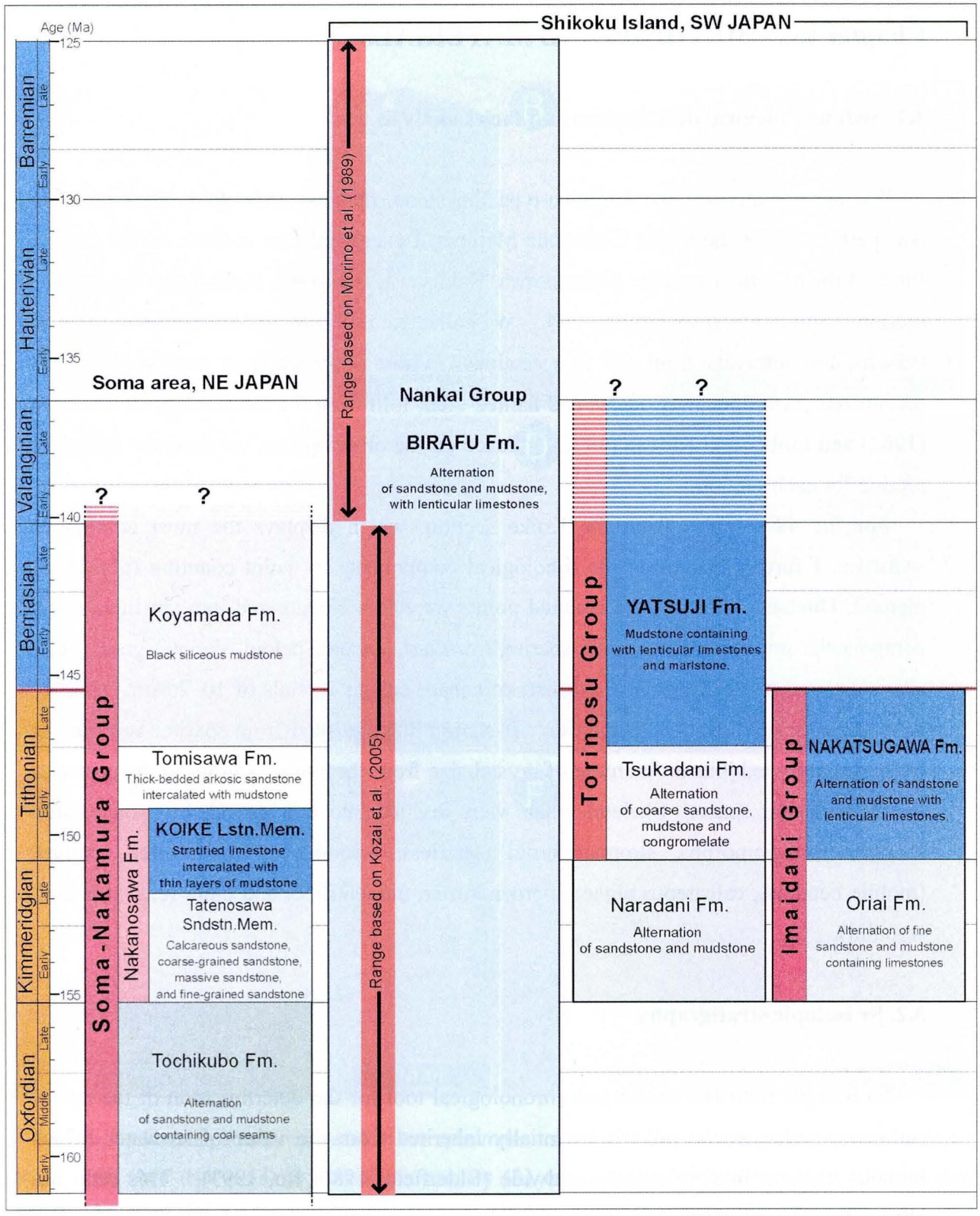

Figure 4. Biostratigraphic age evaluation of the four limestone-bearing units; the Soma-Nakamura Group (Matsuola, 1989; Yanagisawa et al., 1996; Sato and Taketani, 2008), the Nankai Group (Morino et al., 1989; Kozai et al., 2005), the Torinosu Group (Aita and Okada, 1986; Kano, 1988; Matsuoka, 1992), and the Imaidani Group (Yao et al., 1982; Takei and Matsuoka, 2003). The absolute ages follow to Ogg (2004).

Chapter #3. METHODS AND MATERIALS

3.1. Sedimentological descriptions and facies analysis

As representative of the Torinosu-type limestone, detailed sedimentological analyses was performed for the Koike Limestone Member. I examined five sections on the eastern flank of the anticlinorium; the Nakanosawa, Kakusawa, Bunazaka, Koike, and Tatenosawa sections from north to south (Fig. 2B). We collected a total of 177 limestone samples at 0.5- to 2-m intervals from the five sections. From observation of thin sections, we recognized six sedimentary facies and named them following the terminology of Dunham (1962) and Embry and Klovan (1972). Based on the observations, we drew the columnar section for each section.

For the 48 samples from the Koike section, which displays the most continuous sequence, I further quantified the lithological components by point counting (grain-bulk method; Dunham, 1962). The counted points were first categorized into ten lithological components: micrite, microsparite, sparite, intraclast, oncoid, peloid, skeletal grain, ooid, siliciclast, and clay. Microspar consists of equant calcite crystals of 10–20 μm diameter formed by recrystallization of micrite. It can be distinguished from sparite, because the latter generally exhibits an increase of crystal size from the rim of a grain to the center of the intergranular space. Skeletal grains were divided into brachiopod, bryozoan, coral, sponge, Spongiomorpha, stromatoporoid (sessiles), echinoderm, foraminifer, mollusk (mobile benthos), calcareous algae, microencruster, unidentified, and other (e.g., ostracod, serpulid).

3.2. Sr isotopic stratigraphy

Sr isotopic ratio is a useful geo-chronological tool for the determination of the age of carbonate rocks, as the ratio is essentially inherited from the value of seawater, which remains uniform in the oceans worldwide (Elderfield, 1986; Ito, 1993). This ratio has changed with time, principally due to the relative importance between the flux of a low ratio from the mid-ocean ridge and the continental flux having a high ratio (Edmond, 1992), and the global trend from the Ordovician to the Present has already been established (McArthur et al., 2001). I can evaluate the age of deposition of the Torinosu-type

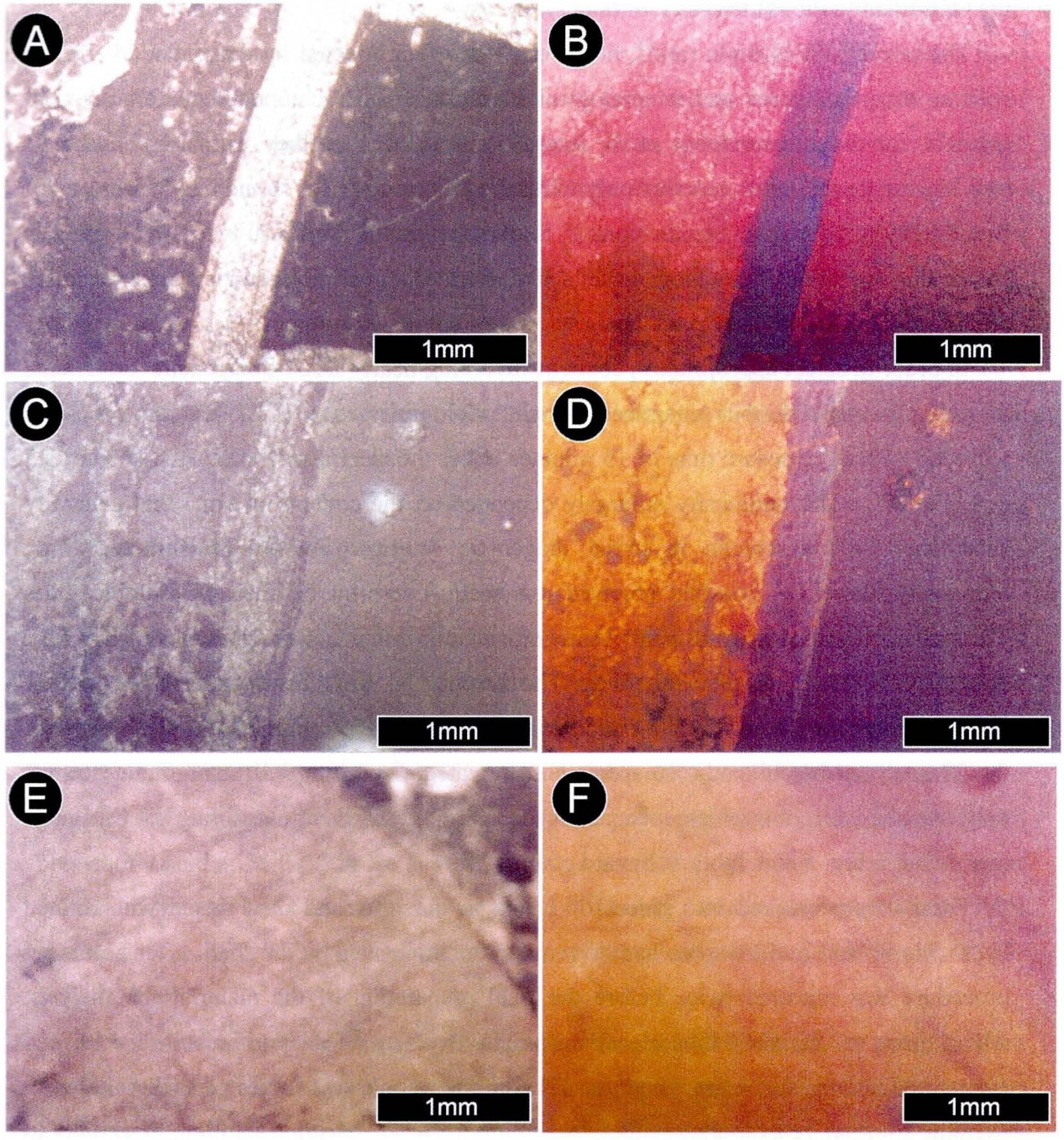

Figure 5. Cathodoluminescence views of the specimens used for Sr isotopic analysis. A non-luminescent brachiopod shell (Nar-N-14) in optical microscopic **(A)** and cathodoluminescence views **(B)**. A dull brachiopod shell (Nk-A-1) in optical microscopic **(C)** and cathodoluminescence views **(D)**. A bright belemnite collected from the Nakatsugawa limestone body (Belemnite) in optical microscopic **(E)** and cathodoluminescence views **(F)**. Other CL results are shown in Table 1.

limestone by Sr isotopic ratio, as the ratio had a monotonic increase during the period from the Oxfordian to the Barremian (Jones et al., 1994).

The primary Sr isotopic ratios, however, were often affected by diagenetic alteration, such as recrystallization and mineralogical stabilization. Brachiopod shells are an ideal material for the measurement of Sr isotopic ratios, because they primarily consist of low-Mg calcite that often receives only minimized alteration (e.g. Brand and Veizer, 1980; Brand, 1991). Previous application of Sr isotope to the Torinosu-type limestone has shown that the ratios of brachiopod shells demonstrated a good reproductivity, therefore are reliable (Shiraishi et al, 2005).

In order to select appropriate specimens involving nearly free of diagenetic alterations, the samples were further examined by cathodoluminescence (CL) images that were recorded with an exposure time of 15 minutes under the electronic beam of 20 kV and 1.5 mA (Fig. 5). The luminosity is largely depended on the content of Mn^{2+} that generally substitutes Ca^{2+} in calcite in burial diagenetic settings. The shells emitting strong luminosity, therefore, possibly received diagenetic overprint on their Sr isotopic ratio. The luminosities are conventionally categorized into three: non-luminescence (Fig. 5B), dull (Fig. 5D), and bright (Fig. 5F). The brachiopod shell commonly shows weaker luminescence than the surrounding micritic sediments (compare Fig. 5A and B), and out of the 22 analyzed brachiopods, 16 specimens are categorized into dull or no-luminescence, only two show bright luminescence, and 4 shells are too small for examining the CL image (see detail in Fig. 5 and Table 1; Savard et al., 1995).

Fossils were crushed into pieces of 2 mm in diameter and then rinsed with diluted hydrochloric acid in ultra-sonic bath to remove the impurities on the shell. This cleaning procedure was repeated twice before the final preparation of the material for analysis. About 1 mg of the shell thus cleaned was dissolved in 0.5 N purified nitric acid, and evaporated into nitrate on the hot plate. The nitrate sample was subjected to dissolution in pyridine solution, re-evaporation, and dissolution in DCTA pyridine solution, essentially to improve separation between Sr and the other alkaline earth elements, such as Ca and Mg. Sr was separated by a use of chromatography with ion exchange resin (AG 50W X12) and then dissolved in purified nitric acid in a concentration of ~ 120 mg/l. 0.8 ml of this nitric acid solution added with a drop of tantalum solution was put and heated on a tungsten filament. The Sr isotopic ratio ($^{87}Sr/^{86}Sr$) was measured by a thermal ionizing mass spectrometer (TIMS; Thermo Finnigan TORITON) at Center for Advanced Marine Core

Research of Kochi University.

The measured $^{87}Sr/^{86}Sr$ ratios were calibrated based on the recommended ratio NIST987 in Look-up Table Version 4: 08/03 ($^{87}Sr/^{86}Sr$ = 0.7102480, revised from McArthur et al., 2001). The calibrated ratios were projected on the standard age-profile of Look-up Table that consists of three curves (upper, mean, and lower) that cover 95% of the Sr isotopic age dataset collected worldwide. I have evaluated three ages (younger limit, mean, older limit) for each measured value. The mean age is the point of the mean isotopic ratio on the mean age-ratio curve. The younger and older limit ages correspond to the point of the mean plus 2σ on the lower curve and the point of the mean minus 2σ on the upper curve, respectively. The measuring error (2σ) was always below 130×10^{-7}, which corresponds to uncertainty less than 2.5 m.y. during the period from the Kimmeridgian to the Hauterivian.

3.3. Carbon isotopic stratigraphy

For geochemical analysis, powdered samples were used, avoiding large fossils, calcite veins, and weathered material. The samples were dissolved in 10% acetic acid and the concentrations of trace elements (Mn and Sr) were analyzed by absorption spectrophotometer (Shimadzu AA-646). The measurement error was less than 5%. To measure stable isotope compositions, 5 mg of the powdered samples were reacted with phosphoric acid at 55.0 C° in He at 1 atm. CO_2 was introduced into a mass spectrometer (Thermo Finnigan MAT Delta Plus). $\delta^{13}C$ and $\delta^{18}O$ were calculated relative to the VPDB standard in per mil. The measurement errors were typically 0.1‰ for $\delta^{13}C$ and 0.15‰ for $\delta^{18}O$ (1σ).

Unweathered micritic matrix was extracted from total 188 limestone samples from the four sections collected at ~1m intervals (37 from the Nakanosawa section, 48 from the Koike section, 15 from the Kubokawa section, and 48 from the South Furuichi section) by using a dental drill. To measure stable isotope compositions, 5 mg of the sample was reacted with phosphoric acid at 55.0 C° in a 12-m*l* glass vial filled with 1-atm He for three hours. The CO_2 gas was introduced with He gas into gas chromatography and separated from water vapor, N_2 and O_2. Then, the $\delta^{13}C$ and $\delta^{18}O$ of the CO_2 was measured in a mass spectrometer (Thermo Finnigan MAT Delta Plus) and calculated relative to the

VPDB standard in per mil. The measurement errors were typically less than 0.2‰ for $\delta^{13}C$ and 0.3‰ for $\delta^{18}O$ (2σ).

Table 1. The results of the Sr isotopic age of 22 brachiopods and 1 belemnite estimated by LOWESS Look-up Table version 4: 08/03 (revised from McArthur, 2001). $^{87}Sr/^{86}Sr$ ratios were calibrated by measuring the standard sample (NIST 987).

	horizon (m)	Sample	CL	$^{87}Sr/^{85}Sr$	2σ	Age (Ma) (Older - Mean - Youngest)	Range (Myr)	Geologic Time
Koike Limestone								
Nakanosawa section								
1	68	Nk-A-1	dull	**0.7070735**	100	150.0-149.6-149.15	0.85	**Early Tithonian** (150.6-149.15Ma)
2	68	Nk-A-2	bright	**0.7070506**	78	150.6-150.3-149.95	0.65	
Nankai Group								
Kubokawa section								
3	6	KBK-7	-	**0.7072421**	88	142.6-142.0-141.5	1.1	**Late Berriasian**
Shiraishi section								
4	1.5	SH-3-2	dull	**0.7074164**	62	134.7-134.25-133.75	0.9	**Early - Late Hauterivian** (136.15-132.1Ma)
5	1.5	SH-3-4	dull	**0.7074435**	88	133.4-132.8-132.1	1.3	
6	1.5	SH-3-5	no	**0.7073915**	58	136.15-135.65-135.2	0.95	
7	1.5	SH-3-6	dull	**0.7074391**	130	133.85-133.1-132.1	1.75	
Torinosu Group								
North Naradani section								
8	78	Nar-S-8	dull	**0.7071692**	126	146.75-145.7-144.4	2.35	**Latest Tithonian -Late Berriasian** (146.75-140.25Ma)
9	128	Nar-N-1-4	no	**0.7072148**	72	143.75-143.15-142.6	1.15	
10	128	Nar-N-1-17	dull	**0.7072254**	84	143.35-142.7-142.1	1.25	
11	128	Nar-N-1-21	dull	**0.7071921**	72	145.05-144.25-143.55	1.5	
12	128	Nar-N-1-22	dull	**0.7072348**	88	142.9-142.3-141.75	1.15	
13	128	Nar-N-1-24	dull	**0.7072004**	74	144.55-143.8-143.15	1.4	
14	128	Nar-N-1-25	dull	**0.7072335**	50	142.75-143.3-141.95	0.8	
15	143	Nar-N-4-9	bright	**0.7072616**	72	141.75-141.3-140.95	0.8	
16	143	Nar-N-4-08	-	**0.7072440**	76	142.45-141.9-141.45	1.0	
17	143	Nar-N-4-09	-	**0.7072214**	76	143.5-142.85-142.3	1.2	
18	152	Nar-N-2-9	dull	**0.7072851**	82	140.95-140.55-140.25	0.7	
Imaidani Group (Nakatsugawa rock body)								
South Furuichi section								
19	27	Fur-S-31	dull	**0.7071629**	128	147.1-146.15-144.85	2.25	**Late Tithonian -Late Berriasian** (147.55-142.95Ma)
20	29	Fur-S-33	dull	**0.7071501**	96	147.55-146.9-146.0	1.55	
21	31	Fur-S-35	dull	**0.7071553**	114	147.4-146.6-145.5	1.9	
22	49	Fur-S-50	-	**0.7072015**	114	144.7-143.65-142.95	1.75	
23	-	Belemnite	bright	**0.7071761**	124	146.35-145.25-144.25	2.1	

Jan. '07

Nakanosawa, Kubokawa, and North Naradani sections

No.	Measured ratio	2σ
1	0.7102492	100
2	0.7102549	70
3	0.7102467	88
AVERAGE	0.7102503	86
Difference	0.0000023	

Feb. '08 **Nakatsugawa Belemnite**

1	0.7102609	68
2	0.7102501	78
3	0.7102485	74
4	0.7102508	92
5	0.7102566	68
AVERAGE	0.71025338	76
Difference	0.0000054	

Jul. '07 **Shiraishi and South Furuichi sections**

No.	Measured ratio	2σ	Status
1	0.7102704	70	Accepted
2	0.7102690	72	Accepted
3	0.7102720	76	Accepted
4	0.7102702	98	Accepted
5	~~0.7102763~~	~~264~~	Abandoned
6	0.7102692	72	Accepted
7	0.7102659	52	Accepted
8	0.7102662	114	Accepted
9	0.7102715	110	Accepted
AVERAGE	0.7102693	83	
Difference	0.0000213		

TOTAL AVERAGE 0.7102576

Sr isotopic ratio of NIST987 in Look-up table 0.7102480

(McArthur and Haworth, 2004)

Chapter #4. RESULTS

4.1. Sedimentology of the Koike Limestone Member

4.1.1. Six sedimentary facies recognized from five study sections

Based on the observation of 177 limestone samples collected from the five study sections that appear variable thickness and facies cycles (Fig. 6), I recognized six basic sedimentary facies: sandy limestone, intraclastic grainstone, oncoidal facies, peloidal wacke–grainstone, coral floatstone, and boundstone. The six facies are all exposed in the Koike section, where the lithological components of the limestone were quantitatively evaluated by point counting. Figure 7A shows the average percentages of the ten lithological components for each facies. For the skeletal components, the percentages given indicate the percentage within the count of the skeletal grains (Fig. 7B).

4.1.1.1. Sandy limestone facies

The sandy limestone facies occurs mainly in thin beds (<4 m thick) in the basal part of the Nakanosawa, Bunazaka, and Koike sections (Fig. 6), where it conformably overlies a calcareous sandstone at the top of the Tatenosawa Sandstone Member. An exception occurs in the Kakusawa section, where this facies is developed near the middle of the section.

The sandy limestone facies is rich in subangular to subrounded siliciclastics (17%; Fig. 7A) of 0.25–1 mm diameter (Fig. 8A). This facies has a characteristically high content of oncoids (34%) with siliciclastic nuclei and thin micritic cortices. Intraclasts are common.

Mollusks (20%) and microencrusters (28%) are dominant among the skeletal grains (Fig. 7B). This facies contains more molluskan shells than other facies, and most of them are fragmented. Microbial filaments (*Girvanella tosaensis*) are seen to cover bivalve shells and to trap some siliciclastics (Fig. 8B).

4.1.1.2. Intraclastic grainstone facies

The intraclastic grainstone facies is thinly (<5 m thick) developed in the lower horizons of the Koike Limestone Member at the Nakanosawa and Koike sections (Fig. 6). The grains of this facies are 0.5–2 mm in diameter and are dominated by intraclasts (34%) and

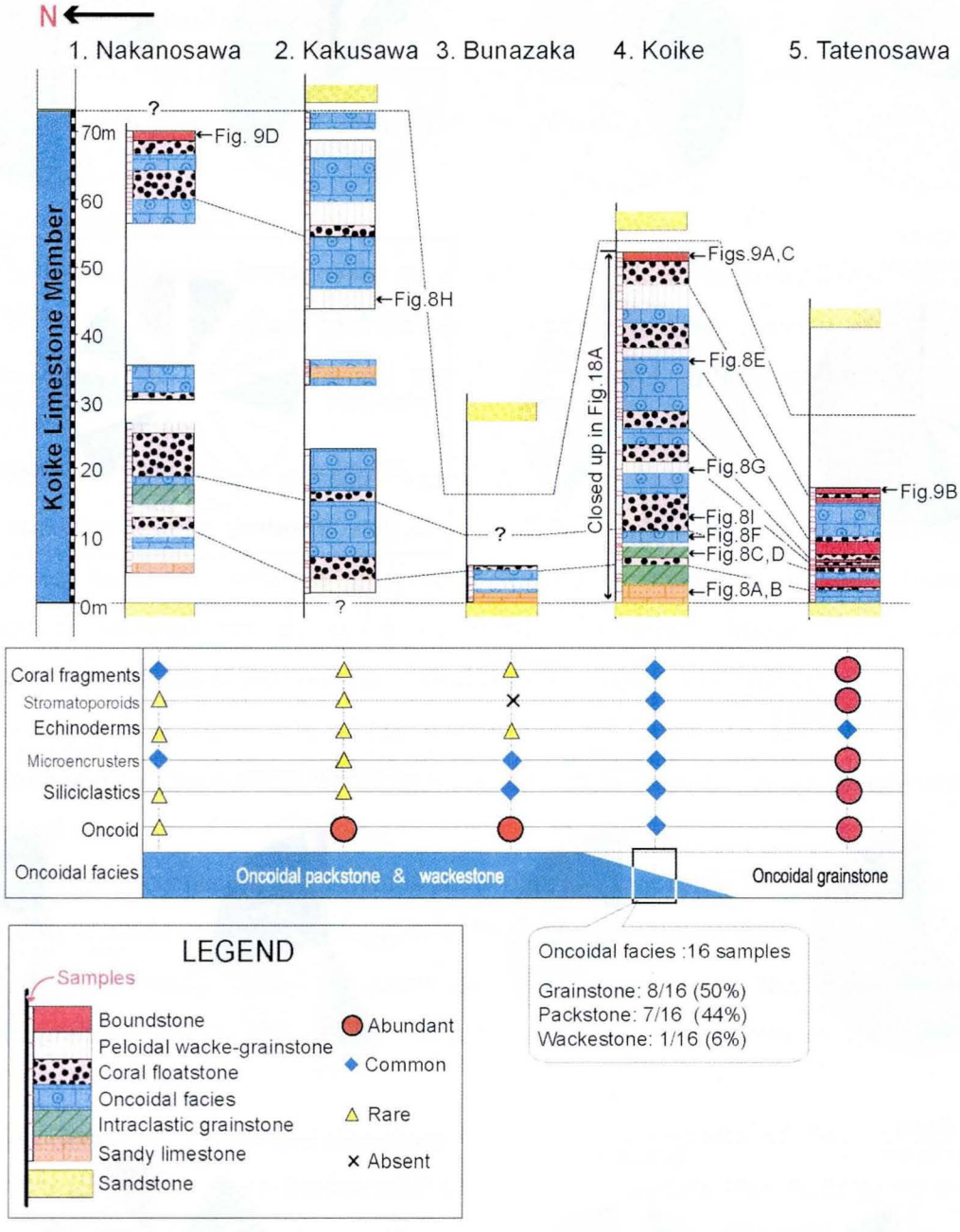

Figure 6. Logs of the five studied sections of the Koike Limestone Member. Abundance of components of limestone and texture of oncoidal facies are also shown for each section. Locations of the sections are shown in Fig. 2B. Arrows indicate horizons of samples shown in Figs. 8 and 9.

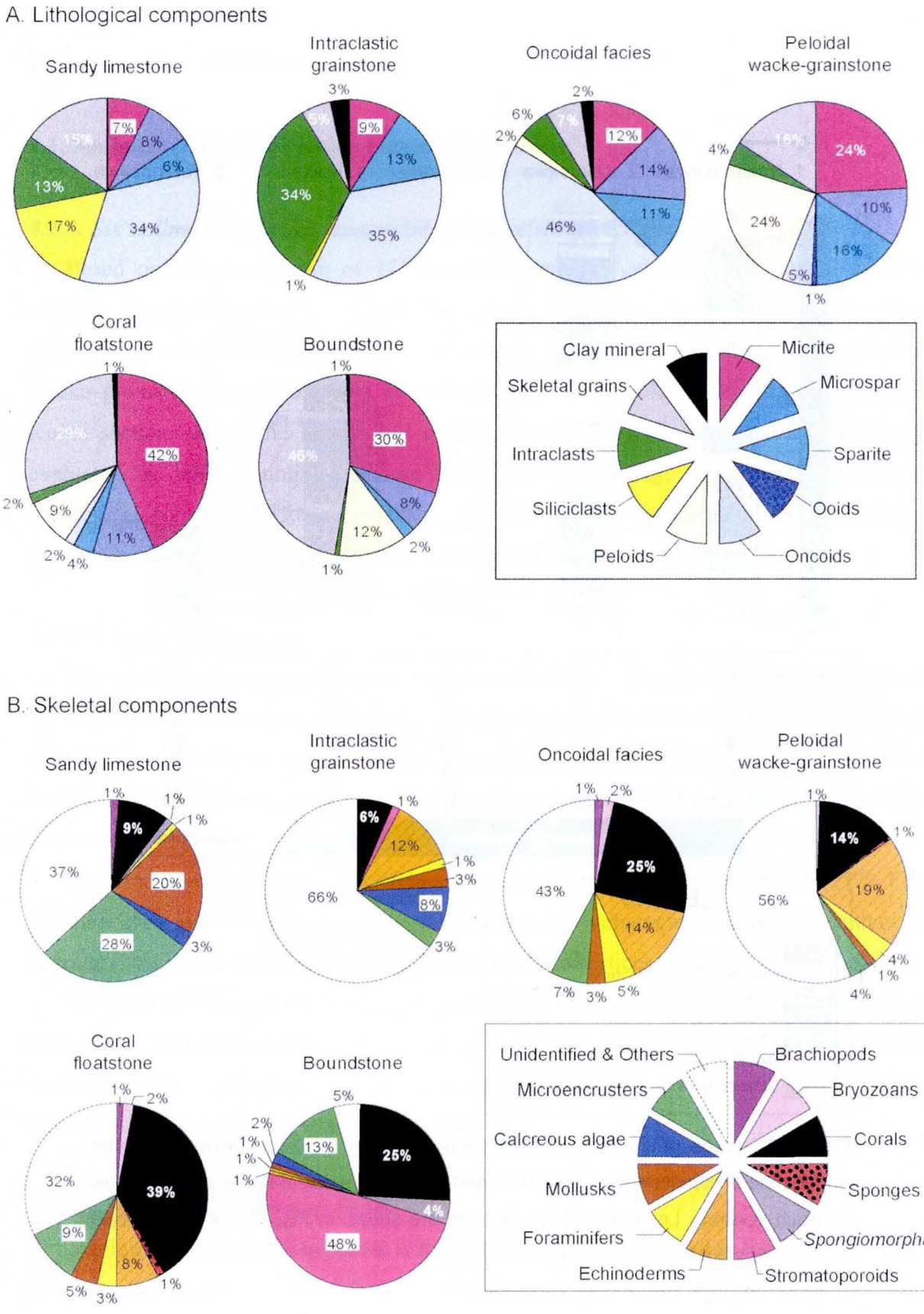

Figure 7. Average composition of the six sedimentary facies of the Koike Limestone Member based on the results of point-counting. **(A)** Lithological components. **(B)** Skeletal components (the values are percentages of skeletal grains).

oncoids (35%; Figs. 7A and 8C). The intraclasts are mainly rounded grains containing agglutinated oncoids and bioclasts (Fig. 8D). Oncoids commonly consist of a thin micritic cortex around an intraclast nucleus, and they are smaller and less mature than those seen in the oncoidal facies. The intergranular spaces are mainly filled with sparite. The most common fossil component is echinoderm (14%; Fig. 7B).

4.1.1.3. Oncoidal facies

The oncoidal facies is one of the most common facies in the Koike Limestone Member (Fig. 6). Oncoids are coarse grained (up to 2 mm in diameter, average ~1 mm; Fig. 8E) and easily identified in the field, and they are the dominant lithological component in this facies (46%; Fig. 7A).

There is a clear spatical variation in texture of the oncoidal facies. Packstone-wackestone texture is well developed in the northern sections (Nakanosawa and Kakusawa sections), whereas grainstone texture is dominant in the southernmost Tatenosawa sections but absent in the northern sections. These textures coexist in oncoidal facies of the Koike section. Grainstone occupies 50%, packstone occupies 44%, and wackestone occupies 6% of the whole oncoidal facies (16 samples) of the Koike section (Fig. 6). No lateral change in the diameter of oncoids was observed between the studied sections.

The micritic cortices of the oncoids show obscure concentric laminations (Fig. 8F) and commonly contain encrusting microbionts such as foraminifers and *Girvanella tosaensis*. The nuclei are mostly sand-sized quartz and feldspar particles in the lower horizons, and skeletal grains in the upper horizons. Oncoids in the lower horizons are generally smaller than those in the upper horizons.

The matrix of the oncoidal packstone commonly consists of fine-grained equant microspar (Fig. 8F). This texture has been described as grainstone in previous studies of the Koike Limestone Member (Eguchi and Shoji, 1965; Morino, 1992; Uematsu; 1997; Kiyama and Iryu 1998) and the microspar was interpreted as pore-filling cement. However, microspar commonly forms by recrystallization from micrite in a mixing zone (Lasemi and Sandberg, 1984; Melim et al., 2004). Thus, I suggest that most of the intergranular spaces of the oncoidal facies were initially filled with micrite.

4.1.1.4. Peloidal wacke–grainstone facies

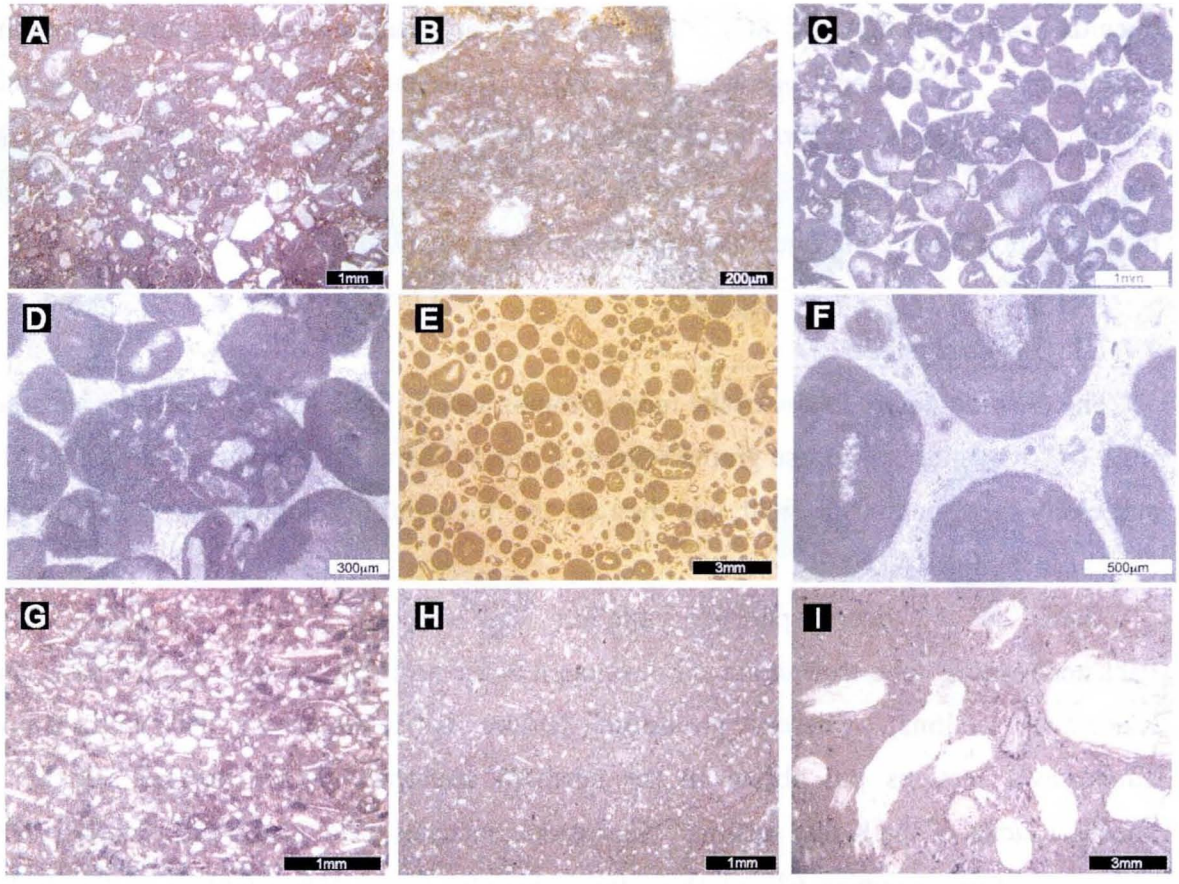

Figure 8. Sedimentary facies recognized in the Koike Limestone Member. **(A)** Sandy limestone in the lowermost horizon of the Koike section (Koi-01). **(B)** Filamentous calcified microbes (*Girvanella tosaensis*) trapping quartz grains (Koi-01). **(C)** Intraclastic grainstone (Koi-06). The intergranular space is filled with sparite and microspar. **(D)** A rounded intraclast in grainstone (Koi-06). **(E)** Oncoidal wackestone in the upper horizon of the Koike Limestone Member (Koi-33) showing microspar matrix. **(F)** Oncoids in packstone showing irregular lamination in the cortex (Koi-08). Intergranular space is filled with equant fine-grained calcite crystals (microspar). **(G)** Packstone containing fine-grained peloids and bioclasts (Koi-21). **(H)** Peloidal wackestone containing small unidentified skeletal grains (Kk-11). **(I)** Coral floatstone consisting of fragments of branching corals and wackestone matrix (Koi-14).

The peloidal wacke–grainstone facies is commonly exposed in the study sections, with the exception of the Tatenosawa section (Fig. 6). This facies is closely associated with coral floatstone and oncoidal facies. It is characterized by high contents of peloids (24%) and bioclasts (16%, Fig. 7A) and includes a wide range of textures, from grainstone with sparitic cement (Fig. 8G) to wackestone sparsely containing smaller (<0.1 mm) grains (Fig. 8H). Common skeletal components are echinoderms (19%) and corals (14%; Fig. 7B). Many of the small bioclasts are unidentifiable.

4.1.1.5. Coral floatstone facies

The coral floatstone is a major facies in the Koike Limestone Member. It is thickly developed in the Koike section and in five intervals of the Nakanosawa section. In the Tatenosawa section, this facies is thinly developed in six intervals closely associated with boundstone facies. This facies is less common in the Kakusawa section. In general, this facies is covered by the oncoidal facies but the boundary is commonly obscure due to gradual decrease in coral content and grain size. On the other hand, the base of this facies is clearly recognized by an abrupt facies change.

The coral floatstone facies is characterized by branching coral (Fig. 8/I) such as *Aplosmilia* sp. and *Thamnasteria* sp., occurring in a wackestone matrix. Fragments of coral branches without preferential orientation and toppled domical colonies indicate that these are allochthonous. The dominant lithological components are micrite (42%) and large (mainly > 20 mm) skeletal grains (29%; Fig. 7A). Corals are the most common (39%; Fig. 7B) among the skeletal grains. Microencrusters (9%) and echinoderms (8%) are also common in this facies.

4.1.1.6. Boundstone

Boundstone is a common facies in the southernmost Tatenosawa section, in which this facies is repeatedly developed in six 1-3m thick horizons accompanied by the coral floatstone. This facies is also developed in the uppermost horizons of the Koike and Nakanosawa sections (Fig. 6). Boundstone is similar in appearance with coral floatstone in the field, but is distinguishable by the occurrence of autochthonous reef builders.

In the boundstone at the top of the Koike section, the important skeletal components are stromatoporoids (48%, mainly *Parastromatopora* sp.), corals (25%), microencrusters (13%), and Spongiomorpha (4%; Fig. 7B). Sessiles constitute 92% of the skeletal grains in this facies. The boundstones of the Tatenosawa and Koike sections show mostly a framestone or bafflestone fabric formed mainly by branching forms of corals and stromatoporoids (Figs. 9A, B). Domal corals are rarely found in the bafflestone. The average height of the coral colonies observed in the outcrops ranges from 30 to 50 cm. There is fine-grained carbonate with large bioclasts in the spaces between the coral branches. Corals and stromatoporoids frequently associate together, and most of stromatoporoids cooperatively construct robst framework with corals. For example, stromatoporoids (*Parastromatopora*?) associate within coral framework developed in the

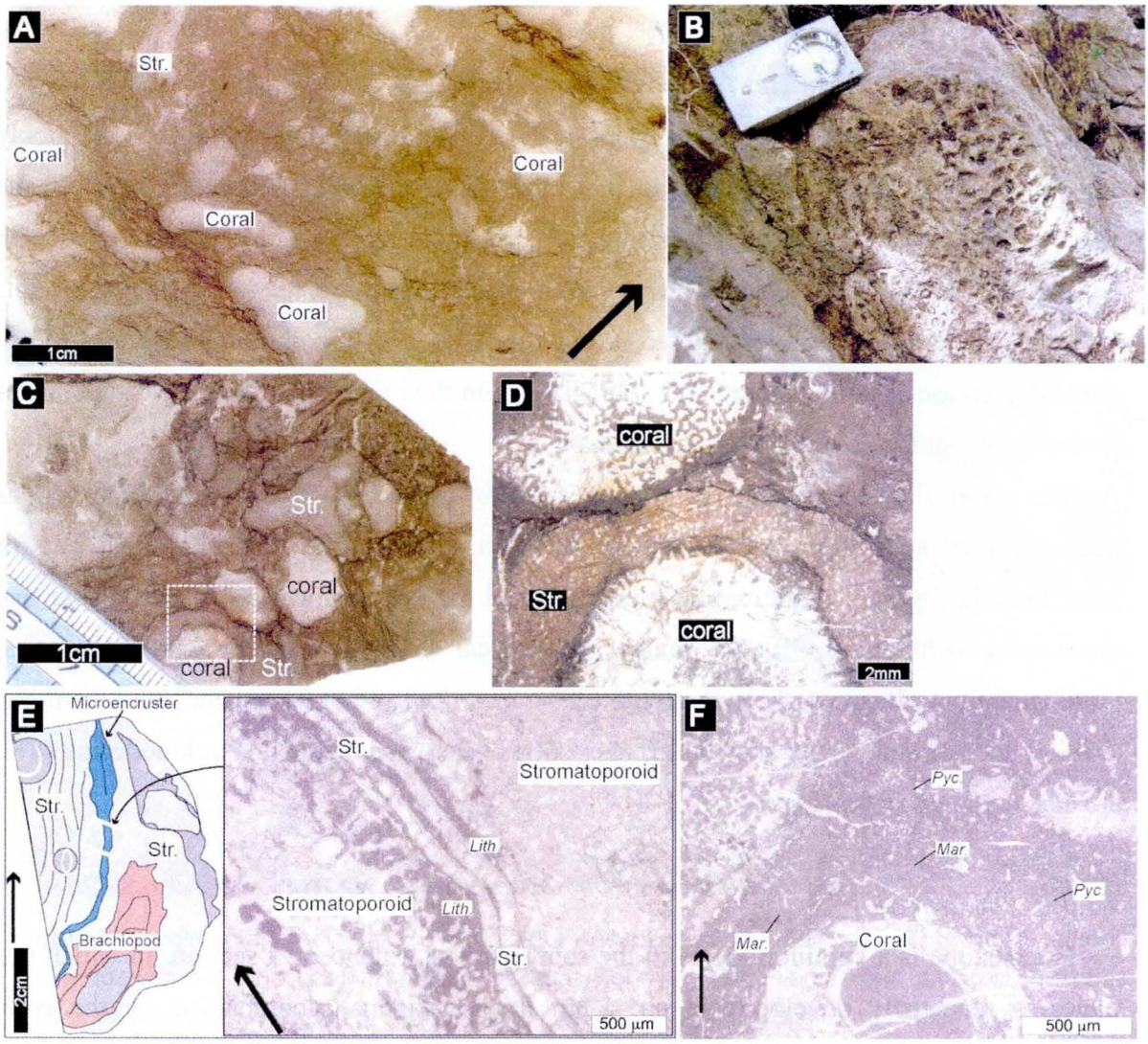

Figure 9. Boundstone facies of the Koike Limestone Member. The arrows show the stratigraphic upward. **(A)** Bafflestone consisting of corals and stromatoporoids (Str.) of branching and massive forms in the uppermost horizon of the Koike section (Koi-48). **(B)** A branching coral in bafflestone at the top of the Tatenosawa section. **(C)** The typical bafflestone in the uppermost horizon (Koi-52). **(D)** The magnified view of squared area in Figure 9C. A stromatoporoid encrusts coral cylinder. **(E)** Bindstone of the Koike section (Koi-48). **Left:** a sketch showing a binding texture by stromatoporoids and microencrusters. Stromatoporoids are bored by bivalves, and encrust a brachiopod. **Right:** a magnified view of a microencruster *Lithocodium* sp. intercalated with stromatoporoids. **(F)** Bindstone in the uppermost horizon of the Nakanosawa section (Nk-16). The predominant microencrusters are bush-shaped *Pycnoporidium lobatum* (*Pyc.*) and *Marinella lugeoni* (*Mar.*) having a micritic texture.

uppermost part of the Koike section (Fig. 9C), and stromatoporoid encrusts coral cylinder (Fig. 9D).

Bindstone fabric consisting of stromatoporoids and microencrusters is thinly (~ 0.5 m thick) developed of the Koike section. There, stromatoporoids and microencrusters (*Lithocodium* sp. and *Marinella lugeoni*) encrust each other and form a rigid domal

framework (Fig. 9E). These framework structures are commonly bio-eroded by bivalves and may also incorporate brachiopods (Fig. 9E). The boundstone at the top of the Nakanosawa section exhibits a bindstone fabric, but differs from the bindstone of the Koike section by its abundance of microencrusters. Two dominant spiecies, *Pycnoporidium lobatum* and *Marinella lugeoni* (Imaizumi, 1965), encrust fragments of corals and sponges (Fig. 9F). Autochthonous corals and stromatoporoids were not found in this bindstone. The thickness of the bindstone is 1.5m or potentially thicker because the upper extent of this facies was unexposed.

4.1.2. Lateral facies change of the Koike Limestone Member

The thicknesses and facies associations of the Koike Limestone Member vary considerably among the sections. The thickness tends to increase from the southernmost Tatenosawa section to the Koike section and decreases toward the Bunazaka section located in the middle of the surveyed area (Fig. 2B). From there, the thickness abruptly increases to the north in the Kakusawa and Nakanosawa sections (Fig. 6).

In the Tatenosawa section, the exposed Koike Limestone Member is about 15 m thick (Fig. 6). Bafflestone including reef builders such as corals, stromatoporoids, and microencrusters is thickly developed. Oncoidal facies always exhibit grainstone fabrics. Limestones in the Tatenosawa section are richer in non-carbonate grains (e.g., quartz and feldspar) than in the other four sections.

In the Koike section, the exposed Koike Limestone Member is 52 m thick. Three facies, coral floatstone, oncoidal faceis, and peloidal wacke–grainstone, are dominant and repeatedly developed. Oncoidal facies shows grainstone-wackestone fabric (Fig. 6). High siliciclastic content is only seen in the lower part of the section.

An 8-m-thick sequence exposed in the Bunazaka section shows a gradual facies transition from sandy limestone facies to a pure carbonate facies of coral floatstone. Repetition of facies cannot be observed due to lacking outcrop (Fig. 6). The limestone at this section is likely thicker than 8 m but still thinner than in the adjacent Koike and Kakusawa sections (Fig. 6). The limestone rarely yields large fossils but commonly contains microencrusters. Oncoidal facies is most common in this section.

The thickest (72 m) limestone sequence occurs in the Kakusawa section that shows repeated facies associations consisting of oncoidal facies, coral floatstone, and peloidal wackestone. Oncoidal facies with packstone-wackestone texture is developed thickly (up

to 8 m) in six layers. Coral floatstone is developed in only three thin layers (max. 3 m thick; Fig. 6). Peloidal facies in this section normally exhibit wackestone fabric. Contents of large fossils are lower than in the two southern sections (Fig. 6).

The Nakanosawa section exposes a 70 m thick limestone sequence that mainly consists of shallow water facies including oncoids, intraclasts, and bioclasts. The base of the limestone sequence is made up of a sandy limestone that conformably rests on the lower-lying mudstone and sandstone. The 1-m-thick bindstone is developed in the uppermost horizon (Fig. 6).

4.1.3. The facies cycles in the Koike section

The vertical repetition of facies associations was recognized in all studied sections except for the Bunazaka section, and it appears most clearly in the continuous outcrop of the Koike section. Each set of the facies association consists of coral floatstone, oncoidal facies, and peloidal wackestone-grainstone, in ascending order. Five such upward-fining cycles are recognized in the Koike section (Fig. 10A). The base of each cycle corresponds to the base of coral floatstone where an abrupt facies change normally occurs. The massive coral floatstone generally stands out clearly from the underlying thinly-bedded peloidal wackestone-grainstone (Fig. 10A). The boundary surface is sharp but lacks any evidence of erosion or subaerial exposure.

The five facies cycles are illustrated in Figure 10A. The cycles are from 3 to 11m thick. The first cycle (from 5 to 9 m in the section) consists of coral floatstone, intraclastic grainstone, and peloidal wacke–grainstone. The intraclastic grainstone contains oncoids. The second cycle lies between 10 and 21 m, the third between 21 and 26 m horizon, the fourth between 26 and 38 m, and the fifth between 38 and 47 m. Only the third cycle lacks peloidal wacke–grainstone; the other four cycles display the complete succession of coral floatstone, oncoidal facies, and peloidal wacke–grainstone.

The cyclic facies changes in the Koike section have been analyzed in previous sedimentological studies. Eguchi and Shoji (1965) and Kiyama and Iryu (1998) defined coral floatstone as the uppermost facies of each of their depositional units. However, I observed that the coral floatstone, followed by the oncoidal facies and peloidal wacke–grainstone, constitutes an upward-fining cycle. Accordingly, I defined the coral floatstone facies as the lowermost part of the facies cycle.

A schematic model of the repeated facies cycle is shown in Fig. 10B. The cycle is

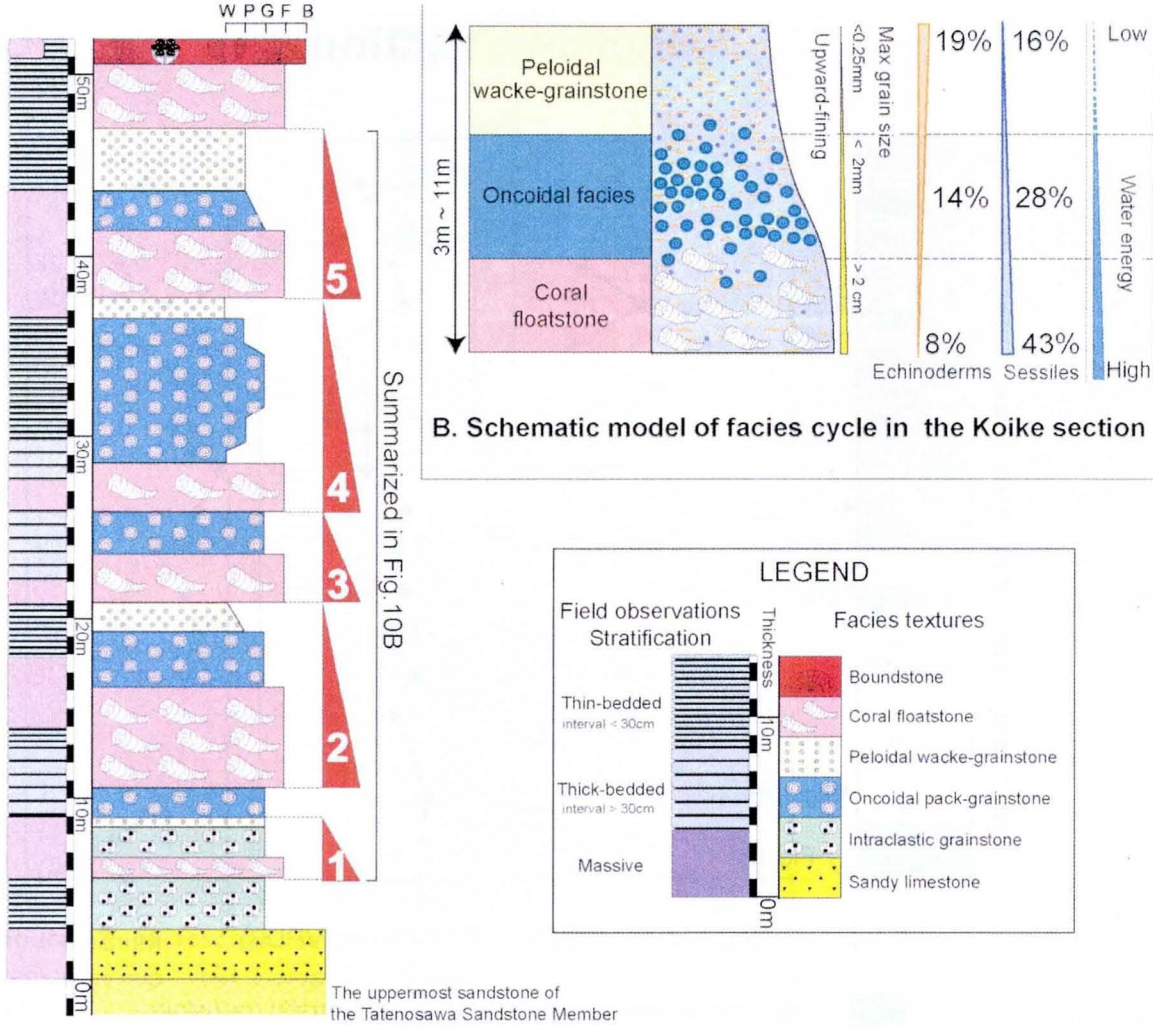

Figure 10. **(A)** Detailed log of the Koike Limestone Member in the Koike section. Widths of the columns reflect the limestone texture based on the Dunham (1962) classification. **(B)** A typical upward-fining cycle identified in the Koike section.

characterized by a gradual decrease in grain size. Skeletal components also change: the proportion of echinoderms increases upward from 8 to 19 %, whereas the proportion of sessiles (e.g., corals and stromatoporoids) decreases from 43 to 16 %. The base of each cycle is marked by an abrupt lithological change, with a grain size increase compared with the underlying peloidal wacke–packstone.

I identified the repeated facies association in four of the five study sections. In the Tatenosawa section, boundstone is developed in six intervals appearing coral floatstone. These six coral-bearing boundstone can be correlated with the six intervals of the relevant facies in the Koike section, and possibly in the Nakanosawa section (Fig. 6). Coral

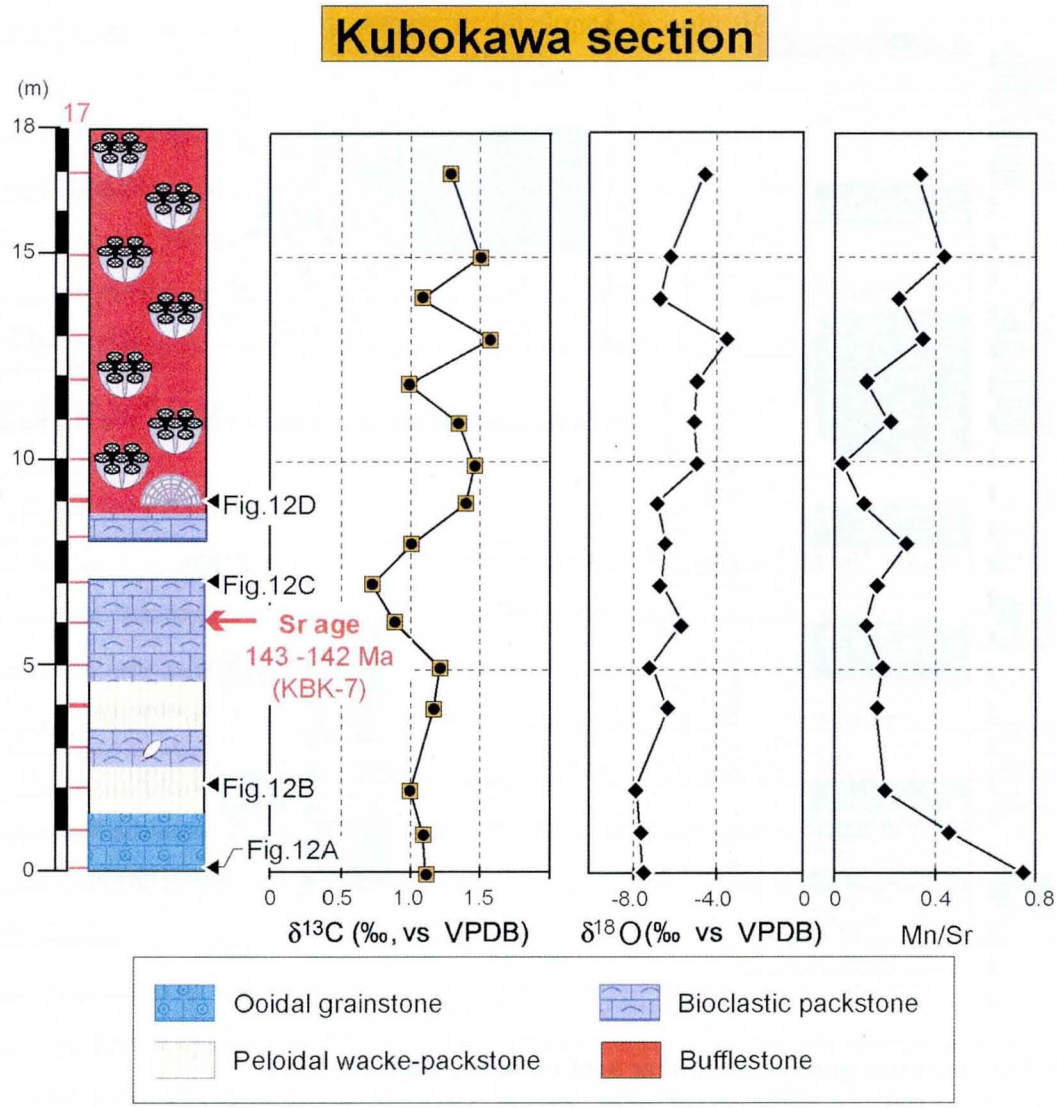

Figure 11. The geochemical profiles of $\delta^{13}C$ and $\delta^{18}O$, and the Mn/Sr ratios, and stratigraphic column of the Kubokawa section.

floatstone is developed only in three intervals of the Kakusawa section, in which the facies cycles are mainly composed of oncoidal facies and peloidal wacke-grainstone in the middle-upper part.

4.2. Sedimentology of the Nankai Group in the Kubokawa and the Shiraishi sections

The 18-m-thick limestone sequence exposed in the Kubokawa section is broadly divided into the lower clastic limestone and the upper bafflestone (Fig. 11). The clastic limestone exhibits grainstone, wackestone-packestone, and packstone facies, and these facies consist of thick bedding in outcrop. On the other hand, bafflestone shows massive

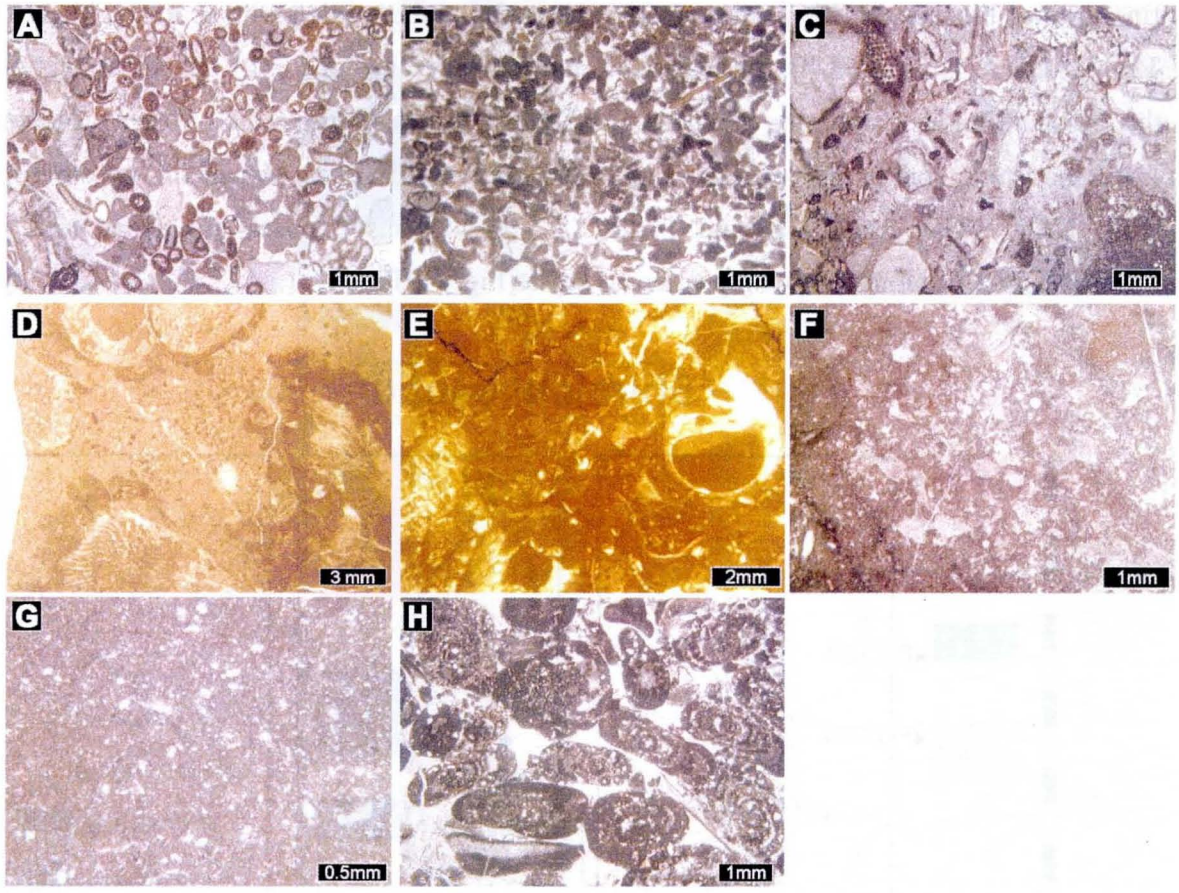

Figure 12. Microscopic views of sedimentary facies in the Kubokawa and Shiraishi sections, the Nankai Group. **(A)** Ooidal grainstone (KBK-01, 1m horizon). **(B)** Peloidal wacke-packstone (KBK-03, 2m horizon). **(C)** Bioclastic packstone (KBK-07, 6m horizon). **(D)** Bafflestone (KBK-10, 9m horizon). **(E)** Bioclastic wackestone (SH-04, 2.5m horizon). **(F)** Bindstone (SH-05, 3m horizon). **(G)** Limemudstone (SH-10, 12m horizon). **(H)** Foraminiferal grainstone (SH-11). The foraminifers mainly belong to Lituolidae.

lithofacies without bedding in the outcrop. The grainstone of the lowermost 1.5 m contains fine ooids and well-rounded bioclastics (Fig. 12A). The wackestone occurs in two intervals and is characterized by an abundance of peloids (Fig. 12B). The bioclastic packstone contains coarse-grained skeletal fragments (Fig. 12C), and is thickly developed at the interval between 4.5 and 8.7 m horizons (Fig. 11). The bafflestone of the upper section is 9.5 m thick, and appears to have a robust framework formed by corals, stromatoporoids, and microencrusters (Fig. 12D).

The limestone sequence in the Shiraishi section is 19 m thick and appears to contain four lithofacies (Fig. 13). The sequence starts from the 2.5-m-thick wackestone (Fig. 13) containing coarse fragments of corals and brachipods (Fig. 12E). The overlaying 2 m thick bindstone contains microbial crusts (*Lithocodium aggregatum*), which trap

fine-grained bioclasts and appear irregularly shaped chambers filled with sparite (Fig. 12F). The bindstone is covered by the 2-m-thick bioclastic wackestone. In the upper section, the discontinuous outcrops expose different facies from the lower section. Lime-mudstone containing very fine bioclastics and peloids is developed in two outcrops (Fig. 12G). The outcrop around 14 to 15 m horizons exposes grainstone rich in foraminifers (Lituolinids) having poriferous septa (Fig. 12H).

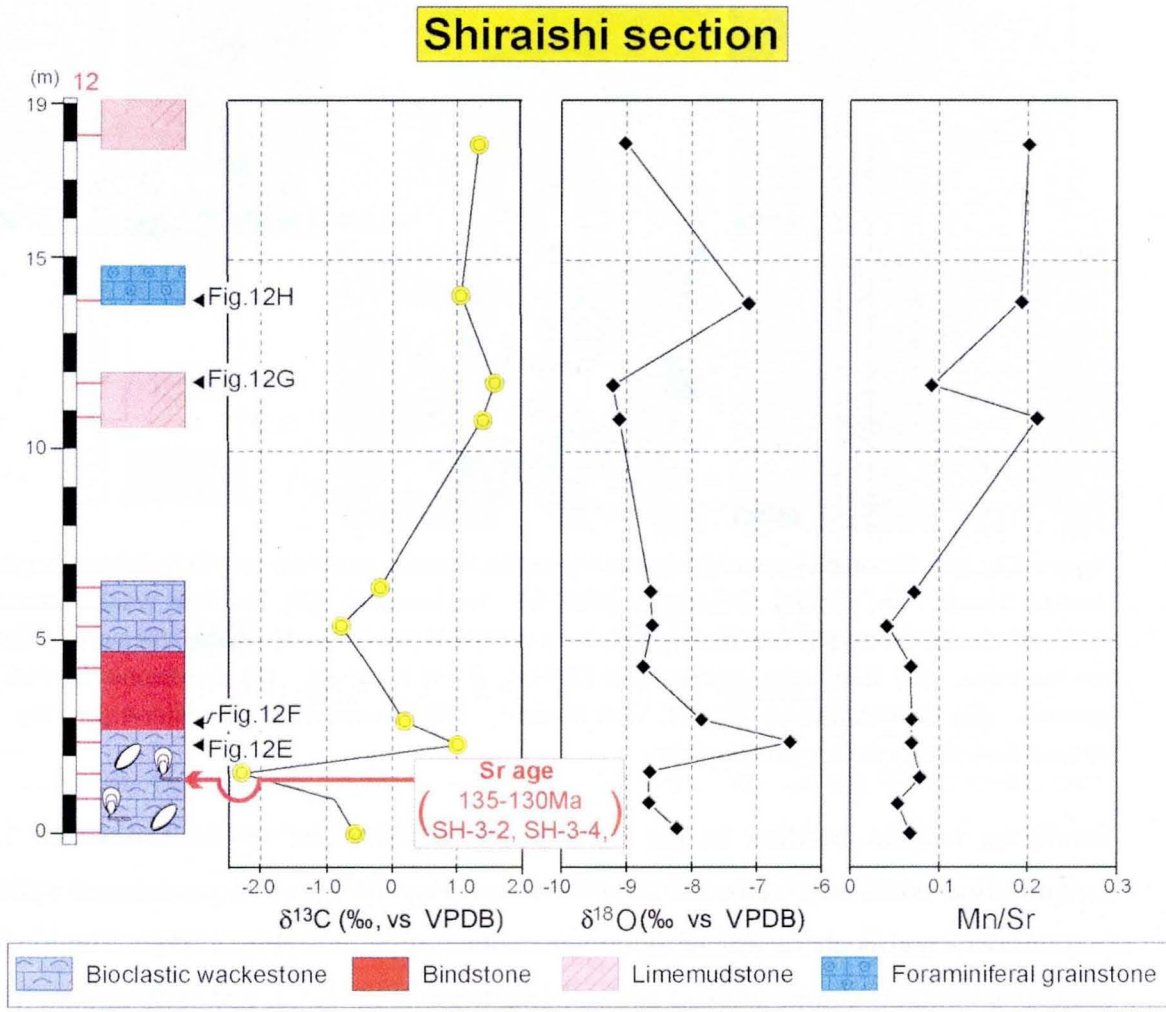

Figure 13. The geochemical profiles of $\delta^{13}C$ and $\delta^{18}O$, and the Mn/Sr ratios, and stratigraphic column of the Shiraishi section.

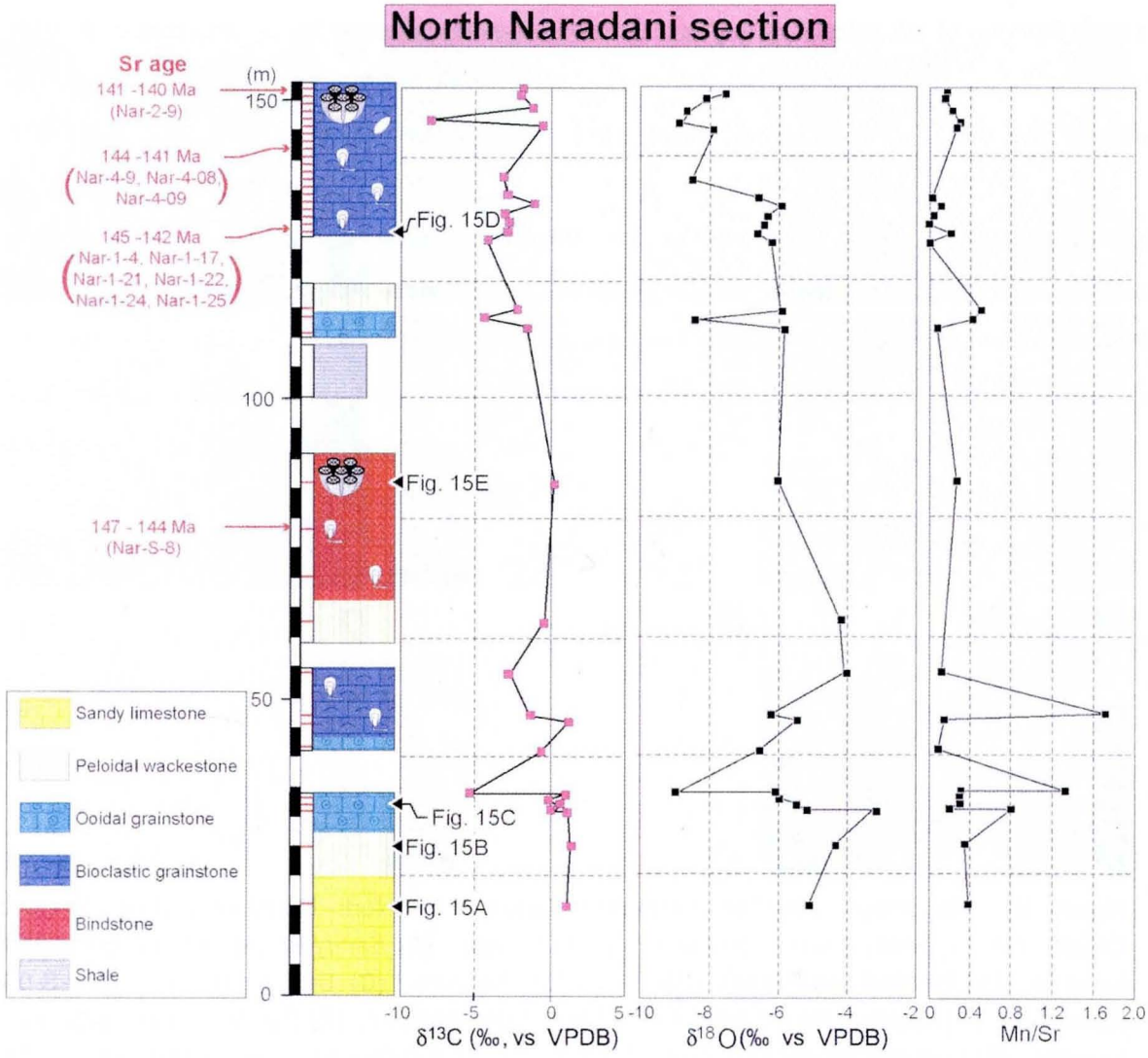

Figure 14. The geochemical profiles of $\delta^{13}C$ and $\delta^{18}O$, and the Mn/Sr ratios, and Stratigraphic column of the North Naradani section.

4. 3. Sedimentology of the Torrinosu Group in the North Naradani section

The exposure at 153-m-thick North Naradani section consists of two limestone sequences separated by an 8-m-thick calcareous shale (Fig. 14). The lower limestone (0 to 92 m interval) shows five lithofacies. The sandy limestone exposed in the lowermost 20 m contains sand-sized siliciclastics, coatoids, and micrite (Fig. 15A). This sandy facies is overlain by the peloidal wackestone (Fig. 15B), ooilitic grainstone (Fig. 15C), and bioclastic grainstone that yield brachiopods and bivalves (Fig. 15D). The 25-m-thick bindstone (Fig. 15E) occurring at the top of the lower limestone sequence contains corals, microencrusters (*Tubiphytes* sp.), and brachiopods. There is a 9-m-thick unexposed

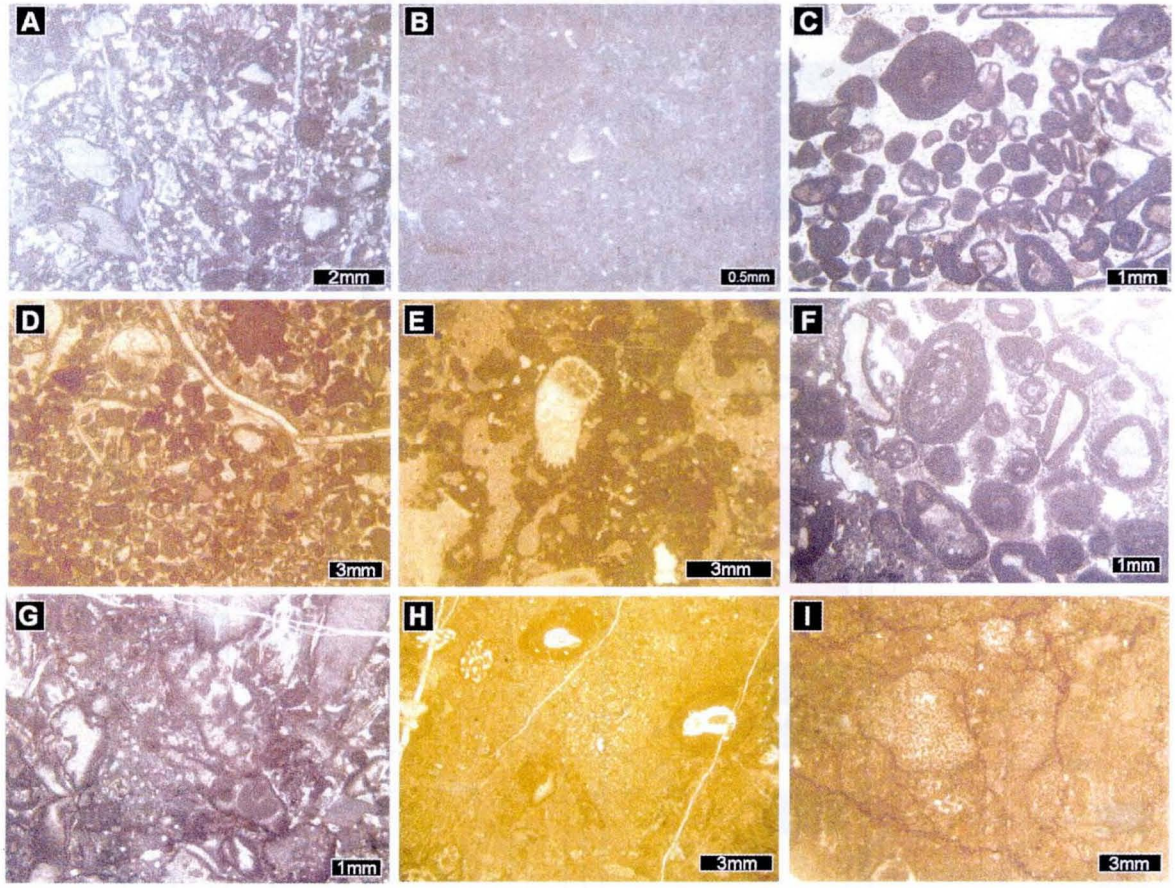

Figure 15. Microscopic views of sedimentary facies in the North Naradani section (Torinosu Group) and the South Furuichi section (Imaidani Group). **(A)** Sandy limestone (Nar-S-01, 15m horizon). **(B)** Peloidal wackestone (Nar-S-02, 25m horizon). **(C)** Ooidal grainstone (Nar-S-03, 32m horizon). **(D)** Bioclastic grainstone (Nar-N-01, 128m horizon). **(E)** Bindstone (Nar-S-15, 86m horizon). **(F)** Oncoidal grainstone (SFur-27, 28m horizon). **(G)** Bioclastic packstone (SFur-09, 9m horizon). **(H)** Bioclastic floatstone (SFur-11, 11m horizon). **(I)** Bafflestone (SFur -06, 6m horizon).

interval between the bindstone and the overlying 8-m-thick calcareous shale. At the 110 m horizon, the oolitic grainstone occurs at the base of the upper limestone sequence, and is overlain by the peloidal wackestone. Beyond the 8 m thick unexposed interval, the bioclastic limestone of 25 m thickness occurs at the top of the North Naradani section. This facies contains an abundance of fossils including brachiopods (Figs. 5A, B), and some of them were used for measurement of Sr isotopic ratios.

4.4. Sedimentology of the Imaidani Group in the South Furuichi section

The limestone exposed in the South Furuichi section exhibits a 50 m thick continuous limestone sequence consisting of four lithofacies (Fig. 16).

The oncoidal grainstone is the most common facies that occurs in the lowermost 4.5 m, and in the middle-upper section (Fig. 15F). It yields brachiopod shells at 27 to 31 m interval. The bioclastic packstone (Fig. 15G) and floatstone (Fig. 15H) are mainly developed in the lower section.

The bafflestone, that shows a reefal framework constructed by calcareous sponges and microencrusters, is developed in several horizons of the lower section (at 13 to 21 m interval: Fig. 15/I). In this section, calcareous sponges are predominant as a potential reef-builder. Coral-stromatoporoid-microencrusters assemblage is absent unlike other sections of Torinosu-type limestone.

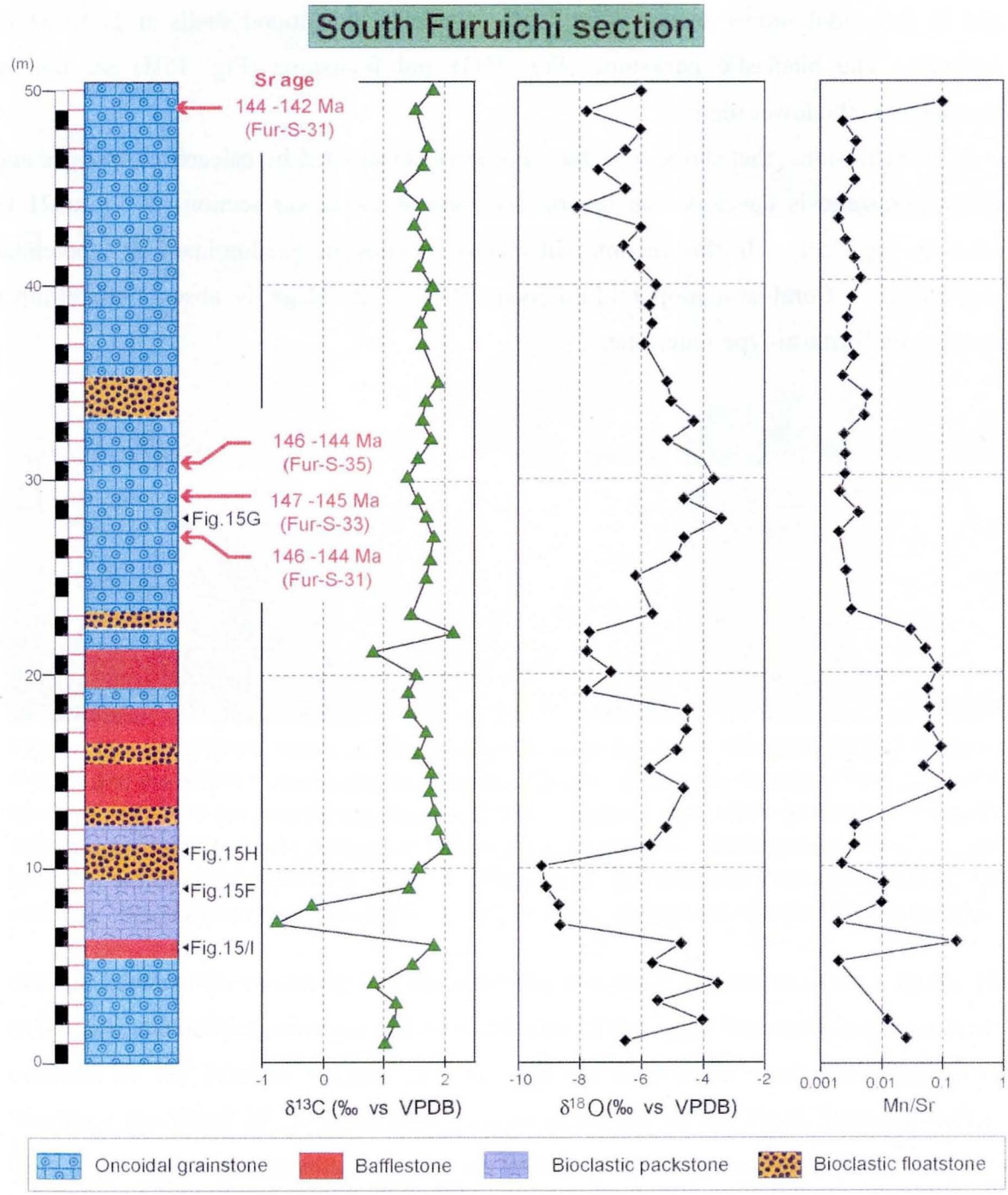

Figure 16. The geochemical profiles of $\delta^{13}C$ and $\delta^{18}O$, and the Mn/Sr ratios, and Stratigraphic column of the South Furuichi section. Only Mn/Sr ratios are shown in logarithmic scale.

4.5. Chemostratigraphy

Sr isotopic ages, stable carbon-oxygen isotpic composition, and minor element concentrations of the carbonate fraction are presented for each of the five sections. The results of measurement of Sr isotopic ratios, and ages estimated on Look-up Table are shown in Table 1.

4.5.1. The Koike sections (the Kike Limestone Member)

Results of the geochemical analyses of samples from the Koike section are shown in Table 2 and Fig. 17. The $\delta^{13}C$ values range from –2.5 to +1.9‰, with several negative excursions. The lowest values were recorded in three samples of intraclastic grainstone in the lower part of the section (3–5 m interval). The values gradually increase upwards with obvious negative values recorded in oncoidal-peloidal facies of the 8.5-10.0 m interval and oncoidal facies of 33.0-36.5 m interval (Fig. 17). Values as high as 1.8-1.9‰ were recorded from levels above 40.0 m (Table 2).

The $\delta^{18}O$ values range from –14 to –4‰, and also showed an upward increasing trend. The values from the lowermost 8 m are mostly lower than –8.0‰, and one sample of intraclastic grainstone (at 4.5 m) displays a significantly negative value (–13.9‰, Table 1). From 8 to 48 m, the $\delta^{18}O$ values generally keep in a narrow range from –8.0 to –6.0‰ (Fig. 8). The uppermost four samples record high $\delta^{18}O$ values around -4.0‰ (Table 1).

Mn concentrations are high at the bottom of the section (max. 660 ppm) and decrease rapidly to 90 ppm at 6.5 m. They again increase up to 380 ppm, and from 10 m upward stay at around 200 ppm (Table 2). Sr concentrations are nearly constant at 350–400 ppm and record the highest value (660 ppm) at 16 m (Table 2). The Mn/Sr ratio, which is often used as an index of diagenetic alteration, is mostly below 0.8 (Fig. 17) but reaches 1.66 in the lowermost horizon (Table 2). These ratios are lower than the value indicative of significant diagenesis that alter the $\delta^{13}C$ value (> 2.0; Jacobsen and Kaufman, 1999).

Because of lack of appropriate specimens for Sr isotopic ratio analysis, any ages were evaluated in this section. However, age of the Koike Limestone will be discussed later based on the Sr isotopic ratio from the Nakanosawa section and available occurrence of age-diagnostic fossils.

Table 2. Results of geochemical analyses of the Koike section. Following abbreviations are used for facies; Sand. (Sandy limestone), Intra. (Intraclastic grainstone), Onc. (Oncoidal facies), Pel. (Peloidal wacke-packstone), Coral. (Coral floatstone), and Bound. (Boundstone).

No.	Horizon (m)	Facies	$\delta^{13}C$ (‰)	$\delta^{18}O$ (‰)	Mn (ppm)	Sr (ppm)	Mn/Sr	Carbonate (wt %)
1	2.0	Sand.	0.72	-9.81	660	400	*1.66*	70.8
2	3.0	Intra.	-2.01	-9.21	560	370	*1.51*	75.9
3	4.0	Intra.	-2.53	-10.77	360	390	*0.94*	93.5
4	4.5	Intra.	-2.46	-13.91	280	260	*1.07*	92.6
5	6.5	Coral.	0.72	-7.80	90	400	*0.23*	98.5
6	7.5	Intra.	0.91	-8.41	120	530	*0.23*	98.1
7	8.0	Onco.	0.85	-8.30	100	390	*0.25*	98.7
8	8.5	Onco.	-0.23	-6.15	360	490	*0.74*	87.2
9	9.0	Pel.	-0.84	-7.81	230	390	*0.59*	96.3
10	9.5	Onco.	0.73	-7.64	270	410	*0.67*	94.5
11	10.0	Onco.	-0.35	-7.57	330	400	*0.83*	91.9
12	10.5	Coral.	1.56	-6.43	220	500	*0.44*	94.8
13	11.0	Coral.	0.73	-6.58	260	390	*0.65*	85.9
14	13.5	Coral.	0.90	-6.08	280	430	*0.65*	89.6
15	16.0	Onco.	0.94	-8.26	320	660	*0.49*	84.2
16	17.0	Onco.	0.34	-7.63	380	300	*1.25*	92.7
17	18.5	Onco.	1.46	-6.97	210	520	*0.40*	94.7
18	19.0	Onco.	0.99	-7.94	240	370	*0.63*	95.1
19	20.0	Pel.	0.64	-7.62	200	420	*0.47*	95.1
20	22.5	Coral.	1.36	-7.01	200	430	*0.47*	94.8
21	23.0	Coral.	0.93	-9.81	250	390	*0.64*	91.2
22	24.0	Onco.	-	-	250	500	*0.50*	91.8
23	25.0	Coral.	1.06	-8.14	250	360	*0.70*	94.4
24	27.5	Coral.	1.16	-7.32	190	370	*0.50*	94.6
25	28.0	Coral.	1.79	-6.87	220	430	*0.51*	93.7
26	29.0	Onco.	0.38	-7.59	260	390	*0.67*	90.9
27	29.5	Onco.	0.65	-7.12	230	320	*0.73*	93.0
28	30.5	Onco.	1.14	-7.16	260	400	*0.65*	90.2
29	31.0	Onco.	1.23	-4.74	190	280	*0.66*	92.5
30	32.0	Onco.	1.21	-6.36	190	460	*0.42*	94.8
31	33.0	Onco.	-0.51	-6.51	180	280	*0.65*	93.5
32	34.0	Onco.	-0.28	-7.24	190	330	*0.58*	95.2
33	35.0	Onco.	1.49	-5.10	220	430	*0.51*	95.0
34	36.5	Onco.	-1.14	-7.11	230	370	*0.61*	95.6
35	38.0	Pel.	1.10	-7.54	210	430	*0.48*	95.0
36	39.0	Coral.	1.74	-7.45	180	450	*0.40*	96.6
37	39.5	Coral.	1.40	-7.07	160	350	*0.47*	94.3
38	40.0	Coral.	1.92	-6.64	160	430	*0.37*	92.7
39	41.5	Coral.	1.92	-6.10	170	440	*0.39*	93.0
40	43.0	Onco.	1.42	-7.12	120	440	*0.27*	97.7
41	44.5	Onco.	1.72	-6.78	190	460	*0.40*	96.2
42	45.5	Coral.	1.43	-6.77	300	490	*0.61*	96.1
43	47.0	Coral.	1.23	-6.81	240	390	*0.61*	94.6
44	48.0	Coral.	1.87	-6.83	210	460	*0.45*	95.0
45	49.5	Coral.	1.84	-3.65	220	440	*0.49*	93.5
46	50.5	Coral.	1.69	-4.02	180	440	*0.40*	93.5
47	51.5	Bound.	1.83	-3.92	150	320	*0.45*	98.1
48	52.0	Bound.	1.90	-4.48	190	380	*0.51*	98.0

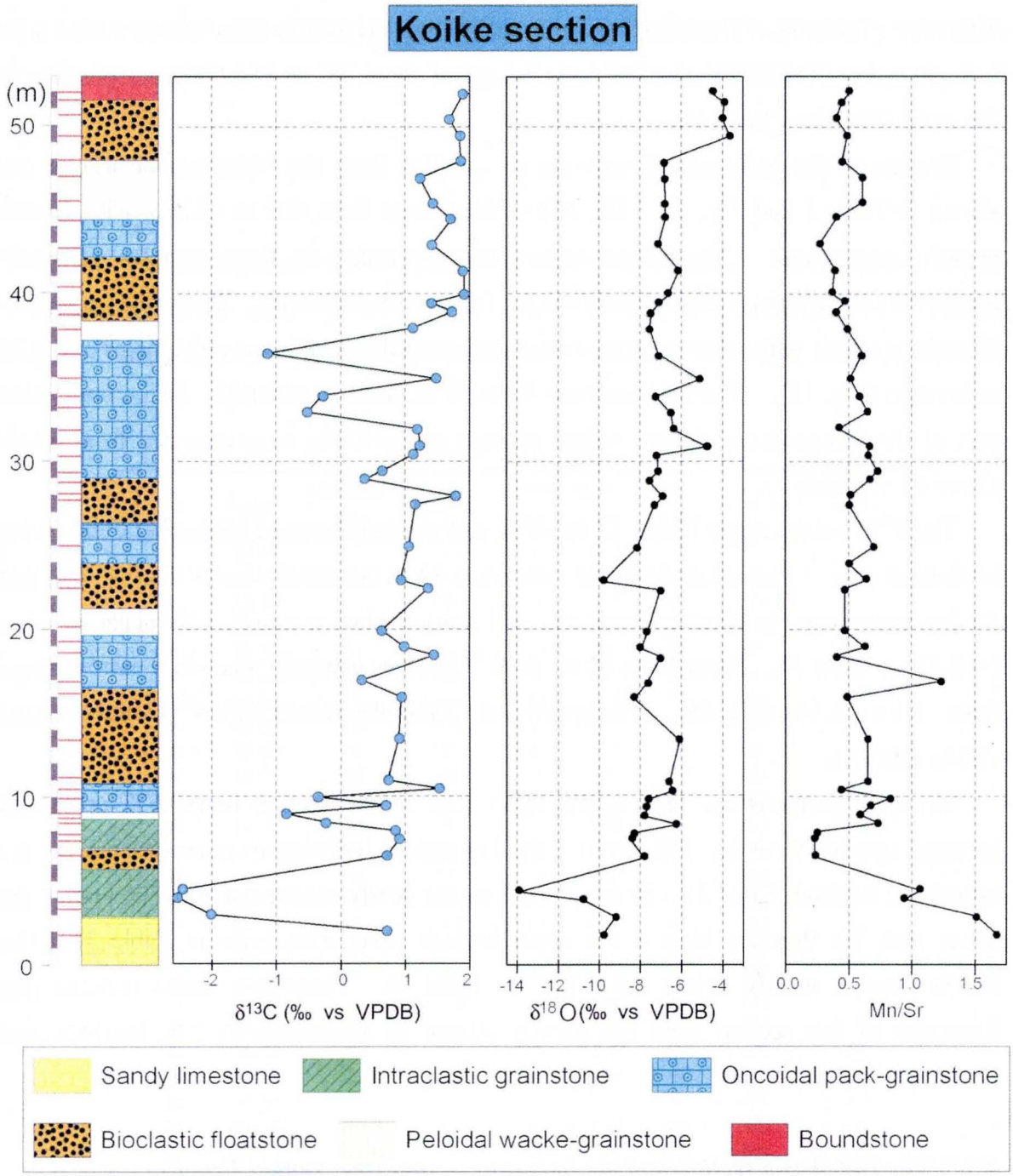

Figure 17. The geochemical profiles of $\delta^{13}C$ and $\delta^{18}O$, and the Mn/Sr ratios, and stratigraphic column of the Koike section.

4.5.2. The Nakanosawa sections (the Kike Limestone Member)

Two brachiopod shells were collected from the bioclastic limestone of the upper section (Fig. 18). The specimen exhibiting dull CL (Nk-A-1) recorded a Sr isotopic ratio of 0.707035 that indicates the age of about 150 to 149 Ma corresponding to the early

Tithonian (Table 1). The other specimen exhibiting bright CL (Nk-A-2) recorded a Sr isotopic ratio of 0.7070506 that indicates the age of about 151 to 150 Ma corresponding to the early Tithonian (Table 1).

Results of the geochemical analyses of samples from the Nakanosawa section are shown in Table 3 and Fig. 18. The $\delta^{13}C$ values range from -1.9 to +2.2‰, with several negative excursions. The lowest values were recorded in three samples of sandy limestone and peloidal wacke-grainestone (at 1m and 4m horizons). The values gradually increase upwards with some negative values and reach the peak in oncoidal facies of the 33 m horizon (Fig. 18). The interval from 34 to 56 m lacks an outcrop. In the uppermost part of the Nakanosawa section, values as high as 1.9-2.0‰ were recorded from levels above 67 m (Table 3).

The $\delta^{18}O$ values range from –12 to –6‰, and show an upward increasing trend in the lowermost part. The values from the lowermost 14 m are mostly lower than –7.0‰, and the lowermost sample of sandy limestone (at 1.5 m) displays a significantly negative value (–12.37‰, Table 3). From 14 to 69 m, the $\delta^{18}O$ values generally keep in a narrow range from –8.0 to –6.4‰ (Fig. 18). The uppermost 13 samples record high $\delta^{18}O$ values around -7.5‰ (Table 1).

Mn concentrations are high at the upper part of the section (max. 637 ppm) and increase upward from ca. 150 ppm (at the lowermost horizon) to over 400ppm (at the uppermost horizon; Table 3). Sr concentrations are nearly constant at 500–700 ppm at the lower part, but they are high in the upper horizon (over 57m horizon: Table 3). The Mn/Sr ratio is mostly below 0.5 (Fig. 18, Table 3). These low ratios indicate that limestone of this section were not heavily altered by diagenesis (> 2.0; Jacobsen and Kaufman, 1999).

4.5.3. The Kubokawa section and the Shiraishi section (the Nankai Group)

In the Kubokawa section, one brachiopod shell was obtained from the bioclastic packstone at 6 m horizon (KBK-7). The Sr isotopic ratio of this specimen is 0.7072421 that indicates an age range of about 143 to 142 Ma that corresponds to the early to the late Berriasian (Table 1).

Results of the geochemical analyses of samples from the Kubokawa section are shown in Table 4 and Figure 11. The $\delta^{13}C$ values range from +0.7 to +1.6‰. The lowest values were recorded in bioclastic packstone in the middle part (7 m horizon). The values

gradually decrease from the base to 7 m horizon (Fig. 11). In contrast, $\delta^{13}C$ values gradually increase upward and reach the peak in bafflestone at 13 m horizon (1.6‰; Table 4).

Table 3. Results of geochemical analyses of the Nakanosawa section. Following abbreviations are used for facies; Sand. (Sandy limestone), Intra. (Intraclastic grainstone), Onc. (Oncoidal facies), Pel. (Peloidal wacke-packstone), Coral. (Coral floatstone), and Bound. (Boundstone).

No.	Name	Horizon (m)	Facies	$\delta^{13}C$ (‰)	$\delta^{18}O$ (‰)	Mn (ppm)	Sr (ppm)	Mn/Sr
1	Nk-01	1.5	Sand.	-1.74	-12.37	31	775	*0.04*
2	Nk-02	2.5	Pel.	0.52	-9.45	177	656	*0.27*
3	Nk-03	3.5	Pel.	-1.90	-11.21	144	626	*0.23*
4	Nk-04	4.5	Onc.	0.16	-9.92	226	579	*0.39*
5	Nk-05	5.5	Onc.	0.18	-9.80	223	455	*0.49*
6	Nk-06	6.5	Pel.	0.79	-7.01	139	463	*0.30*
7	Nk-07	7.5	Coral.	1.40	-9.05	117	450	*0.26*
8	Nk-08	8.5	Coral.	1.33	-7.06	150	517	*0.29*
9	Nk-09	9.5	Pel.	0.67	-7.55	175	548	*0.32*
10	Nk-10	10.5	Pel.	2.21	-7.43	169	626	*0.27*
11	Nk-11	11.5	Int.	1.29	-8.22	121	605	*0.20*
12	Nk-12	12.5	Int.	1.91	-7.80	194	510	*0.38*
13	Nk-13	14	Int.	1.58	-6.40	125	480	*0.26*
14	Nk-14	14.5	Onc.	0.59	-6.67	157	450	*0.35*
15	Nk-15	16	Coral.	1.29	-6.56	145	631	*0.23*
16	Nk-16	17	Coral.	1.98	-6.56	87	542	*0.16*
17	Nk-17	18	Coral.	1.55	-7.37	120	545	*0.22*
18	Nk-18	19	Coral.	2.06	-7.34	96	507	*0.19*
19	Nk-19	20	Coral.	1.26	-7.40	332	791	*0.42*
20	Nk-27	28.5	Coral.	1.73	-8.30	154	487	*0.32*
21	Nk-28	29	Onc.	1.91	-7.40	101	470	*0.22*
22	Nk-29	30	Onc.	1.87	-7.24	83	378	*0.22*
23	Nk-31	32	Onc.	1.98	-7.32	89	479	*0.19*
24	Nk-u-01	57	Onc.	1.40	-8.09	424	1062	*0.40*
25	Nk-u-02	57.5	Onc.	1.40	-7.72	455	645	*0.71*
26	Nk-u-03	58	Onc.	0.99	-7.51	394	1583	*0.25*
27	Nk-u-04	58.5	Onc.	1.07	-7.46	515	2290	*0.22*
28	Nk-u-06	60	Coral.	1.45	-7.55	364	1198	*0.30*
29	Nk-u-07	61	Coral.	1.09	-7.74	473	2281	*0.21*
30	Nk-u-08	61.5	Coral.	1.12	-7.79	455	2000	*0.23*
31	Nk-u-09	62.5	Coral.	1.16	-7.13	546	2228	*0.25*
32	Nk-u-10	63	Coral.	0.99	-7.81	424	1941	*0.22*
33	Nk-u-11	64	Coral.	0.96	-7.17	412	934	*0.44*
34	Nk-u-12	65	Onc.	0.98	-7.91	576	2736	*0.21*
35	Nk-u-13	66	Coral.	1.97	-6.85	594	3045	*0.20*
36	Nk-u-14	68.5	Coral.	1.92	-7.28	637	4373	*0.15*
37	Nk-u-15	69	Bound.	1.86	-7.60	534	2663	*0.20*

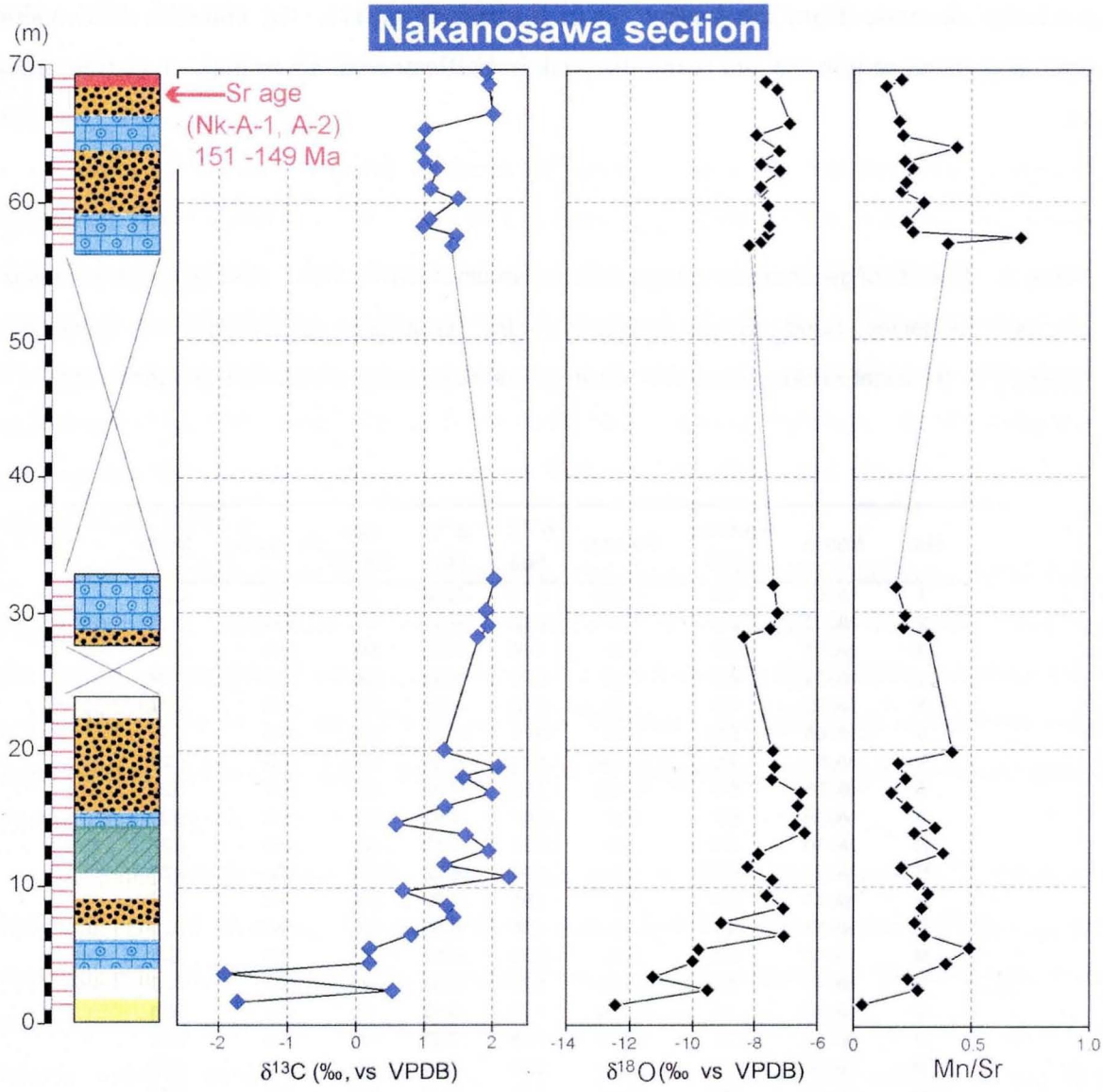

Figure 18. The geochemical profiles of $\delta^{13}C$ and $\delta^{18}O$, and the Mn/Sr ratios, and stratigraphic column of the Nakanosawa section.

The $\delta^{18}O$ values range from –8 to –4‰, and also showed a stable trend. The values at the lowermost horizon are lower than –8.0‰, and the values increased upward gently (Fig. 11). Mn concentrations are highiest at the bottom of the section (max. 561 ppm) and decrease to 33 ppm at 10 m horizon. They again increase up to 374 ppm in the upper part of the section (Table 4). Sr concentrations are nearly constant at 450–600 ppm and record the highest value (515 ppm) at 12 m horizon (Table 4). The Mn/Sr ratio is mostly below 0.4 (Fig. 11) but reaches 1.4 in the lowermost horizon (Table 4). These ratios are lower than the value indicative of significant diagenetic alteration (> 2.0; Jacobsen and Kaufman, 1999).

In the Shiraishi section, four brachiopod shells were collected from the lowermost bioclastic wackestone (SH-3-2, SH-3-4, SH-3-5, SH-3-6), and their Sr isotopic ratios range from 0.7073915 to 0.7074435, which correspond to the ages of about 136 to 132 Ma (the early to the late Hauterivian). Among the four specimens, SH-3-5 that exhibited no luminescence yielded the highest isotopic ratio and the oldest age (Table 1).

Results of the geochemical analyses of samples from the Shiraishi section are shown in Table 5 and Figure 13. The $\delta^{13}C$ values record a relatively wide range from -2.3 to +1.6‰. The lowest values were recorded in bioclastic wackestone in 1.5 m horizon. The values largely increase in 1.5-2.5 m interval, and exceed 1.0 ‰. From the 2.5 m horizon, the $\delta^{13}C$ values rapidly decrease upward to -0.77‰ at 5.2m horizon, and then gradually increase to the uppermost horizon (Fig. 13).

The $\delta^{18}O$ values record a wide range from –9.2 to –7.1‰ (Fig. 13). The two distinct peaks occur around 2.5 m and 13.8 m horizons. Except for these peaks, the $\delta^{18}O$ values are mostly below -8.0‰. Mn concentrations are mostly low (below 200 ppm), except for two uppermost samples (Table 5). Sr concentrations range from 600 to 1300 ppm and record the highest value (1300 ppm) at 4.2 m horizon (Table 5). The Mn/Sr ratio is mostly below 0.2 (Fig. 13) and gently increases upwards.

4.5.4. The North Naradani section (the Torinosu Group)

Sr isotopic ratios were measured for 11 brachiopod shells collected from four horizons (78 m horizon: Nar-S-08, 130 m horizon: Nar-N-1 series, 140 m horizon: Nar-N-4 series, and 152 m horizon: Nar-N-2-9: Table 1; Fig. 14). The ratios generally show the upward-increasing trend that demonstrates stratigraphic consistency of the evaluated ages. The Sr isotopic ratio of the 78 m horizon (0.7071692) indicates the age of about 147 to 144 Ma (the late Tithonian to the earliest Berriasian). The ratios of the six specimens from the 128 m horizon range from 0.707192 to 0.7072348 that corresponds to the ages ranging from about 145 to 142 Ma (the Berriasian). Three samples of brachiopods from the 147 m horizon that possess a bright CL record have the ratios ranging from 0.707214 to 0.7072616 that indicate the age of about 144 to 141 Ma (the Berriasian). The ratio of the specimen from 152 m horizon is 0.7072851 that corresponding to the age of about 141 to 140 Ma (the late Berriasian, Table 1).

Table 4. Results of geochemical analyses of the Kubokawa section. Following abbreviations are used for facies; Ooi. (Ooidal grainstone), Pel. (Peloidal wacke-packstone), Bio. (Bioclastic packstone), Baf. (Bafflestone).

No.	Name	Horizon (m)	Facies	$\delta^{13}C$ (‰)	$\delta^{18}O$ (‰)	Mg (ppm)	Mn (ppm)	Sr (ppm)	Fe (ppm)	Mn/Sr	Carbonate (wt %)
1	KBK01	0	Ooi.	1.12	-7.09	3316	561	400	5466	*1.40*	85.1
2	KBK02	1	Ooi.	1.04	-7.47	2790	338	381	4366	*0.89*	84.2
3	KBK03	2	Pel.	1.18	-6.03	3895	194	477	3010	*0.41*	86.2
4	KBK05	4	Pel.	1.22	-6.75	3794	173	515	3115	*0.34*	86.8
5	KBK06	5	Bio.	0.91	-5.29	4165	223	572	2634	*0.39*	86.2
6	KBK07	6	Bio.	0.73	-6.29	5755	151	591	1510	*0.26*	93.1
7	KBK08	7	Bio.	1.02	-6.11	5765	173	515	1622	*0.34*	100.0
8	KBK09	8	Bio.	1.41	-6.43	5349	274	477	2012	*0.57*	91.4
9	KBK10	9	Baf.	1.48	-4.55	3831	108	458	1588	*0.24*	–
10	KBK11	10	Baf.	1.37	-4.65	3619	33	477	2706	*0.07*	88.5
11	KBK12	11	Baf.	1.00	-4.61	4355	216	491	2145	*0.44*	81.2
12	KBK13	12	Baf.	1.60	-3.11	5869	137	515	1804	*0.27*	83.3
13	KBK14	13	Baf.	1.08	-6.22	4804	252	362	3113	*0.70*	78.5
14	KBK15	14	Baf.	1.53	-5.88	3830	230	438	2480	*0.53*	83.9
15	KBK16	15	Baf.	1.31	-4.16	4575	374	438	4604	*0.85*	81.9
16	KBK17	16	Baf.	-	-	5642	302	458	2376	*0.66*	-

Table 5. Results of geochemical analyses of the Shiraishi section. Following abbreviations are used for facies; Bio. (Bioclastic wackestone), Bin. (Bindstone), Lim. (Lime-mudstone), For. (Foraminiferal grainstone).

No.	Horizon (m)	Facies	$\delta^{13}C$ (‰)	$\delta^{18}O$ (‰)	Mn (ppm)	Sr (ppm)	Mn/Sr
1	0	Bio.	-0.55	-8.21	42	610	0.07
2	1	Bio.	-0.86	-8.66	44	802	0.05
3	1.5	Bio.	-2.30	-8.65	40	499	0.08
4	2.5	Bio.	1.04	-6.44	44	628	0.07
5	3	Bin.	0.17	-7.85	68	975	0.07
6	4.2	Bin.	-0.38	-8.74	92	1331	0.07
7	5.2	Bio.	-0.77	-8.59	39	876	0.04
8	6.2	Bio.	-0.18	-8.63	56	760	0.07
9	10.8	Lim.	1.43	-9.11	187	882	0.21
10	11.8	Lim.	1.58	-9.20	88	948	0.09
11	13.8	For.	1.09	-7.12	228	1177	0.19
12	18.2	Lim.	1.33	-8.99	224	1112	0.20

Results of the geochemical analyses of samples from the North Naradani section are shown in Table 6 and Figure 14. The $\delta^{13}C$ values record a considerably wide range from -8.3 to +1.3‰, and show two distinct negative excursions; one is developed in ooidal grainstone at 34 m horizon, the other is developed in bioclastic grainstone at 146 m horizons (Fig. 14). Especially, the value of the latter specimen is as low as -8.3‰, which is the lowest value among the samples measured in this study.

The $\delta^{18}O$ profile shows trend, which is roughly synchronized with $\delta^{13}C$ profile. The $\delta^{18}O$ profile shows three large negative excursions; the first in ooidal grainstone at 34m horizon, the second in ooidal grainstone at 113m horizon, and the third in bioclastic grainstone at 146m horizons (Table 6). The $\delta^{18}O$ profile shows the higher value at the lowermost part, and shows an upward decreasing trend to the lower values of $\delta^{18}O$ in the uppermost section (Fig. 14).

Mn concentrations are high at the bioclastic grainstone in the upper section (in 110-140m interval). Mn concentrations are mostly below 100 ppm in other horizons (Table 6). In contrast, Sr concentrations are high at the lower to middle horizon (Max. 599 ppm at 11.5 m horizon). Sr concentrations are lower at bioclastic grainstone of the upper section (Table 6). The Mn/Sr ratio is mostly below 0.8 (Fig. 14), except for at 34 m and 47 m horizons, in which the $\delta^{13}C$ and the $\delta^{18}O$ profiles show large negative excursions. A similar tendency was recognized around 113 m horizon. The ratio is not so large in the bioclastic grainstone of the uppermost horizon, which records the lowest $\delta^{13}C$ value.

4.5.5. The South Furuichi section (Nakatsugawa limestone body, the Imaidani Group)

Samples of brachiopods were collected from the oncoidal grainstone at four horizons; three in the middle section (27 m horizon: Fur-S-31, 29 m horizon: Fur-S-33, 31 m horizon: Fur-S-35), and one near the top (1 sample; 49 m horizon, Fur-S-50, Fig. 16). The three ratios of the middle section are within a relatively narrow range of 0.7071501 to 0.7071629 that indicates an age of about 148 to 145 Ma (the early Tithonian to the earliest Berriasian). The ratio from the uppermost horizon (0.7072015) indicates a younger age of about 145 to 143 Ma (the early Berriasian). Hence, the Jurassic/Cretaceous boundary is expected at somewhere in the middle or the upper section.

I also measured the Sr isotopic ratio of a belemnite collected from the same limestone body (Fig. 3E). The ratio (0.7071761) indicates an age of about 146 to 144 Ma (Table 1), which conforms to the range of the middle section of the South Furuichi.

In the South Furuichi section, $\delta^{13}C$ values range mainly from -0.8 to +2.2‰ (Fig. 16; Table 7). The profile is mainly stable in the range from +0.8 to +2.0 ‰, except for a negative excursion in 7-8 m interval. In the lower part of the section (in 0–11 m interval), the $\delta^{13}C$ profile roughly shows an increasing trend from +0.8 to +2.0‰. In addition, the $\delta^{13}C$ profile shows a negative and positive shfts of a small amplitude at 21 m and 22 m horizons, respectively.

The $\delta^{18}O$ values range from -9.2 to -3.6‰. The profile shows two large negative excursionsin 7-10 m and 19–22 m intervals. The $\delta^{18}O$ profile shows a trend roughly synchronized with the $\delta^{13}C$ profile.

Mn concentrations are generally low at the all horizons, especially in the specimens above 23 m horizon. All of they are below 60 ppm (Table 7). Sr concentrations are generally higher at the lowermost horizon, and the maximum value (2495ppm) is recorded in the upper section (30 m horizon; Table 2). The Mn/Sr ratio is mostly below 0.1 (Fig. 16), and these values are the lowest level among the study sections. These ratios are certainly lower than the value indicative of significant diagenetic alteration (> 2.0; Jacobsen and Kaufman, 1999).

Table 6. Results of geochemical analyses of the North Naradani section. Following abbreviations are used for facies; Sand. (Sandy limestone), Ooi. (Ooidal grainstone), Pel. (Peloidal wackestone), Bio. (Bioclastic grainstone),. Mcr. (Microbal bindstone).

No.	Sample	Horizon (m)	Facies	$\delta^{13}C$ (‰)	$\delta^{18}O$ (‰)	Sr (ppm)	Mn (ppm)	Mn/Sr
1	S01	15	Snd.	1.04	-5.05	191	79	*0.42*
2	S02	25	Pel.	1.27	-4.28	210	79	*0.38*
3	S03	31	Ooi.	1.11	-3.11	153	130	*0.85*
4	S04	31	Ooi.	0.12	-5.12	191	43	*0.23*
5	S05	32	Ooi.	0.59	-5.44	172	58	*0.34*
6	S06	33	Ooi.	-0.31	-5.92	153	50	*0.33*
7	S07	34	Ooi.	0.96	-6.04	481	162	*0.34*
8	S08	34	Ooi.	-5.60	-8.92	57	79	*1.38*
9	S10	41	Ooi.	-0.74	-6.50	191	22	*0.11*
10	S11	46	Bio.	1.16	-5.39	286	50	*0.18*
11	S12	47	Bio.	-1.54	-6.17	133	238	*1.78*
12	S14	54	Bio.	-2.87	-3.98	343	50	*0.15*
13	S15	63	Pel.	-0.48	-4.11	343	65	*0.19*
14	S17	86	Mcr.	0.13	-5.96	343	101	*0.29*
15	N01	111.5	Ooi.	-1.77	-5.77	599	60	*0.10*
16	N02	113	Ooi.	-4.65	-8.35	95	43	*0.45*
17	N03	114.5	Pel.	-2.41	-5.90	104	191	*0.54*
18	N04	126	Bio.	-4.44	-6.17	10	805	*0.01*
19	N05	127.5	Bio.	-3.12	-6.59	130	535	*0.24*
20	N06	129	Bio.	-3.03	-6.40	10	632	*0.02*
21	N07	130.5	Bio.	-3.26	-6.28	39	602	*0.06*
22	N08	132	Bio.	-1.18	-5.88	67	495	*0.14*
23	N09	133.5	Bio.	-3.03	-6.56	33	679	*0.05*
24	N11	136.5	Bio.	-3.35	-8.54	22	-	-
25	N14	145	Bio.	-0.66	-7.85	172	50	*0.29*
26	N15	146	Bio.	-8.27	-8.86	95	32	*0.33*
27	N16	148	Bio.	-1.36	-8.60	114	29	*0.25*
28	N17	150	Bio.	-2.12	-8.07	122	22	*0.18*
29	N18	151	Bio.	-1.97	-7.48	153	32	*0.21*

Table 7. Results of geochemical analyses of the South Furuichi section.Following abbreviations are used for facies; Onc. (Oncoidal grainstone), Baf. (Bafflestone), Biof. (bioclastic floatstone), Biop. (Bioclastic packestone).

No.	Name	Horizon (m)	Facies	$\delta^{13}C$ (‰)	$\delta^{18}O$ (‰)	Mn (ppm)	Sr (ppm)	Mn/Sr
1	SFur-01	1	Onc.	1.03	-6.49	60	2233	*0.027*
2	SFur-02	2	Onc.	1.21	-3.98	14	1093	*0.013*
3	SFur-03	3	Onc.	1.23	-5.45	-	-	-
4	SFur-04	4	Onc.	0.86	-3.45	-	-	-
5	SFur-05	5	Onc.	1.46	-5.68	2	1233	*0.002*
6	SFur-06	6	Baf.	1.82	-4.66	15	87	*0.175*
7	SFur-07	7	Biop.	-0.77	-8.59	3	1358	*0.002*
8	SFur-08	8	Biop.	-0.18	-8.63	7	681	*0.010*
9	SFur-09	9	Biop.	1.43	-9.11	6	555	*0.011*
10	SFur-10	10	Biof.	1.58	-9.20	2	832	*0.002*
11	SFur-11	11	Biof.	2.00	-5.68	1	361	*0.004*
12	SFur-12	12	Biop.	1.89	-5.17	2	633	*0.004*
13	SFur-13	13	Biof.	1.82	-4.87	-		-
14	SFur-14	14	Baf.	1.76	-4.56	34	248	*0.139*
15	SFur-15	15	Baf.	1.79	-5.66	34	694	*0.049*
16	SFur-16	16	Biof.	1.62	-4.82	48	471	*0.101*
17	SFur-17	17	Baf.	1.71	-4.49	37	569	*0.065*
18	SFur-18	18	Baf.	1.43	-4.44	33	504	*0.065*
19	SFur-19	19	Onc.	1.40	-7.74	33	541	*0.060*
20	SFur-20	20	Baf.	1.55	-6.89	51	578	*0.088*
21	SFur-21	21	Baf.	0.83	-7.77	26	462	*0.055*
22	SFur-22	22	Onc.	2.17	-7.67	22	709	*0.031*
23	SFur-23	23	Biof.	1.47	-5.56	1	442	*0.003*
24	SFur-24	25	Onc.	1.72	-6.14	5	1721	*0.003*
25	SFur-25	26	Onc.	1.76	-4.84	-	-	-
26	SFur-26	27	Onc.	1.82	-4.59	1	626	*0.002*
27	SFur-27	28	Onc.	1.69	-3.32	2	469	*0.004*
28	SFur-28	29	Onc.	1.57	-4.58	1	624	*0.002*
29	SFur-29	30	Onc.	1.42	-3.61	1	454	*0.003*
30	SFur-30	31	Onc.	1.56	-3.96	7	2495	*0.003*
31	SFur-31	32	Onc.	1.79	-5.08	4	1756	*0.003*
32	SFur-32	33	Biof.	1.63	-4.19	1	274	*0.005*
33	SFur-33	34	Biof.	1.69	-4.97	7	1109	*0.006*
34	SFur-34	35	Onc.	1.93	-5.12	2	867	*0.002*
35	SFur-36	36	Onc.	1.65	-5.83	2	633	*0.004*
36	SFur-37	37	Onc.	1.64	-5.61	1	501	*0.003*
37	SFur-38	38	Onc.	1.75	-5.69	1	481	*0.003*
38	SFur-39	39	Onc.	1.77	-5.43	1	381	*0.003*
39	SFur-40	40	Onc.	1.60	-6.03	6	1260	*0.005*
40	SFur-41	41	Onc.	1.71	-6.55	2	563	*0.004*
41	SFur-42	42	Onc.	1.52	-5.93	2	574	*0.003*
42	SFur-43	43	Onc.	1.65	-8.07	1	632	*0.002*
43	SFur-44	44	Onc.	1.26	-6.44	1	549	*0.002*
44	SFur-45	45	Onc.	1.66	-7.35	3	754	*0.004*
45	SFur-46	46	Onc.	1.72	-6.49	2	484	*0.003*
46	SFur-47	47	Onc.	1.62	-5.94	1	320	*0.004*
47	SFur-48	48	Onc.	1.51	-7.77	1	536	*0.002*
48	SFur-49	49	Onc.	1.82	-5.92	4	38	*0.108*

Chapter #5. DISCUSSIONS

5.1. Sedimentology of the carbonate platform of the Koike Limestone

5.1.1. Platform architecture and depositional environments

Lateral facies changes between the five sections (Fig. 6) show that the carbonate platform of the Koike Limestone Member was generally deepened to the north. Clear evidence of the northward-deepening trend is the variation in texture of the oncoidal facies. The oncoidal facies shows mainly a grainstone texture in the two southern sections (Koike and Tatenosawa) but becomes more micritic (packstone) in the other three sections (Fig. 6). This textural variation likely indicates decreasing water-energy from south to north.

A similar interpretation was given by Kiyama and Iryu (1998) who found that the Koike limestone becomes micritic in the northern part of the study area. This trend is confirmed in my study by the fact that peloidal facies with wackestone texture is well developed in the Kakusawa section and in the lower part of the Nakanosawa section (Fig. 6).

An additional evidence is the spatical distribution of the two types of coral-bearing facies (boundstone and floatstone). Corals and stromatoporoids from the Koike Limestone Member, such as *Thamnastrea* sp. and *Parastromatopora* sp., are typical shallow-water reef-builders of the Late Jurassic (Scott, 1988; Leinfelder et al., 1994). The distribution of boundstone mainly occurs in the Tatenosawa section, and indicates that these reef-builders mainly grew in the southern part of the platform. On the other hand, the corals in the floatstone facies were transported and buried in micritic sediments. They likely originated from the northern platform and were transported southwards to deeper locations (Fig. 19).

The deepening-northward platform is consistent with the northward dip of the landform of the Late Jurassic Southern Kitakami Terrane, as inferred by Takizawa (1985) on the basis of the 3-D geometry of the sediment package and paleo-current directions.

Reconstruction of the deepening-northward trend of the Koike Limestone platform helps interpretation of the depositional environments. Boundstone is likely the shallowest facies because the corals had to live in the photic zone (Fig. 9). Coral floatstone was also deposited in a shallow environment unless the corals were transported over a long distance on a slope. This facies is well developed in the Koike section that is located 500 m north

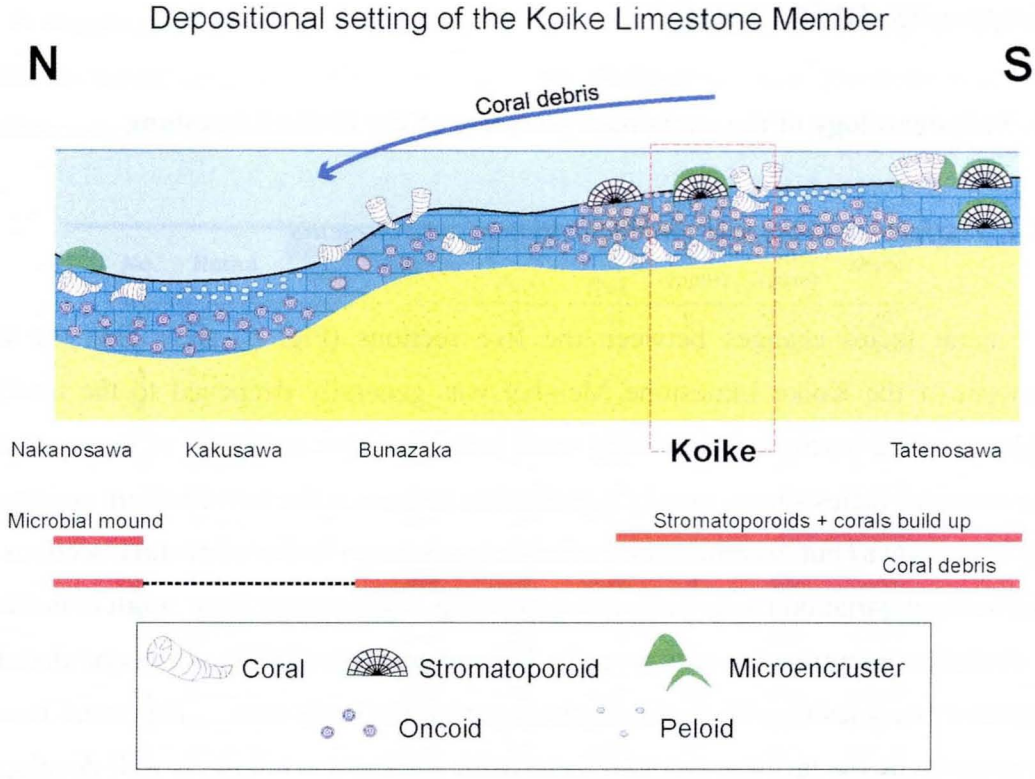

Figure 19. Reconstruction of the carbonate platform of the Koike Limestone

of the Tatenosawa section (Fig. 2B). Difference in depth between the Tatenosawa and Koike section is evaluated at less than 50 m, even with an assumption of a relatively steep bathymetry (6°). Therefore, at least the coral floatstone in Koike section can still be regarded as shallow-water facies.

Oncoidal facies used to be regarded as high-energy facies deposited in a very shallow environment (e.g., Eguchi and Shoji, 1965; Morino, 1992). This reconstruction was largely based on the interpretation that the coated grains of the Koike Limestone Member were ooids. However, the grains consist of micritic envelopes without distinct concentric laminations or preferential orientation of crystals (Fig. 8F), and resemble the "Type C oncoids" of Flügel (2004, pp. 124-142), which are formed by microencrusters. They probably formed in the photic zone inhabited by phototrophic microencrusters (e.g., cyanobacteria) and with some water energy causing the grains to be rolled. They were formed in a shallow environment but not necessary in a high-energy condition. There is no conclusive evidence to compare paleo-depths between oncoidal facies and coral floatstone. However, Figure 6 indicates that the thickest development of oncoidal facies occurs in the Kakusawa section located in a deeper setting on the deepening-northward platform. Considering this facies distribution, the corals lived densely on the shallower

location than the oncoidal sediment.

Peloidal wacke-grainstone is fine-grained carbonate and was likely deposited under low water-energy. This facies does not accompanied with any sedimentary structures that specify the depositional environment. It could be deep water without sufficient influences from wave and current, or shallow water in a calm lagoonal setting. The periodically appearing grainstone texture suggests changes in the position of the wave base, possibly related to storm events.

5.1.2. Origin of the depositional cycles

The cyclic facies change is a characteristic feature of the Koike section have been described and interpreted differently in previous sedimentological studies (Eguchi and Shoji, 1965; Kiyama and Iryu, 1998). Eguchi and Shoji (1965) recognized repetition of "ooidal" and micritic facies, which correspond to my oncoidal facies and coral-peloidal facies, respectively, and interpreted this as having been caused by changes in water energy. Kiyama and Iryu (1998) defined the cycles as depositional units, each consisting of high-energy oncoidal facies and overlying low-energy coral facies. According to their model, each unit corresponds to an upward-shallowing sequence that starts with a transgressive open-marine setting and ends with a restricted low-energy environment.

My definition of the cycle is different from that of Kiyama and Iryu (1998), in terms of the boundary set at the bottom of the coral facies, which normally marks an abrupt facies change. The cycles identified in the Koike section in this study consist of coral floatstone, oncoidal facies, and peloidal wacke–grainstone, in ascending order. The upward-fining trend indicates decrease in water-energy (Fig. 10B).

The data presented in this study are not sufficient to specify the process forming the cycles, nevertheless, two potential models can be proposed. One simple interpretation is cyclic change in water depth due to relative sea-level change. In this case, each cycle started with rising sea-level, and water-depth gradually increased during the transgressive stage whereby the rate of the sea-level rise exceeded the sediment accumulation rate. Alternative interpretation is that sediment accumulation through reef growth gradually blocked wave and current energy. This process commonly forms upward-fining cycles on peritidal platforms (Osleger et al., 1991; Strasser et al., 1999), and develops a protected lagoon, which accommodates fine-grained sediments on the top of the cycle.

5.2. Depositional age and developments of Torinosu-type limestones

5.2.1. Estimation of the depositional rate in the North Naradani and the South Furuichi sections

In the North Naradani section and the South Furuichi section, Sr isotopic ages obtained from several horizons provide the opportunity to estimate the rate of deposition of the limestone. From the available age data set (Table 1), I used the mean age values of the uppermost (at 152 m horizon) and the lowermost horizons (at 78 m horizon) for the North Naradani section, which were evaluated at 140.55, and 145.7 Ma, respectively. The calculated duration of the deposition of the 74-m-thick interval is thus 5.15 m.y., which yields the average rate of deposition of 14.4 m/m.y. Assuming a constant rate of deposition for the entire section, the duration of the deposition of the lower 78 m section was estimated at 5.4 m.y., and the age of the base of the section is around 151 Ma (the late Kimmeridgian). I further conclude that the deposition of limestone in the North Naradani section had lasted for 11 m.y. from the late Kimmeridgian to the late Berriasian.

For the South Furuichi section, I used the oldest and the youngest ages, which are 147 Ma at 29 m horizon and 144 Ma at the 49 m horizon, respectively (Table 1). The age difference of the 20-m-thick interval is 3 m.y. and the estimated rate of deposition is 6.7 m/m.y. Application of this rate makes the duration of the deposition of the lower 29 m section 4 m.y., and the age of the base of the section is calculated at 151 Ma (the late Kimmeridgian), which is almost simultaneous to the base of the North Naradani section. As above, it is estimated that the deposition of limestone in the South Furuichi section had lasted for 8 m.y. from the late Kimmeridgian to the early Berriasian.

5.2.2. Consistency between Sr isotopic ages and the previous biostratigraphies

Sr isotopic ages of the brachiopod shells should be compared to available biostratigraphic ages of the previous studies in order to verify their consistencies.

Ammonoids reported by Sato and Taketani (2008) are one of the biostratigraphic constraints for the Koike Limestone Member. They were collected from the Tatenosawa Sandstone Member that occurs beneath the Koike Limestone Member, and contains *Aulacosphinctoides tairai* and *Hybonoticeras* sp., indicating the age of the Kimmeridgian

to the Tithonian. This biostratigraphic age does not contradict my Sr age of the late Kimmeridgian to the early Tithonian ascertained for the upper horizon of the Koike Limestone Member.

The two examined limestone bodies of the Nankai Group were assigned substantially different ages; the Kubokawa section was to the early to the late Berriasian, and the Shiraishi section to the early to the late Hauterivian. However, these two ages are within the ranges estimated by radiolarians and bivalves, which is extended from the Oxfordian to the Barremian (Morino et al., 1989; Kozai et al., 2004). Geological structure of the Nankai Group (Fig. 3B) indicates that the Shiraishi section is stratigraphically upper than the Kubokawa section. My estimated Sr ages suggest that the Nankai Group was deposited over a relatively long duration of time that included at least two distinct periods of carbonate deposition.

Biostratigraphy of the Torinosu Group and its equivalent strata have been relatively well established by radiolarian assemblages from the mudstone facies (Aita and Okada, 1986; Matsuoka, 1992). The radiolarian biostratigraphy recognized at least two biozones, *Pseudodictyomitra primativa* and *Pseudodictyomitra* sp. cf. *P carpatica* Assemblage zone. In Sakawa area, the limestone bodies most commonly occur within *P primativa* and *P carpatica* zone that correspond to the middle Tithonian to the Berriasian (Kano, 1988). My ages of the North Naradani section are almost identical to the biostratigraphic ages.

The Imaidani Group, that is the lateral extension of the Torinosu Group, has been assigned to the Kimmeridgian to the Tithonian, based on ammonites and radiolarian assemblages from mudstone facies (Yao et al., 1982; Takei and Matsuoka, 2004). Although the age of the Nakatsugawa limestone body was never thoroughly examined, the Kimmeridgian radioralian assemblage was reported from the mudstone beneath the limestone (Yao et al., 1982). This means that the limestone body is younger than the Kimmeridgian, and is consistent with my results. In summary, the Sr isotopic stratigraphy is reliable and provides ages of higher resolution than the previous biostratigraphic ages.

5.2.3. Local tectonic setting for the limestone development on forearc basin

Development of the Torinosu-type limestones is highly variable in different region in Japanese Island, and substantial in the western Shikoku Island (e.g. Tamura, 1960). This is simply demonstrated by comparison of the thickness of limestone bodies studied in this

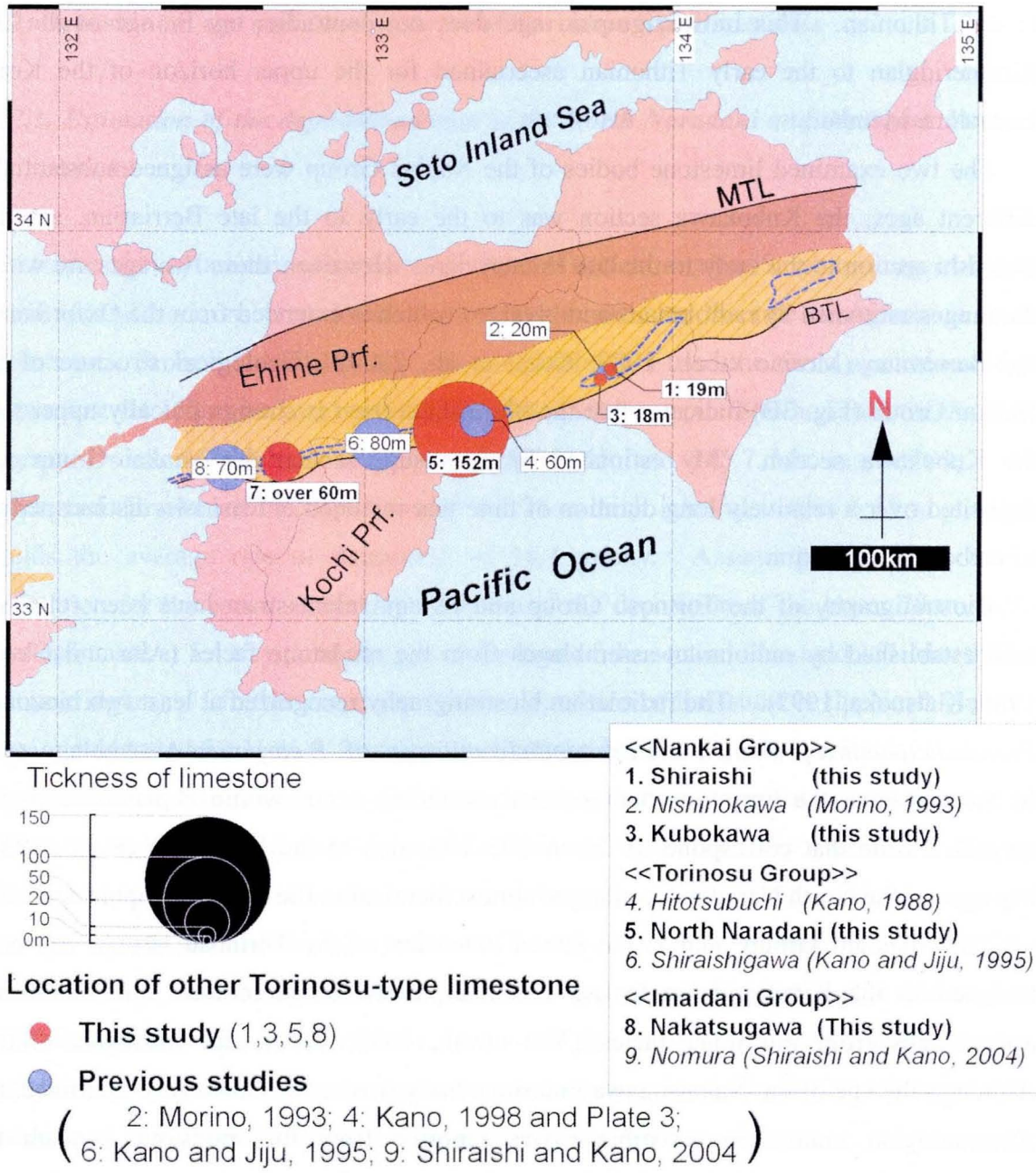

Figure 20. The thickness of Torinosu-type limestones in Shikoku Island. The legend is common to Figure 2B. The diameter of circle indicates the thickness of the limestone. The limestone bodies in this study are shown as filled circles, and other limestone bodies are shown as open circles.

thesis. Thickness of each limestone body is shown in Figure 20. Thick limestone bodies are prone to occur in western Shikoku, such as the North Naradani body (152 m thick; Fig. 14), the Nakatsugawa body (> 60 m: total thickness of the South Furuichi and the North Furuichi sections; see Fig. 16, Plate 7), the Shiraishigawa body (> 80 m thick; Kano and Jiju, 1995) and the Nomura body (70 m thick; Shiraishi and Kano, 2004). In contrast in

the eastern Shikoku, thickness of the Kubokawa body is 17m thick (Fig. 11), that of the Shiraishi body is 19m thick (Fig. 13). The tendency is extended outside of the Shikoku Island, where the Torinosu-type limestone occurs in thin and small bodies, such as in Kii Peninsula (Kashiwagi et al., 2002) and Kyushu Island (Fukuda, 1984).

The concentrated occurrence on the western Shikoku might have been related to the tectonic setting that controlled configuration and stability of the carbonate platform. It is considered that the Torinosu-type limestones were developed on continental shelf, which was formed by the sediment accretion and deformed by the collision of seamounts in the fore-arc margin. During the Jurassic, accreationary prisms were well developed along the Asian Continent, and were widest in the region corresponding to the western Shikoku Island (Matsuoka, 1992). This was likely reflected from the seamount collision that is now exposed as the Triassic limestone body of the Sambosan-Togano Group. The Triassic limestone is thickly developed around Sakawa-Niyodo area where the younger Torinosu-type limestone is also thick. Hence, in such areas, tectonics controlled the regional bathymetry, and resulted in broad development of continental shelf that was necessary for deposition of thick limestone sequence. Favorable conditions for carbonate deposition had lasted over a long period in the western part of the Shikoku Island.

5.2.4. The depositional age of the Torinosu-type limestone.

Among the five examined limestone bodies, three (Kubokawa, North Naradani, and Nakatsugawa) were deposited in a period from the Tithonian to the Berriasian (Fig. 21). A previous study on another limestone body in Niyodo area (the Shiraishigawa section, the location is shown in Fig. 3A), also indicates the Tithonian age (Shiraishi et al., 2005). Hence, it is shown that many of the Torinosu-type limestones in Shikoku Island were simultaneously deposited during the 10-m.y.-period.

Quantitative study on age-distribution of shallow marine carbonate recognizes active carbonate deposition during the period of the Tithonian to the Berriasian (Philip, 2003). This conclusion was drawn essentially from the dataset of the Tethys Ocean, but my age estimate supports that the activated carbonate deposition was global and seen in northwestern Palaeo-Pacific area. Here I discuss potential factors controlling the temporal distribution of the Torinosu-type limestones.

Sea level could be a global control. Generally, shallow marine carbonates were

deposited in transgressive interval or high stand sea-level interval, when shallow shelf area was expanded. According to global eustatic curve during the Kimmeridgian to the Hauterivian by Haq et al. (1987), high stand of sea level was recognized in the early Tithonian and the Hauterivian when the limestone of the Nakanosawa and Shiraishi sections were deposited (Fig. 21). In contrast, a declining trend of sea level was revealed for the late Tithonian to the Berriasian, which was the period of active limestone deposition in Shikoku Island. Sea level of this period is characterized by the third order change with amplitudes of 50 m, which was followed by a distinct regression in the early Valanginian (Fig. 21; Haq et al., 1987). Deposition of the Torinosu-type limestone was discontinuous in some cases, as seen in the North Naradani section and the discontinuity may have been partly reflected from the third order fluctuation. In addition, absence of the Valanginian limestone is possibly related with the global regression.

The discontinuity and the alternation with thick siliciclastics are the prominent features of the Torinosu-type limestone, and are not seen in shallow carbonate platforms in the Tethyan areas. Therefore, this could be related with the tectonic setting in fore-arc areas along northwestern Palaeo-Pacific where environments of deposition were influenced by accretion and collision of seamounts (Matsuoka, 1992). The fore-arc basin on the accretionary complexes was unfavorable for deposition of carbonate in terms of a large amount of terrigenous influx.

5.2.4. Temporal pattern of reef-building assemblage of the Torinosu-type limestone

Major reef-builders of each study section are listed Figure 21 in a relation with the depositional period. Coral frameworks and microbal crusts are developed commonly in all five sections, and also in the Shiraishigawa section that was deposited in early to late Tithonian (Kano and Jiku, 1995; Shiraishi et al, 2005). Corals-stromatoporoids-microencrusters association is predominant reef-building assemblage in the Koike Limestone, and the Kubokawa section. In the Nakatsugawa section, calcareous sponges played a role in reef-building instead of stromatoporoids. In contrast, bindstone consisting of microbal crust are thickly developed in the Shiraishi and North Naradani sections, where frameworks of corals and stromatoporois are rare (Figs. 13 and 14). In summary, I could only recognize a slight faunal variation of reef-builders, but could not determine if it was the variation due to the age from late Kimmeridgian to Hauterivian.

Hence, fauna of reef-builder of Torinosu-type Limestones is considered to have been stable during the 15-m.y.-long period.

Expansion of calcareous plankton (e.g. coccoliths, planktonic foraminifer, and carpionellids) is known as a global evolutionary event around the Tithonian to the Berriasian period, which has been termed the "Biocalcification event" by Weissert and Erba (2004) and Weissert et al. (2008), and was possibly related to the palaeoceanography and seawater chemistry. Since the Oxfordian, seawater had been eutrophied by increased influx from continents, as deduced from an increase in $^{87}Sr/^{86}Sr$ ratio (Jones et al., 1994; Weissert and Mohr, 1996; McArthur et al., 2001). Enhanced primary production reflected on increased diversity of calcareous plankton (Erba, 2004). Their morphological and ecological diversity is also known to have increased especially during the Tithonian to the Berriasian (Roth, 1987; Bralower et al., 1989).

In addition, the continental weathering also intensified the Ca^{2+} influx to the ocean, which enhanced the potential for carbonate deposition. This resulted in the high Ca/alkalinity ratio of seawater, which provided a favorable condition for the photosynthetically induced calcification (Arp et al., 2001). Calcified microbes and microencrusters become important carbonate producers in this period (Riding, 1992), as noticeable from their common occurrence in the Torinosu-type limestone (Imaizumi, 1965; Shiraishi and Kano, 2004).

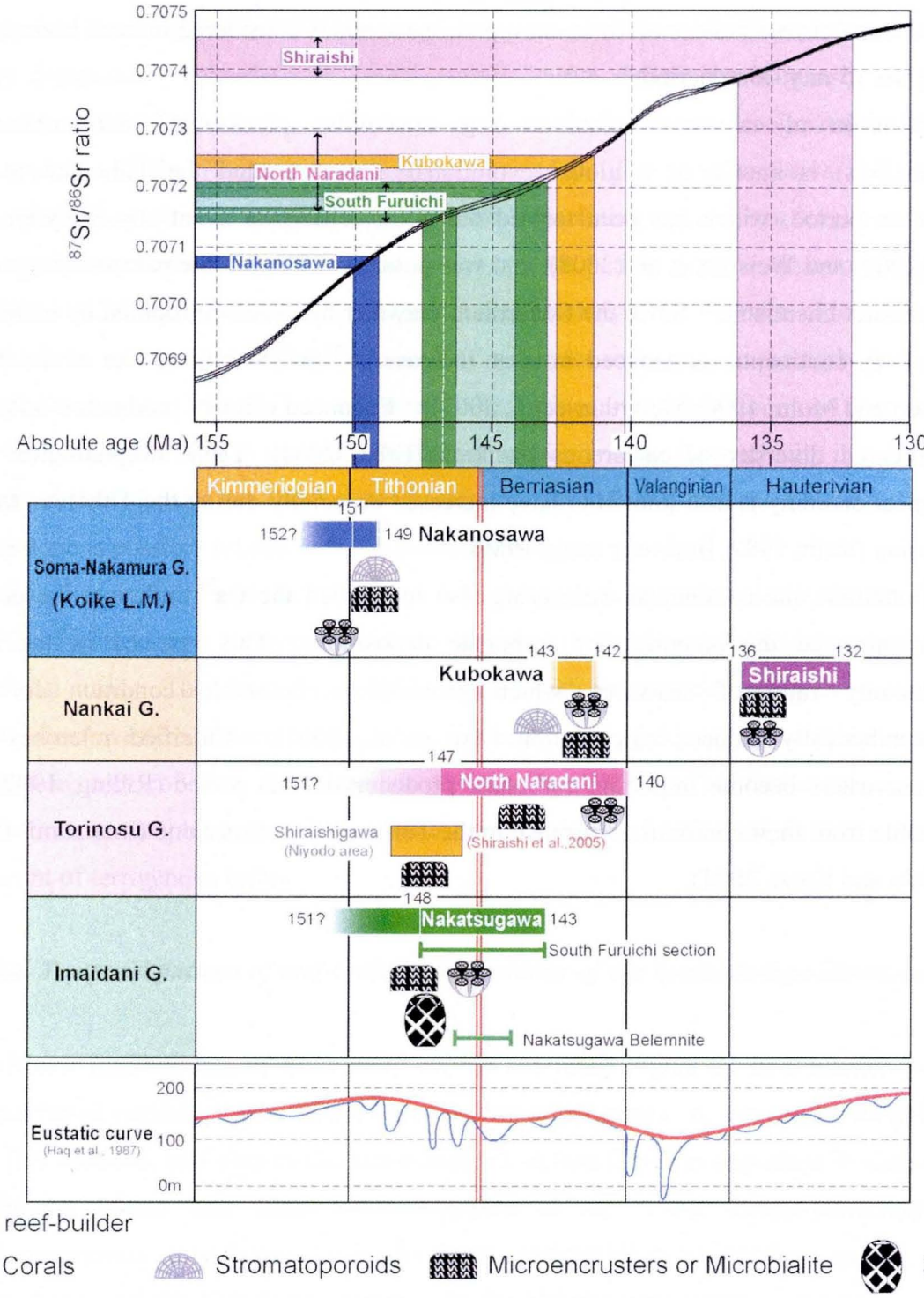

Figure 21. Evaluated Sr isotopic ages and eustatic sea level change (Haq et al., 1987) during the duration of deposition of the Torinosu-type limestones. The ages were evaluated by projection of the Sr isotopic ratio to the standard Sr isotopic curves of the LOWESS Look-up Table version 4: 08/03. Evaluated age of the Shiraishigawa section (Shiraishi et al., 2005) was added. Dominant reef-builders are listed for each study section. The absolute age (Ma) refers to Ogg (2004).

5.3. Carbon isotopic profiles

5.3.1. Evaluation of diagenetic alteration

The carbon isotopic data from the study sections provide basic information to discuss the carbon circulation in the late Jurassic-early Cretaceous ocean system by comparison with the Tethyan data. However, the preservation status of the initial $\delta^{13}C$ signal should be first confirmed. I have measured the Mn/Sr ratios of the carbonate fraction to evaluate the degree of diagenetic alteration. Usually, carbonate having the Mn/Sr below 2 records the $\delta^{13}C$ signal without suffuring a substantial alternation that normally resulted in a negative shift (Jacobsen and Kaufman, 1999). The fact that all samples show the ratio less than 2 (Figs. 11, 13, 14, 16, 17, and 18) indicates that the limestone of the study sections supports the preservation potential of the analyzed specimens. However, some of the sections record distinct negative shifts (e.g., Fig. 17) in the $\delta^{13}C$ signal as well as the $\delta^{18}O$ signal. Co-variation between $\delta^{13}C$ and $\delta^{18}O$ could be an altered signal due to the freshwater diagenesis (Allan and Matthews, 1982) that tends to affect to initially porous lithologies, such as grainstone. Here, effects of the diagenetic alteration are evaluated based on the $\delta^{18}O$ values and the presence in diagenetic feature (sparite and microspar cements).

5.3.1.1. Diagenetic alteration in the Koike section

In the Koike section, the $\delta^{13}C$ curve shows several negative excursions as well as a general increasing trend (Fig. 17). The negative excursions are mainly developed in the horizon with sparitic facies (e.g., intraclastic grainstone and oncoidal grainstone), and may therefore be ascribed to diagenetic alteration probably related to intergranular cement. In order to confirm this facies-dependent diagenesis, the $\delta^{13}C$ and $\delta^{18}O$ values of different facies were plotted in Figure 22. The cross-plot shows that three samples of intraclastic grainstone are positioned far from the other samples. They probably suffered freshwater diagenesis that generally decreases both $\delta^{13}C$ and $\delta^{18}O$ (Allan and Mathews, 1982; Marshall, 1992). Figure 22 also shows that sparitic facies generally record lower $\delta^{13}C$ values than micritic facies. The negative values in the upper section exclusively occur in oncoid facies with grainstone or packstone texture (Fig. 22). Samples of the oncoidal packestone contain a large proportion of microspar (Fig. 8F). Studies on cores from the

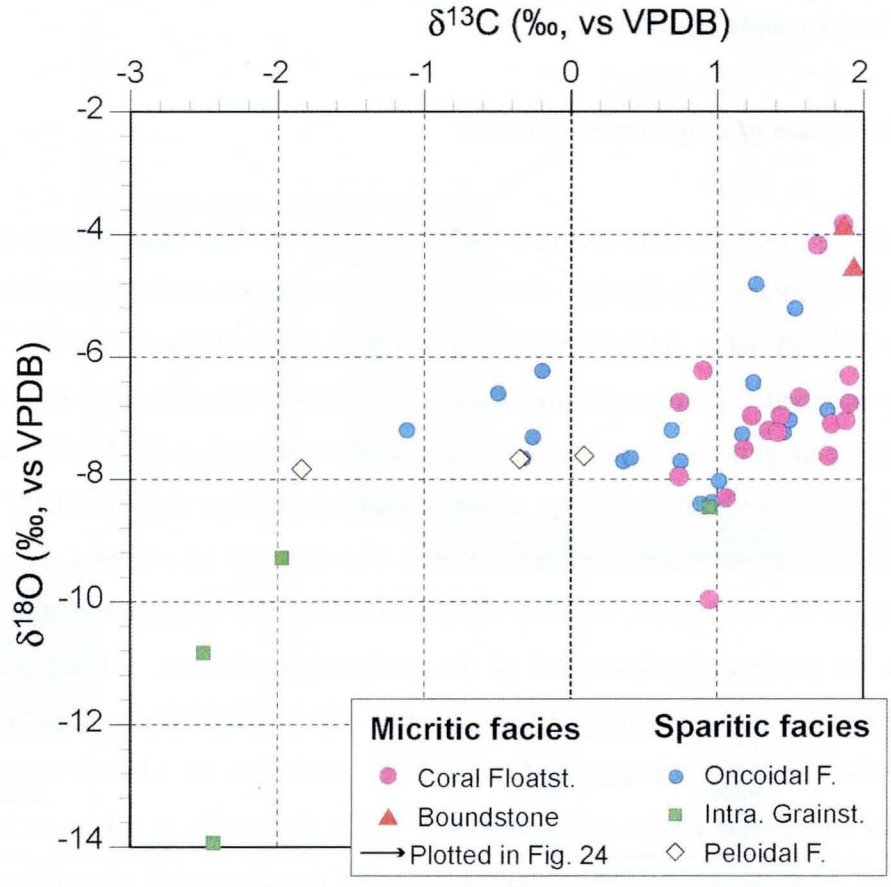

Fig. 22. Cross plot of $\delta^{13}C$ and $\delta^{18}O$ of the different facies of the Koike section.

Pleistocene in the Bahamas and Florida indicate that the equant microspar is produced by burial diagenesis in the mixing zone (Melim et al., 2002; Melim et al., 2004). It has also been suggested that microspar generally records lower $\delta^{13}C$ value than the original micrite (Lasemi and Sandberg, 1984; Melim et al., 2002). Figure 23 shows that samples containing a high percentage of diagenetic components (microspar and sparite) generally display lower values of $\delta^{13}C$.

On the other hand, samples from the micritic facies (coral floatstone and boundstone) show a relatively narrow range in $\delta^{13}C$ (from +0.8 to +2.0‰) and $\delta^{18}O$ (mostly from -8.0 to –4.0‰; Fig. 22), and contain only a small amount of sparite and microspar (Fig. 11A). Based on these data, I only accept the values of coral floatstone and boundstone as initial $\delta^{13}C$ signatures. These show a general increasing trend from 0.7‰ at the bottom to 1.9‰ at the top of the section (Fig. 23).

5.3.1.2. Diagenetic alteration in the other sections

In the Nakanowasa section, all samples have Mn/Sr ratios of the carbonate fraction less

than 2.0 (Table 3), which indicates an insufficient level of diagenetic alteration (Jacobsen and Kaufman, 1999). Lack of distinct correlation on cross-plots of $\delta^{13}C$ and $\delta^{18}O$ (Fig. 24) broadly indicates that influence from freshwater diagenesis was unimportant (Allan and Matthews, 1982; Marshall, 1992). However, seven samples having considerably low values of $\delta^{13}C$ and $\delta^{18}O$ (Fig. 24B) may involved diagenetic alternation, and were therefore excluded from profiles (Fig. 25).

In the Kubokawa section, all samples have Mn/Sr ratios of the carbonate fraction less than 2.0 (Table 4). Lack of distinct correlation on The Cross-plots of $\delta^{13}C$ and $\delta^{18}O$ (Fig. 24B) show an insignificant correlation that indicates high preservation potential of the analyzed specimens. This is consistent to a narrow range in the isotopic values of the 15 samples; +0.7 to +1.6‰ in $\delta^{13}C$ values and -3.1 to -7.5‰ in $\delta^{18}O$ values. There is no sample having the isotopic values diverged largely from other samples (Fig. 24B, Table 4). All $\delta^{13}C$ values of this section were accepted as initial values.

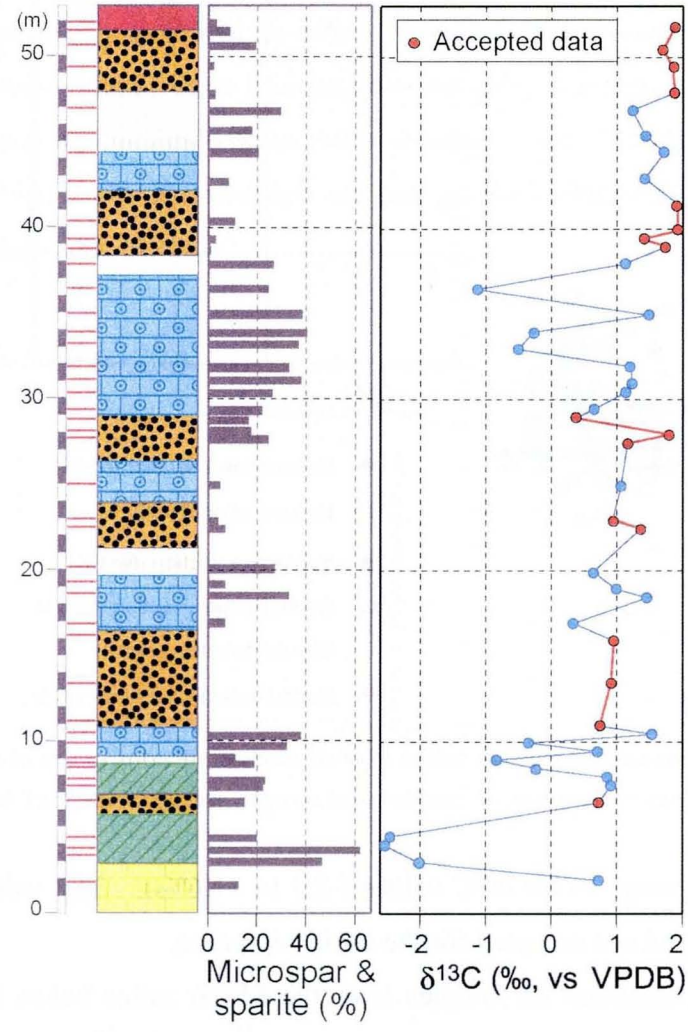

Figure 23. Relation between carbon isotope values and percentage of diagenetic components (microspar and sparite) in the Koike section. Micritic facies (coral floatstone and boundstone) generally recorded higher values that were accepted as initial $\delta^{13}C$ signatures.

In the Shiraishi section, no sample has Mn/Sr ratios of the carbonate fraction more than 2.0 (Table 5), and the correlation between $\delta^{13}C$ and $\delta^{18}O$ values is insufficient (Fig. 24A). These features indicate that diagenetic alternation was not substantial. However, the specimens of this section are characteristic in terms of relatively low $\delta^{18}O$ values (Fig. 24A), and this might be

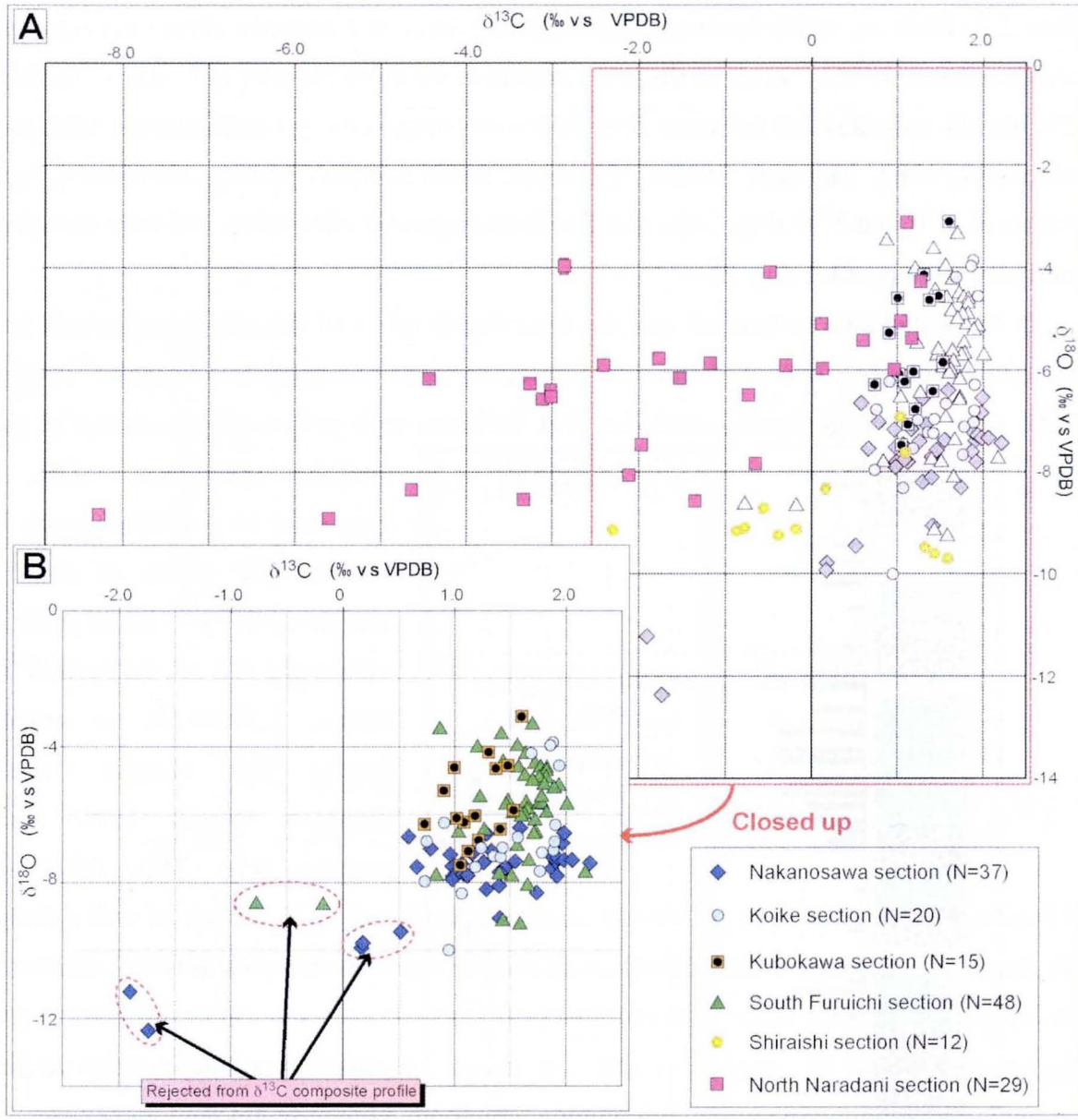

Figure 24. **(A)** Cross-plots of carbon and oxygen isotopic ratios of of all studied sections of the of the Torinosu-type Limestones. **(B)** Closed up cross-plots of carbon and oxygen isotopic ratios of four sections.

responsible for the relatively wide range in the $\delta^{13}C$ values (-2.3 to +1.6‰). The values were likely changed by diagenesis and not accepted for the initial signature.

In the North Naradani section, although all samples have the Mn/Sr ratios below the critical level (2.0) (Table 6), an obvious correlation between $\delta^{13}C$ and $\delta^{18}O$ can be confirmed on cross-plots (Fig. 24A). This trend indicates influence from freshwater diagenesis (Allan and Matthews, 1982; Marshall, 1992). Furthermore, this section shows the largest deviation in $\delta^{13}C$ values ranging from -8.3 to +1.3‰. Samples having low $\delta^{13}C$ values record especially low $\delta^{18}O$ values and relatively high Mn/Sr rations (e.g. at 30m and

113m horizons). Diagenetic alternation is considerable for this section, and I rejected all $\delta^{13}C$ values.

In the South Furuichi section, the Mn/Sr ratios of the samples are all less than 2.0, and even in the lowest level among the 6 analyzed sections (Table 7). Cross-plots of $\delta^{13}C$ and $\delta^{18}O$ show no distinct correlation (Fig. 24) indicating that influence from freshwater diagenesis was unimportant. However, two samples having considerably low values of $\delta^{13}C$ and $\delta^{18}O$ (Fig. 24B) may involved diagenetic alternation, and were therefore excluded.

I conclude that samples of Nakanosawa, Koike, Kubokawa, and South Furuichi sections are highly potential in terms of preservation of the initial $\delta^{13}C$ values. The $\delta^{13}C$-$\delta^{18}O$ cross-plots of these four sections indicates that most of the data are plotted in a relatively narrow domains with in the $\delta^{13}C$-range from 0.5 to 2.2‰ and the $\delta^{18}O$ range from –9 to -3‰. Only six samples are out of the domain and regarded to have received some diagenetic effect.

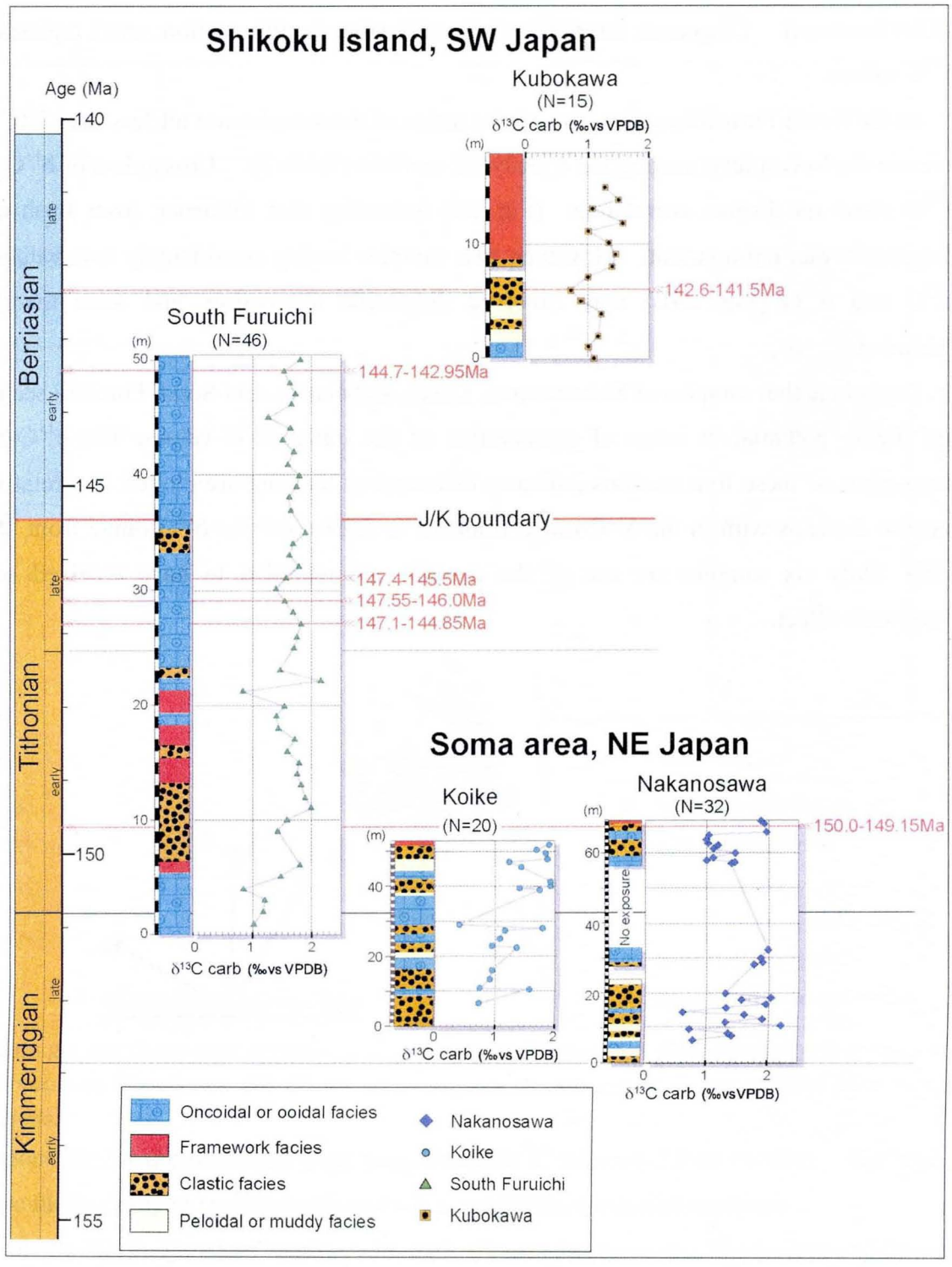

Figure 25. Stratigraphy and carbon isotopic data of the Torinosu-type limestones. Absolute ages of each section were determined by Sr isotopic ratios (Table 1). $\delta^{13}C$ curve of the Koike section is from Kakizaki and Kano (in press). Absolute ages of time units are from Ogg (2004). Symbols as in Figure 24.

5.3.2. Composite $\delta^{13}C$ profile of the Torinosu-type limestones and comparison with Tethyan profile

The accepted $\delta^{13}C$ profiles from the four sections are shown in a relation with the geological age (Fig. 25). The $\delta^{13}C$ values of the two sections of Late Kimmeridgian to Early Tithonian age ranged from +0.5‰ to +2.2‰ and showed fluctuations of ~1‰ amplitude (Fig. 25). Lower values were recorded in the lowest and middle parts of the Koike section and in the lower part of the Nakanosawa section. Higher values occurred in the upper part of the two sections, which are considered to have been deposited contemporaneously (Kakizaki and Kano, 2009). In the coeval part of the South Furuichi section, $\delta^{13}C$ values increased from +0.8‰ to +2.0‰ in the lowest 10 m interval, showing a similar trend with the Koike section. In the rest of the South Furuichi section, $\delta^{13}C$ values were stable in the range of +1.2‰ to +1.9‰, except for two horizons at around 20 m (+0.8‰ and +2.2‰). In the Kubokawa section, carbon isotopic values were stable in a range of +0.7‰ to +1.5‰, with a slight upward-increasing trend.

Results from the four sections provide a continuous $\delta^{13}C$ profile from the Late Kimmeridgian to Late Berriasian (Fig. 26), the first reported from the Palaeo-Pacific province. This profile differs considerably from the Tethyan composite curves of Alpine hemipelagic (Weissert and Erba, 2004) and Alpine shallow-marine carbonates (Padden et al., 2002; Fig. 26). Our profiles are ~1‰ lower than the Tethyan values in late Kimmeridgian but become closer in late Tithonian, when the Tethyan values decrease by 1.0‰ to 1.5‰. In Berriasian, our profiles and the Tethyan profiles almost overlap in the range of +0.7‰ to +1.8‰ (Fig. 26).

5.3.3. Marine carbon cycle and ocean circuation, reconstructed from the $\delta^{13}C$ profile of the Torinosu-type limestones

The Late Jurassic ocean differed substantially from the modern ocean. One of the characteristic fuatures is relatively dense and high-salinity water that was produced in the thalassic Tethys Ocean by strong evaporation at low latitudes and flowed out to the Palaeo-Pacific Ocean, generating a deep-sea flow (Parrish and Curtis, 1982). This water mass is similar to the modern Mediterranean Outflow that inflows to nothern Atlantic (e.g., Kano et al., 2007a), but its magnitude was likely far greater in the case of the Jurassic

Tethys. This outflow must have provided a major driving force to the vertical circulation on an Earth without polar ice caps, and it welled up to the surface mainly along the eastern edge of the Palaeo-Pacific Ocean (Parrish and Curtis, 1982).

Another important feature in the carbon cycle of Late Jurassic to Early Cretaceous was rapid burial rate of organic carbon in the Tethys Ocean. The temporal distribution of oil source rocks (e.g., Middle East, North Sea, and Mexican Gulf Coast) and bituminous sediments (e.g., Kimmeridge clay) peak in the Late Jurassic (Alsharan, 1993; Berner, 2003; Handoh et al., 2003; van Dongen et al., 2006). Organic burial happened mainly in the Tethyan-Atlantic province and was interrupted during the Berriasian. However, in the Palaeo-Pacific no large oil source rock is known from the Late Jurassic.

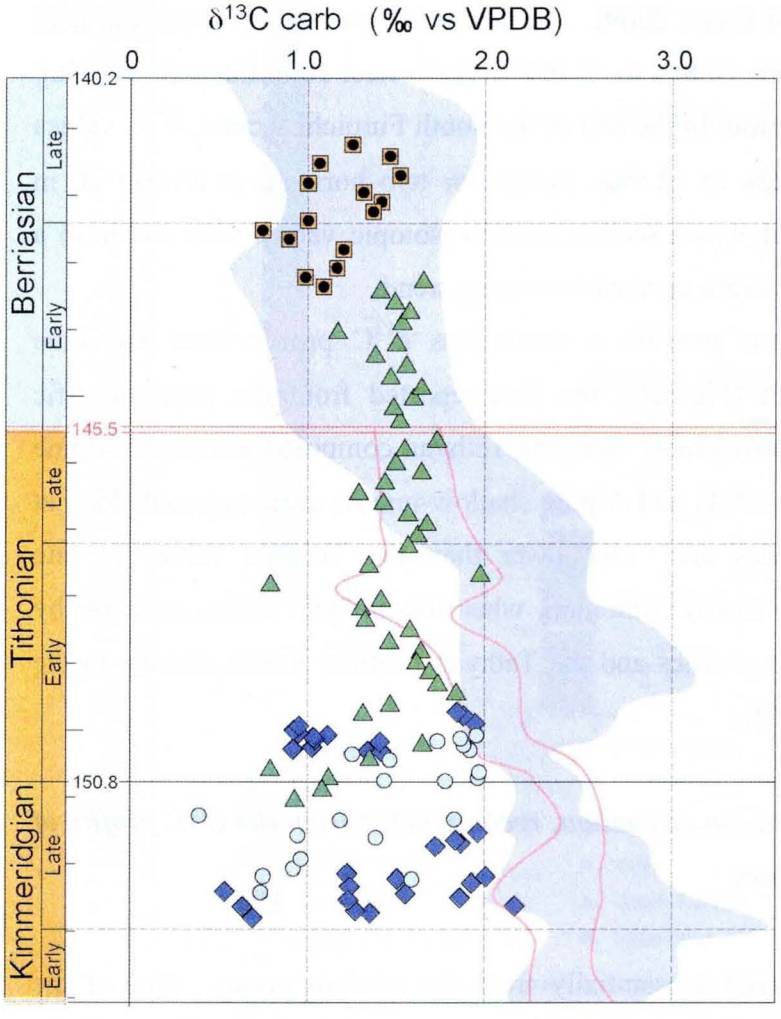

Figure 26. Age plots of carbon isotopic data from four sections of the Torinosu-type limestones. Also shown are a hemipelagic profile (shading; from Weissert and Erba, 2004) and a shallow-marine profile (outline; from Padden et al., 2002) for the Tethyan Ocean. Symbols as in Figure 24.

We propose a model of the changing ocean circulation between the Tethys and Palaeo-Pacific oceans in light of the history of ocean floor spreading from the Kimmeridgian to the Berriasian (Fig. 27). Under the restricted exchange of surface water in the Late Jurassic, organic production and burial were greatly enhanced in the Tethys, where surrounding landmasses provided abundant nutrients. Hence, fixation of ^{13}C-depleted organic carbon likely produced high $\delta^{13}C$ values of DIC in the Tethys. In contrast, carbon fixation was not substantial in the less eutrophic

Palaeo-Pacific, and deep water with lowered $\delta^{13}C$ values was supplied there through upwelling.

This discrepancy in $\delta^{13}C$ values was entirely lost in the Early Berriasian, possibly related to changes in the global ocean circulation that homogenized the carbon isotopes. Two noteworthy geologic events related to exchange of surface water happened in this period. One is expansion of the Hispanic Corridor in the middle proto-Atlantic, which connected the western Tethys to the Palaeo-Pacific. Opening of the Hispanic corridor began in the Early Jurassic (at least Pliensbachian) and triggered interoceanic traffic of ostracodes and ammonoids (e.g., Arias, 2007), and subsequent ocean spreading expanded the corridor (Scotese, 2001; Stampfli and Borel, 2002). The other event is the opening of the Mozambique Corridor connecting the southern Tethys and the southeastern Palaeo-Pacific. Distributions of marine bivalves and marine deposits indicate that this opening happened during the Tithonian (Riccardi, 1991).

Establishment of these two corridors generated dynamic oceanic circulation (Fig. 27B). During the Berriasian, the Tethys joined the global circulation, and marine productivity and organic burial were decreased owing to depleted nutrients and more active exchange of surface water, respectively. As a result, the difference in $\delta^{13}C$ values between the Tethys and Palaeo-Pacific declined. The greater exchange of surface water also decreased formation of high-salinity water in the Tethys and likely weakened the density-driven vertical circulation. The first OAE in the Cretaceous (the Weissert Event of Erba et al., 2004) happened in the Valanginian, possibly related to the weakened circulation and oxygen supply in the deep sea.

Stability in $\delta^{13}C$ values (+0.5‰ to +2.2‰) recorded in the Torinosu-type limestones was the trend in the Palaeo-Pacific, which can thus be regarded as the global trend. The higher values in the Tethys were possibly local signals reflecting rapid burial rate of organic carbon. Late Jurassic to Early Cretaceous ocean models, reconstructed mainly from Tethyan records, should be revised on the basis of Palaeo-Pacific records. More carbonate data are needed from the Palaeo-Pacific Ocean to improve our understanding of the carbon cycle and ocean circulation during this greenhouse epoch and the origin of OAEs.

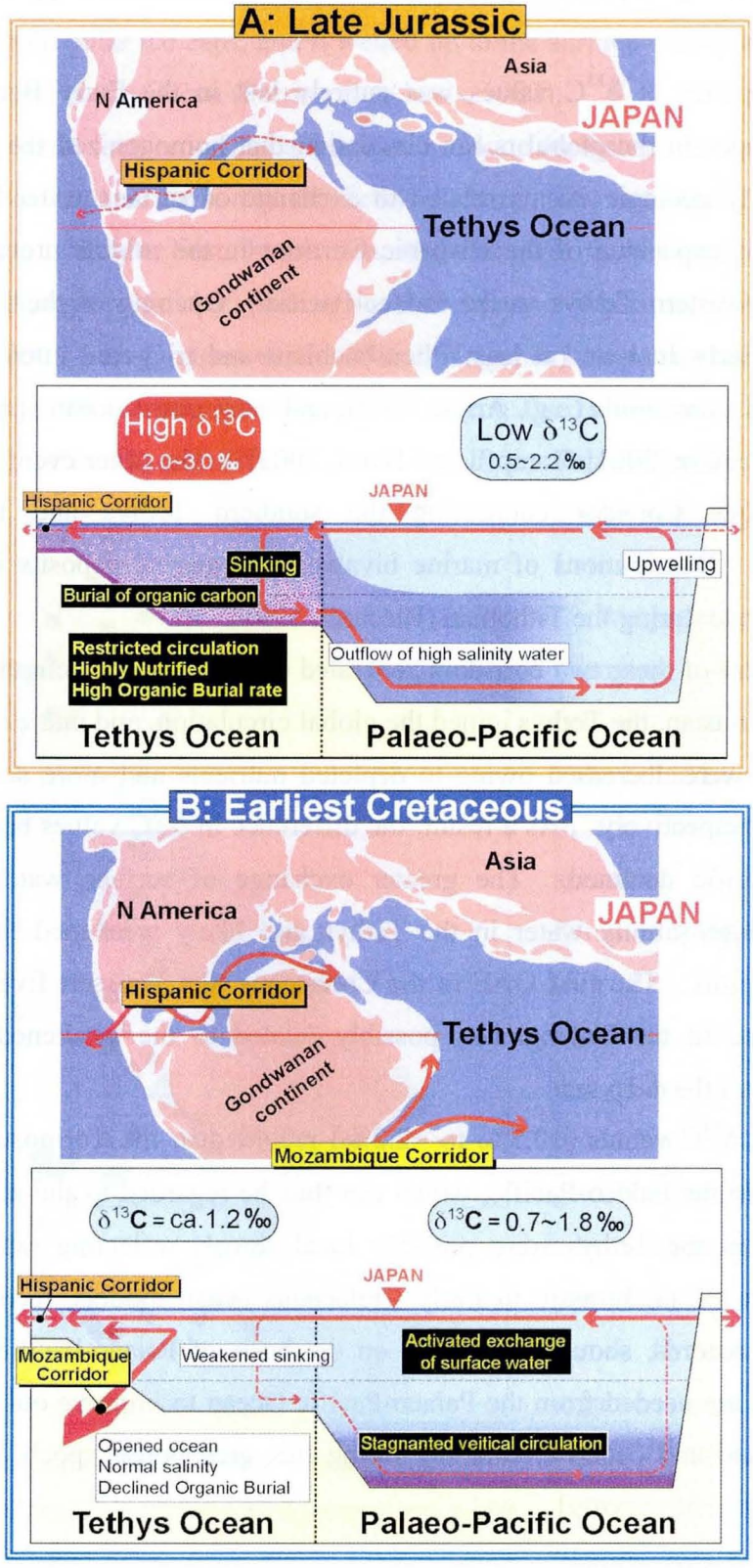

Figure 27. Schematic mid-Mesozoic ocean circulation reconstructed from $\delta^{13}C$ profiles : **(A)** Late Kimmeridgian to Early Tithonian. **(B)** Berriasian.

Chapter #6. CONCLUSIONS

In general, chemostratgraphy has been applied for two different purposes; 1) correlation between the stratigraphic sections, and 2) recognition of the important biological and climatic events. The former purpose was in my mind when I started my PhD study, but now I am realizing the global oceanographic picture hidden in the chemostratigraphy of the Torinosu-type limestone by the end of the five-year study in Hiroshima University. Sporadic and discontinuous occurrence is probably the consequence of the limestone developed in a forearc basin along an active margin, but in another hand has discouraged researchers to deal with the chemostratigraphy. However, the data accumulated from several sections of the Torinosu-type limestones succeeded to construct a continuous record from Kimmeridgian to Berriasian, first from East Asia as well from the Palaeo-Pacific. This thesis revised the previous picture that has been demonstrated based on the data from the Tethys region, and provided insights into the global change during a period when the Earth was coming into its warmest status in the last 600 million years. For the fulfilling palaeoceanographic discussion, different sources of bricks (stratigraphy, lithology, diagensis, strontium, and carbon isotopic compositions) piled up one by one as summarized in the following paragraphs.

1) Sedimentological investigation is a principle requirement in prior to chemostratigraphy. The thesis represented the results in details for the Koike Limestone of the Soma-Nakamura Group.

   Microfacies analysis of the five sections recognized six sedimentary facies of the limestone: sandy limestone, intraclastic grainstone, coral floatstone, peloidal wacke–grainstone, oncoidal facies, and boundstone (Figs. 6 and 8).

   Two types of boundstone are recognized. One is a reefal build-up facies formed by corals, stromatoporoids, and microencrusters, and occurs only in the two southern sections (Koike and Tatenosawa). The other is microbial bindstone, dominated by *Pycnoporidium lobatum* and *Marinella lugeoni*, and observed in the northernmost section (Nakanosawa; Figs. 6 and 9).

   The spatial variation in compositions and textures between the five studied sections shows that the carbonate platform of the Koike Limestone Member generally deepened

to the north (Fig. 19). Occurrence of *in-situ* corals is mostly restricted in the southernmost Kakusawa section, and coral abundance decreases to the north. The deepening-northward trend is confirmed by the texture of the oncoidal facies, which changes from grainstone in the south to pack-wackestone in the north (Fig. 6).

The Koike section displays cycles consisting of coral floatstone, oncoidal packstone–grainstone, and peloidal wacke–grainstone, in ascending order. The upward-fining trend of each cycle indicates a decrease in water energy, which resulted from rising relative sea-level or from restriction of wave and current energy (Fig. 10).

The $\delta^{13}C$ values of the Koike Limestone Member showed a general increasing upward trend from +0.7 to +1.9‰ (Fig. 17). Marked negative excursions from the overall trend with values ranging from –2.5 to +0.5‰ are recorded from sparitic facies and likely result from diagenetic alteration (Figs. 22 and 23).

Excluding the data from sparitic facies, the $\delta^{13}C$ values of the Koike Limestone Member are 1.0-1.5 ‰ lower than those from the Tethyan shallow-marine carbonates of Late Kimmeridgian age. An explanation for this difference may be that marine organic productivity and organic burial rate were higher in the Tethys Ocean than in the western Palaeo-Pacific. The difference almost disappears in the upper part of the section that was deposited during Early Tithonian.

2) I measured $^{87}Sr/^{86}Sr$ ratios in order to assign the depositional ages of the Torinosu-type limestones, because detailed temporal data were needed for inter-regional correlation of limestone sections and for making a composite carbon isotopic profile. It is fortunate that the marine $^{87}Sr/^{86}Sr$ ratios had been continuously increasing, and therefore a certain ratio obtained from the Torinosu-type limestone can be assigned to a specific age range (Fig. 21). Based on the evaluated ages, I found that the temporal frequency of the carbonate deposition was related with the global palaeoceanographic events, such as change in the sea-level, the primary production, and seawater chemistry, and potentially with tectonics on the active margin.

The ages were estimated by the $^{87}Sr/^{86}Sr$ ratio of 22 brachiopods that has a high preservation potential due to the low-Mg calcite mineralogy. The evaluated ages from five sections of the Torinosu-type limestone, are consistent with the previous

biostratigraphy and even better in terms of the time-resolution.

The oldest age that was obtained from the Nakanosawa section (the Koike Limestone Member) indicates late Kimmeridgian to the early Tithonian (Fig. 18), limestones of the three sections (Kubokawa, North Naradani, and South Furuichi) were assigned to the age ranging from the late Kimmeridgian to the late Berriasian (Figs. 11, 14, and 16). The youngest age identified in this study was the Hauterivian, estimated for the Shiraishi section (the Nankai Group: Fig. 13).

The period of deposition of the Nakanosawa and Shiraishi sections are correlated to high-stand or transgressive stage in the global eustatic trend. Other three limestone bodies (Kubokawa, North Naradani, and Nakatsugawa) were deposited during a general decline of the sea level (Fig. 29).

I measured carbon and oxygen isotopic values, and Mn/Sr ratios in 6 sections where Sr isotopic ages were obtained. From late Kimmeridgian to early Tithonian, carbon isotopic values ranged from -2.5 to +1.9‰ in the Koike section (Fig. 17), and ranged -1.9 to +2.2‰ in the Nakanosawa sections (Fig. 18). Carbon isotopic values ranged from -8.3 to +1.3‰ in the North Naradani section from late Kimmeridgian to late Berriasian (Fig. 14), from -0.8 to +2.2‰ in the South Furuichi section from late Kimmeridgian to early Berriasian (Fig. 16), from +0.7 to +1.6‰ in the Kubukawa section from early to late Berriasian (Fig. 11), from -2.3 to +1.6‰ in the Shiraishi section of Hauterivian (Fig. 13).

These profiles apparently record several negative anomalies that have never been reported from other stratigraphic sections of the relevant age. The anomalies could be the diagenetic origin, and I carefully consider the effect of diagenetic alteration, by using $\delta^{13}C$-$\delta^{18}O$ cross-plots (Figs. 24) and Mn/Sr ratios. I recognized that specimens having low $\delta^{13}C$ also brought low $\delta^{18}O$, and such specimens were likely subjected to a substantial diagenetic alternation. In summary, I concluded that carbon isotopic values of all specimens from the North Naradani and the Shiraishi sections, and several specimens from the Nakanosawa and the South Furuichi sections are heavily altered by fresh water diagenesis. After excluding these data, I constructed the composite carbon isotopic profile of the Torinosu-type limestone from late Kimmeridgian to late

Tithonian (corresponding to ca. 12-m.y.-interval; Fig. 25).

The composite carbon isotopic profile of the Torinosu-type limestones was stable in the range from +0.5‰ to +2.2‰ throughout the period, and largely differs from the Tethyan profile (Fig. 26). From the Late Kimmeridgian to the Early Tithonian, the Palaeo-Pacific carbon isotopic values are ca. 1.0‰ lower than the Tethyan values. This difference is consistent with rapid burial rate of organic carbon in the Tethys and restricted interoceanic exchange of surface water during Late Jurassic (Fig. 27A). Then, development of the Hispanic and Mozambique corridors strengthened exchange of surface seawater and weakened the density-driven vertical circulation, erasing the interregional difference in $\delta^{13}C$ values (Fig. 27B).

In this thesis, I could have provided a new $\delta^{13}C$ profile of the mid-Mesozoic age from western Palaeo-Pacific Ocean that occupied more than 80% of the world sea surface. The Late Jurassic to the Early Cretaceous oceanography that has been reconstructed mainly by the Tethyan records should be revised using the Paleo-Pacific records. Studies of carbonates deposited in the Paleo-Pacific Ocean, which are still fragmentary up to now, need more attention in order to improve our understanding on carbon cycle and ocean circulation during this greenhouse epoch and on origin of OAEs.

ACKNOWLEDGEMENTS

My thanks are expressed to Associate Professor Takami Miyamoto (Hiroshima University) and Professor Akihiro Kano (Kyushu University) for their magnificent supervision and encouragement during my five-year study in Department of Earth and Planetary Systems Science, Hiroshima University. I thank people in the department including Professors Hiroshi Shimizu, Toshihiko Shimamoto, Fumiko Tajima, Ryuji Kitagawa and Hiroshi Hidaka who provided useful suggestions and improved my doctor thesis. I express my thanks to Professor Atsushi Matsuoka (Niigata University) for his helpful advice when I have started studying the Torinosu-type limestone.

My thesis would never be completed without supports from the following people; Fumito Shiraishi (Kyushu University) for his constructive comments and suggestion; Dr. Tsuyoshi Ishikawa, Dr. Masaharu Tanimizu (JAMSTEC), Dr. Kazuya Nagaishi, Dr. Jun Matsuoka (Marine Works Japan), and Dr. Masafumi Murayama (Kochi University) for their help in analyzing Sr isotope performed during the cooperative research program (No. 06B011, 07A003, and 07B003) at the Center for Advanced Marine Core Research (CMCR); Yoshihiro Shibata and Hayami Ishisako (Hiroshima University) for their technical support; Dr. Masako Hori, Tetsuhiro Togo, Sho Takeuchi (Hiroshima University), Noriko Kawagoe (WOOD ONE Ltd.), Kazuto Ohmori (Hokkaido University), and Masanori Katagishi (Kyushu University) for joining laboratory and fieldworks. My science was substantially improved by discussion with Professor André Strasser (Fribourg University), Professor Helmut Weissert (ETH Zurich), Mr. Shin-ichi Sano (Fukui Prefectural Dinosaur Museum), Professor Itsuro Kita, Professor Yasuhito Osanai (Kyushu University) and Professor Yasufumi Iryu (Nagoya University). My activity was financially supported by Grand-in-Aid of the Fukada Geological Institute during 2007, and Hiroshima University Support Programs for Improving Graduate School Education during 2007 and 2008.

Finally, I would like to express my sincere thanks to my parents who have continuously offered me unstinted assistance and affection over 27 years.

REFERENCES CITED

Aita, Y., and Okada, H., 1986, Radiolarians and calcareous nannofossils from the uppermost Jurassic and Lower Cretaceous strata of Japan and Tethyan regions. Micropalaeontology, v. 32, p. 97-128.

Allan, J.R., and Matthews, R.K., 1982, Isotope signatures associated with early meteoric diagenesis. Sedimentology, v. 29, p. 797–817.

Aguirre-Urreta, A.B., Price, G.D., Ruffel, A.H., Lazo, D.G., Kalin, R.M., Ogle, N., and Rawson, P.F., 2008, Southern Hemisphere Early Cretaceous (Valanginian-Early Barremian) carbon and oxygen isotope curves from the Neuquen Basin, Argentina. Cretaceous Research, v. 29, p. 87-99.

Alsharan, A.S., 1993, The Jurassic of the Arabian Gulf Basin: Their facies, depositional setting and hydrocarbon habitat. Annual Convention of Cannadian. Society of Petroleum Geologists Abstracts. Cannadian Society of Petroleum Geollogists. Calgary, Canada, p. 3.

Arias, C., 2007, Pliensbachian–Toarcian ostracod biogeography in NW Europe: Evidence for water mass structure evolution. Palaeogeography Palaeoclimatology Palaeoecology, v. 251, p. 398-421.

Arp, G., Reimer, A., and Reitner, J., 2001, Photosynthesis-Induced Biofilm Calcification and Calcium Concentrations in Phanerozoic Oceans. Science, v. 292, p. 1701-1704.

Berner, R. A., 2003, The long-term carbon cycle, fossil fuels and atmospheric composition. Nature, v. 426, p. 323-326.

Bralower, T.J., Monechi S., and Thierstein, H.R., 1989. Calcareous Nannofossil Zonation of the Jurassic-Cretaceous Boundary Interval and Correlation with the Geomagnetic Polarity Timescale. Marine Micropalaeontology, v. 14, p. 153-235.

Brand, U., and Veizer, J., 1980, Chemical diagenesis of a multicomponent carbonate system-1: trace elements. Journal of Sedimentary Petrology, v. 50, p. 1219-1236.

Brand, U., 1991, Strontium isotope diagenesis of biogenic aragonite and low-Mg calcite. Geochimica Cosmochimica Acta, v. 55 (2), p. 505-513.

Channell, J.E.T., Erba, E., and Lini, A., 1993, Magnetostratigraphic calibration of the Late Valanginian carbon isotope event in pelagic limestones from Northern Italy and Switzerland. Earth and Planetary Science Letters, v. 118, p. 145-166.

Dunham, R.J., 1962, Classification of carbonate rocks according to depositional texture.

Memoir of American Association of Petroleum Geologists, v. 1, p. 108–121.

Dunham, R.J., 1962, Classification of carbonate rocks according to depositional texture. Memoir of American Association of Petroleum Geollogists, v. 1, 108–121.

Edmond, J.M., 1992, Himalayan tectonics, weathering processes and the strontium isotope record in marine limestone. Science, v. 258, p. 1594-1597.

Eguchi M., 1951, Mesozoic hexacorals from Japan. Science Report of Tohoku University 2nd series, v. 24, p. 1-96.

Eguchi, M, and Shoji, R., 1965, Sedimentary environments of the Jurassic Limestone in the Kashima-machi, Fukushima Prefecture, Japan. Journal of the Geological Society of Japan, v. 71, p. 237-246. (in Japanese, with English Abstract)

Elderfield, H., 1986, Strontium isotope stratigraphy. Palaeogeography Palaeoclimatology Palaeoecology, v. 57 (1), p. 71-90.

Embry, A.F., and Klovan, J.E., 1972, Absolute water depth limits of late Devonian paleoecological zones. Geologische Rundschau, v. 61, p. 672-686.

Erba, E., Bartolini, A., and Larson, R.L., 2004, Valanginian Weissert oceanic anoxic event. Geology, v. 32, p. 149-152.

Erba, E., 2006, The first 150 million years history of calcareous nannoplankton: Biosphere - geosphere interactions. Palaeogeography Palaeoclimatology Palaeoecology, v. 232 (2-4), p. 237 – 250.

Flügel, E., 2004, Microfacies of Carbonate Rocks, Analysis, Interpretation and Application. Springer, Berlin. 976p.

Fukuda, S., 1984, Geological study on the Torinosu-type limestone along Ohtani River, Futami Hon-cho, Yatsushiro City. Journal of Kumamoto Earth Science Society, v. 75, p. 2-15.

Gröcke, D.R., Price, G.D., Ruffel, A.H., Mutterlose, J., Baraboshkin, E., 2003, Isotopic evidence for Late Jurassic-Early Cretaceous climate change. Palaeogeogrraphy Palaeoclimatology Palaeoecology, v. 202(?), p. 97-118.

Harada, T., 1890, Die japanische Inseln. Geological Survey of Japan. 126p.

Hayami, I., 1962, Jurassic pelecypod faunas in Japan with special reference to their stratigraphical distribution and biogeographical provinces. Journal of the Geological Society of Japan, v. 68, p. 96-108. (in Japanese with English Abstract)

Handoh, I.C., Bigg, G.R., and Jones, E.J.W., 2003, Evolution of upwelling in the Atlantic Ocean basin. Palaeogeography Palaeoclimatology Palaeoecology, v. 202, p. 31-58.

Haq, B.U., Hardenbol, J., Vail, P.R., 1987, Chronology of Fluctuating Sea levels Since the Triassic. Science, v. 235, p. 1156-1167.

Igarashi, T, and Fujinuki, T., 1972, The impure minerals and trace components of the Soma limestone, Fukushima Prefecture. Journal of the Sedimentological Society of Japan, v. 8, p. 2-7. (in Japanese)

Imaizumi, R., 1965, Late Jurassic algae from Honshu and Shikoku, Japan. Science Report of Tohoku University 2nd series, v. 37, p. 49-62.

Ito, T., 1993, Sr isotope stratigraphy of Cenozoic seawater: An evaluation of published seawater Sr isotopic data. Journal of the Geological Society of Japan, v. 99, p. 739-753 (in Japanese with English Abstract).

Jacobsen, S.B., and Kaufman, A.J., 1999, The Sr, C and O isotopic evolution of Neoproterozoic seawater. Chemical Geology, v. 161, p. 37-57.

Jenkyns, H.G., Jones, C.E., Gröcke, D.R., Hesselbo, S.P, and Parkinson, D.N., 2002, Chemostratigraphy of the Jurassic System: applications, limitations and implications for palaeoceanography. Journal of the Geological Society in London, v. 159, p. 351-378.

Jones, C.E., Jenkyns, H.C., Angela, L.C., Hesselbo, S.P., 1994, Strontium isotopic variations in Jurassic and Cretaceous seawater. Geochimica et Cosmochimica Acta, v.58 (14), p.3061-3074.

Kakizaki, Y., and Kano, A., 2009, Architecture and chemostratigraphy of Late Jurassic shallow marine carbonates in NE Japan, western Paleo-Pacific, Sedimentary Geology, 214, 49-61.

Kano, A., 1988. Facies and Depositional Conditions of a Carbonate Mound (Tithonian-Berriasian, SW-Japan). Facies, v. 18, p. 27-47.

Kano, A., and Jiju, K., 1995, The Upper Jurassic-Lower Cretaceous carbonate-terrigenous succession and the development of the carbonate mound in Western Shikoku, Japan. Sedimentary Geology, v. 99, p. 165-178.

Kano, A., Kambayashi, T., Fujii, H., Matsuoka, J., Sakura, K., and Ihara, T., 1999, Seasonal variation in water chemistry and hydrological conditions of tufa deposition of Shirokawa, Ehime Prefecture, southwestern Japan. Journal of the Geological Society of Japan, v. 105, p. 289-304.

Kano, A., Ferdelman, T.G., Williams, T., Henriet, J.-P., Ishikawa, T., Kawagoe, N., Takashima, C., Kakizaki, Y., Abe, K., Sakai, S., Browning, E.L., Li, X. and The IODP

Expedition 307 Scientists, 2007a, Age constraints on the origin and growth history of a deep-water coral mound in NE Atlantic drilled in IODP Expedition 307. Geology, v. 35, p. 1051-1054.

Kano, A., Kakizaki, Y., Takashima, C., Wang, W. and Matsumoto, R., 2007b, Facies and depositional environment of the uppermost Jurassic stromatoporoid biostromes in the Zagros Mountains of Iran. GFF, v. 128, p. 107-122.

Kashiwagi, K., Yamagiwa, N., Yao, A., Ezaki, Y., Sakaori, Y., and Shoji, Y., 2002. Late Jurassic cridanian and poriferan fossils from the Torinosu-type limestones in the Kurosegawa Terrane, western Kii Peninsula, Southwest Japan and their geological significance. Fossil, v. 72, p. 5-16 (in Japanese with English Abstract).

Kiessling, W., 2001, Phanerozoic reef trends based on the paleoreef database. In, Stanley, G. D. Jr. ed. The History and Sedimentology of Ancient Reef Systems. Topics in Geology, v. 17, Kluwer Academic /Plenum Publishers, p. 41-88.

Kimura, T., 1953, The origin of pyrite in the Nakanosawa Formation. Journal of Earth Science, Nagoya University, v. 1, p. 35-41.

Kimura, T., 1956, Stratigraphy and limeston of the Torinosu Group. Journal of the Geological Society of Japan, v. 62, p. 515-526.

Kiyama, O., and Iryu, Y., 1998, Sedimentation of the Upper Jurassic Koike Limestone, Somanakamura district, northeastern Japan. Journal of the Sedimentological Society of Japan, v. 47, p. 17–31 (in Japanese with English Abstract).

Kozai, T., Ishida, K., and Kondo, Y., 2004, Radiolarian ages and bivalve fauna of the Birafu Formation, Central Shikoku. News of Osaka Micropaleontologists, Special volume 13, p. 149-165 (in Japanese with English Abstract).

Lasemi, Z., and Sandberg, P.A., 1984, Transformation of aragonite-dominated lime muds to microcrystalline limestones. Geology, v. 12, p. 420-423.

Leinfelder, R.R., Krautter, M., Laternser, R., Nose, M., Schmid, D.U., Schweigert, G., Werner, W., Keupp, H., Brugger, H., Herrmann, R., Rehfeld-Kiefer, U., Schroeder, J.H., Reinhold, C., Koch, R., Zeiss, A., Schweizer, V., Christmann, H., Menges, G., and Luterbacher R., 1994, The Origin of Jurassic Reefs: Current Research Developments and Results. Facies, v. 31, p. 1-56.

Leinfelder, R.R., Schmid, D.U., Nose, M., and Werner, W., 2002, Jurassic reef patterns - the expression of a changing globe. In: Kiessling, W., Flügel, E. and Golonka, J. (Eds.), Phanerozoic Reef Patterns. SEPM (Society for Sedimentary Geology) Special

Publication 72, SEPM, Tulsa, OK, p. 465-520.

Matsuoka, A., 1992, Jurassic-Early Cretaceous tectonic evolution of the Southern Chichibu terrane, southwest Japan. Palaeogeography Palaeoclimatology Palaeoecology, v. 96, p. 71-88.

Matsuoka, A., Yamakita, S., Sakakibara, M., Hisada, K., 1998, Unit division for the Chichibu Composite Belt from a view point of accretionary tectonics geology of western Shikkoku, Japan. Journal of the Geological Society of Japan, v. 104, p. 634-653 (in Japanese with English Abstract).

Marshall, J.D., 1992, Climatic and oceanographic isotopic signals from the carbonate rock record and their preservation. Geological Magazine, v. 129, p. 143-160.

Maruyama, S., and Seno, T., 1986, Orogeny and relative plate motions: example of the Japanese islands. Tectonophysics, v. 127, p. 305-329.

McArthur, J.M., Haworth, R.J., and Baily, T.R., 2001, Strontium isotope stratigraphy: LOWESS version 3: best fit to the marine Sr- isotope curve for 0-509 Ma and accompanying look-up table for deriving numerical age. Journal of Geology, v. 109, p. 155-170.

Melim, L.A., Westpal, H., Swart, P.K., Eberli, G.P., and Munnecke, A., 2002, Questioning carbonate diagenetic paradigms: evidence from the Neogene of the Bahamas. Marine Geology, v. 185, p. 27-53.

Melim, L.A., Swart, P.K., and Eberli, G.P., 2004, Mixing-zone diagenesis in the subsurface of Florida and the Bahamas. Journal of Sedimentary Research, v. 74, p. 904-913.

Metelkin D.V., Gordienko I.V., and Klimuk, V.S., 2007, Paleomagnetism of Upper Jurassic basalts from Transbaikalia: new data on the time of closure of the Mongol-Okhotsk Ocean and Mesozoic intraplate tectonics of Central Asia. Russian Geology and Geophysics, v. 48, p. 825–834.

Minoura, K., 1985, Where did Kitakami and Abukuma come from? Kagaku, v. 55, p. 14-23 (in Japanese).

Mori, K., 1963, Geology and paleontology of the Jurassic Somanakamura Group, Fukushima Prefecture, Japan. Science Reports of Tohoku University 2nd series, v. 35, p. 33-65.

Morino, Y., Kozai, T., Wada, T., and Tashiro, M., 1989, On the Lower Cretaceous Birafu Formation including the torinosu type limestone in the Monobe area, Kochi Prefecture. Research Reports of Kochi University, v. 38, p. 73-83 (in Japanese with English

Abstract).

Morino, Y., 1992, Depositional environments of Upper Jurassic Koike Limestone. Journal of the Sedimentological Society of Japan, v. 37, p. 122-124 (in Japanese).

Morino, Y., 1993, Depositional environments of the Lower Cretaceous Torinosu type limestone in the Monobe area, Kochi Prefecture. Journal of Geological Society of Japan v. 99, p. 173-183 (in Japanese with English Abstract).

Ogg, J.G., 2004, The Jurassic Period. In: Gradstein, F.M., Ogg, J.G., Smith, A.G., Agterberg, F.P., Bleeker, W., Cooper, R.A., Davydov, V., Gibbard, P., Hinnov, L.A., House, M.R., Lourens, L., Luterbacher, H.P., McArthur, J., Melchin, M.J., Robb, L.J., Shergold, J., Villeneuve, M., Wardlaw, B.R., Ali, J., Brinkhuis, H., Hilgen, F.J., Hooker, J., Howarth, R.J., Knoll, A.H., Laskar, J., Monechi, S., Plumb, K.A., Powell, J., Raffi, I., Röhl, U., Sadler, P., Sanfilippo, A., Schmitz, B., Shackleton, N.J., Shields, G.A., Strauss, H., Van Dam, J., van Kolfschoten, T., Veizer, J., and Wilson, D., (Eds.), A Geologic Time Scale 2004. Cambridge University Press, Cambridge, UK, 307-343p.

Olesger, D., 1991, Subtidal carbonate cycles: Implications for allocyclic vs. autocyclic controls. Geology, v.19, p. 917-920.

Opdyke, B.N. and Wilkinson, B.H., 1988, Surface area control of shallow cratonic to deep marine carbonate accumulation. Paleoceanography, v. 3, p. 685-703.

Opdyke, B.N. and Wilkinson, B.H., 1990, Paleolatitude distribution of Phanerozoic marine ooids. Palaeogeography Palaeoclimatology Palaeoecology, v. 78, p. 135-148.

Padden, M., Weissert, H., Funk, H., Schneider, S., and Gansner, C., 2002, Late Jurassic lithological evolution and carbon-isotope stratigraphy of the western Tethys. Eclogae Geologicae Helvetiae, v. 95, p. 333–346.

Parrish, J., and Curtis, R.J., 1982, Atmospheric circulation, upwelling and organic-rich rocks in the Mesozoic and Cenozoic Eras, Palaeogeography Palaeoclimatology Palaeoecology, v. 40, p. 31-66.

Philip, J., 2003, Peri-Tethyan neritic carbonate areas: distribution through time and driving resultors. Palaeogeography Palaeoclimatology Palaeoecology, v. 196, p. 19-37.

Read, J.F., 1985, Carbonate platform facies models. Bulletin of American Association of Petroleum Geologists, v. 69, p. 1-21.

Ren, J., Tamaki, K., Li, S., and Junxia, Z., 2002, Late Mesozoic and Cenozoic rifting and its dynamic setting in Eastern China and adjacent areas. Tectonophysics, v. 344, p. 175–205.

Riccardi, A.C., 1991, Jurassic and Cretaceous marine connections between the Southeast Pacific and Tethys. Palaeogeography Palaeoclimatology Palaeoecology, v. 87, p. 155-189.

Riding, R., 1992, Temporal variation in calcification in marine cyanobacteria. Journal of Geological Society London, v. 149, p. 979-989.

Roth, P.H., 1987, Mesozoic calcareous nannofossil evolution: related to paleoceanographic events. Paleoceanography, v. 2, p. 601-611.

Sato, T., 1962, Études biostratigraphiques des ammonites du Jurassique du Japon. Mémoires Société Géologique de France nouvelle Série, n. 94, p. 1-122. (in French)

Sato, T., Taketani, Y., Suzuki, C., Yamaki, Y., Taira, M., Ara, Y., Aita, Y., and Furukawa, Y., 2005, Newly collected ammonites from the Jurassic-Cretaceous Somanakamura Group. Bulletin of Fukushima Museum v. 19, p. 1-41 (in Japanese).

Sato, T., and Taketani, Y., 2008, Late Jurassic to Early Cretaceous ammonite fauna from the Somanakamura Group in Northeast Japan. Palaeontological Research, v. 12, p. 261-282.

Savard, M.M., Veizer, J., Hinton, R., 1995, Cathodoluminescence at low Fe and Mn concentrations : a SIMS study of zones in natural calcites. Journal of Sedimentary Research, v. 1, p. 208-213.

Scotese, C.R., 2002, PALEOMAP website: http://www.scotese.com (December, 2008).

Scott, R.W, 1988, Evolution of Late Jurassic and Early Cretaceous reef biotas. Palaios, v. 3, p. 184-193.

Shikama, T., Yui, S., 1973, On some Nerineid gastropoda in Japan (preliminary report). Science Report of Yokohama National University, Section 2, v. 21, p. 9-69.

Shiraishi, F., and Kano, A., 2004, Composition and spatial distribution of microencrusters and micro crusts in upper Jurassic-lowermost Cretaceous reef limestone (Torinosu limestone, southwest Japan). Facies, v. 50, p. 217-227.

Shiraishi, F., Hayasaka, Y., Takahashi, Y., Tanimizu, M., Ishikawa, T., Matsuoka, A., Murayama, M., and Kano, A., 2005, Strontium isotopic age of the Torinosu Limestone in Niyodo Village, Kochi Prefecture, SW Japan. Journal of the Geological Society of Japan, v. 111, p. 610-623 (in Japanese with English Abstract).

Shiraishi, F., and Yoshidomi, K., 2005, Depositional environment of the upper Jurassic-lower Cretaceous reef limestone in western Yamaguchi Prefecture, Southwest

Japan. Journal of the Geological Society of Japan, v. 111, p. 21-28 (in Japanese with English Abstract).

Strasser, A., Pittet, B., Hillgärtner, H., and Pasquier, J.B., 1999, Depositional sequences in shallow carbonate-dominated sedimentary systems: concepts for a high-resolution analysis. Sedimentary Geology, v. 128, p. 201-221.

Stampfli, G.M., and Borel, G.D., 2002, A plate tectonic model for the Paleozoic and Mesozoic constrained by dynamic plate boundaries and restored synthetic oceanic isochrones. Earth and Planetary Science Letters, v. 196, p. 17-33.

Stanley, S.M., Hardie, L.A., 1999, Secular oscillations in the carbonate mineralogy of reef-building and sediment-producing organisms driven by tectonically forced shifts in seawater chemistry. Palaeogeography Palaeoclimatology Palaeoecology, v. 144, p. 3-19.

Takei, M., and Matsuoka, A., 2004, Mega fossil-bearing mudstone blocks in the Oriai Formation of the Upper Jurassic Imaidani Group in the Shirokawa area, Ehime Prefecture, Southwest Japan. Journal of the Geological Society of Japan, v. 110, p. 146-157 (in Japanese with English Abstract).

Takizawa, F., 1985. Jurassic sedimentation in the South Kitakami Belt, Northeast Japan. Bulletin of the Geological Survey of Japan, v. 36, p. 203-320.

Takizawa, F., 1996, Soma-Nakamura Group (Jurassic –Lower Cretaceous). In: Yanagisawa, Y., Yamamoto, T., Sakano, Y., Tazawa, J., Yoshioka, T., Kubo, K., and Takizawa F. (Eds.), 1996, Geology of the Somanakamura district with Geological Sheet Map at 1:50,000. Geological Survey of Japan, Tokyo, p. 35-49 (in Japanese with English Abstract).

Tamura, M., 1960, A stratigraphic study of the Torinosu Group and its relatives. Memoir of Faculty of Education, Kumamoto University, v. 8, p. 1-40 (in Japanese, with English Abstract).

Tamura, M., 1961a, The Torinosu Series and fossils therein. Japan Journal of Geology and Geography, v. 32, p. 219-252.

Tamura, M., 1961b, The geologic history of the Torinosu Epoch and the Mesozoic reef-limestone in Japan. Japan Journal of Geology and Geography, v. 32, p. 253-278.

Tashiro, M., 1985, The Cretaceous System of the Chichibu Belt in Shikoku –On the Early Cretaceous lateral fault in the Chichibu belt. Fossil, v. 38, p. 23-35 (in Japanese with English Abstract).

Tazawa, J., 1993, Pre-Neogene tectonics of the Japanese Islands from the viewpoint of palaeobiogeography. Journal of the Geological Society of Japan, v. 99, p. 525-543 (in Japanese with English Abstract).

Tazawa, J., 2004, The strike-slip model: A synthesis on the origin and tectonic evolution of the Japanese Islands. Journal of the Geological Society of Japan, v. 110, p. 503-517 (in Japanese with English Abstract).

Uematsu, H., 1997, Foraminifera and depositional environment of Torihosu-type Limestone, in Soma-Nakamura district of Fukushima prefecture. Reports of the Fukada grant-in-aid for 1996, p. 225-234 (in Japanese).

van Dongen B.E., Schouten S., and Sinninghe Damsté, J.S., 2006, Preservation of carbohydrates through sulfurization in a Jurassic euxinic shelf sea: Examination of the Blackstone Band TOC cycle in the Kimmeridge Clay Formation, UK. Organic Geochemistry, v. 37, p. 1052–1073.

Weissert, H. and Mohr, H., 1996. Late Jurassic climate and its impact on carbon cycling. Palaeogeography Palaeoclimatology Palaeoecology, v. 122 (1-4), p. 27-43.

Weissert, H., and Erba, E., 2004. Volcanism, CO2 and palaeoclimate: a Late Jurassic-Early Cretaceous carbon and oxygen isotope record. Journal of Geological Society of London, v. 161, p. 695-702.

Weissert, H., Joachimski, M., and Sarnthein, M., 2008. Chemostratigraphy. Newsletters on Stratigraphy, v. 42, p. 145-179.

Weissert, H., Lini, A., Föllmi, K.B., and Kuhn, O., 1998, Correlation of Early Cretaceous carbon isotope stratigraphy and platform drowning events: a possible link? Palaeogeography Palaeoclimatology Palaeoecology, v. 137, p. 189-203.

Yabe, H., and Toyama, S., 1928, On some rock-forming algae from the younger Mesozoic of Japan. Science Reports of Tohoku Imperial University 2nd series, v.12, p. 141-152.

Yabe, H., and Sugiyama, T., 1935, Jurassic stromatoporoids from Japan. Science Reports of Tohoku Imperial University 2nd series, v.14, p. 135-192.

Yao, A., Matsuoka, A., and Nakatani, T., 1982, Triassic and Jurassic radioralian assemblages in Southwest Japan. Proceedings of Radiolarian Symposium, Special volume 5, p. 27-43 (in Japanese with English Abstract).

Plates

(14 plates)

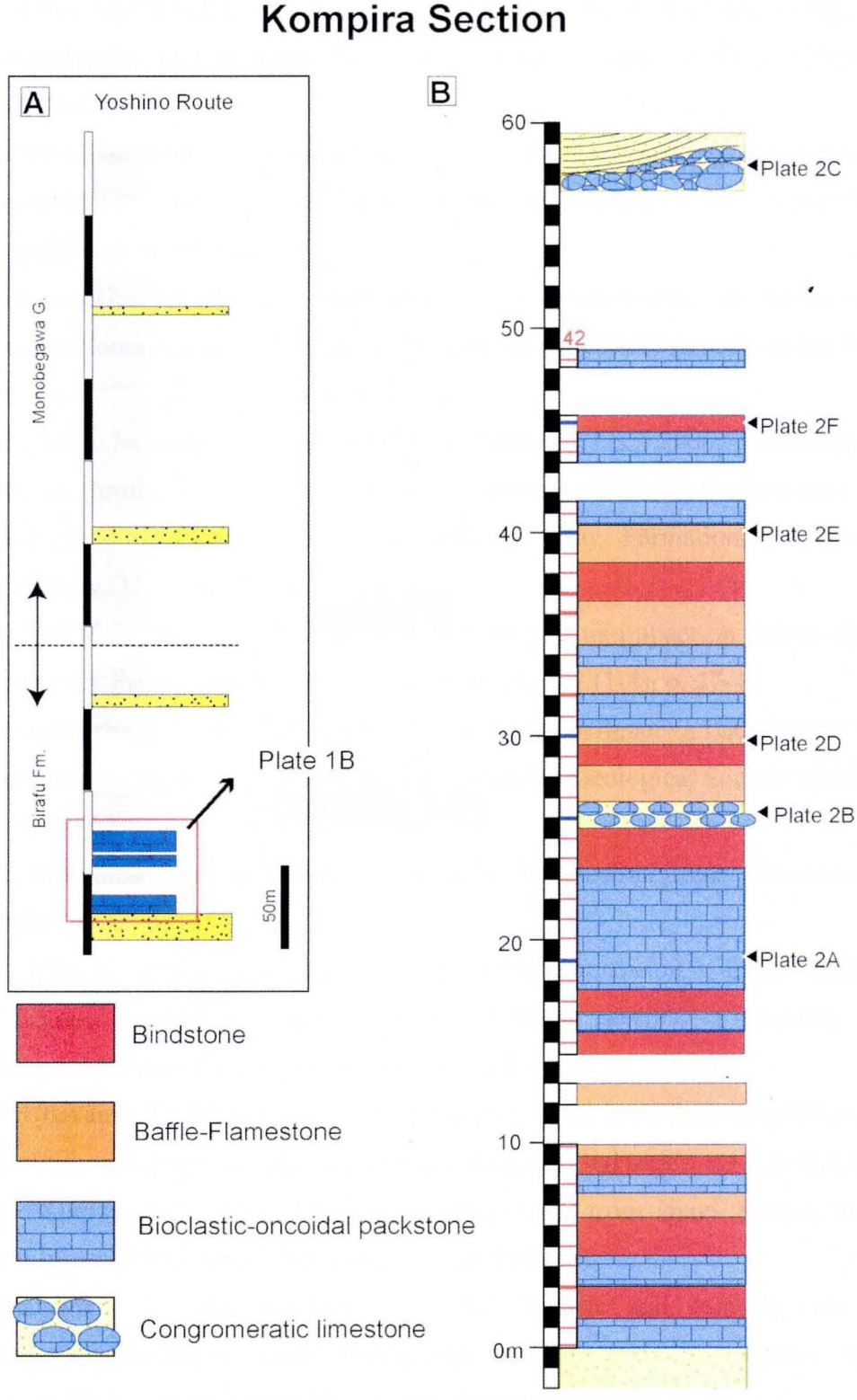

Plate 1. Columnar section of the Kompira section (Nankai Group) in Kochi Prefecture. Locality of this section is shown in Figure 3B. **(A)** Columnar section of Yoshino route modified after Kawagoe (2006, MS). **(B)** Columnar section of the Kompira section.

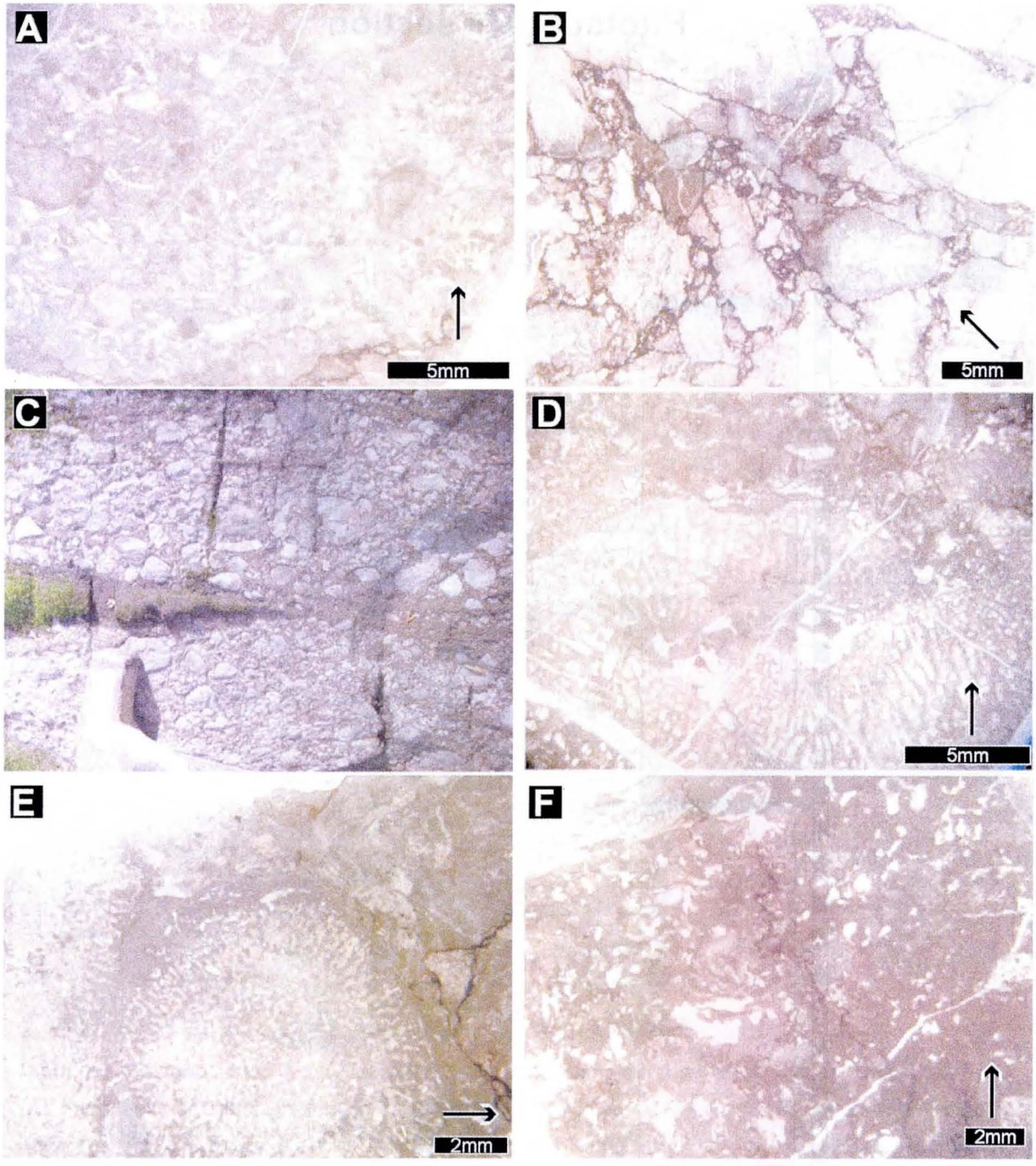

Plate 2. Limestone facies recognized in the Kompira section. Horizons of microscopic photographs are shown in the Plate 1B.

(A) Bioclasic-oncoidal packstone in the middle part of the Kompira section (KPR-16). **(B)** Congromeratic limestone in the middle part (26m horizon). **(C)** Congromerate containing limestone pebble in the uppermost part of the Kompira section (58m horizon). This conglomeratic bed overlies the limestone body and underlies fine-grained sandstone. **(D)** Baffle-framestone in the middle part (30m horizon), which contains corals constructing a robst framework. ***(E)*** Baffle-framestone in the middle part (40m horizon) containing stromatoporoid-microencruster association. **(F)** Bindstone constructed by microbial crusts (46m horizon).

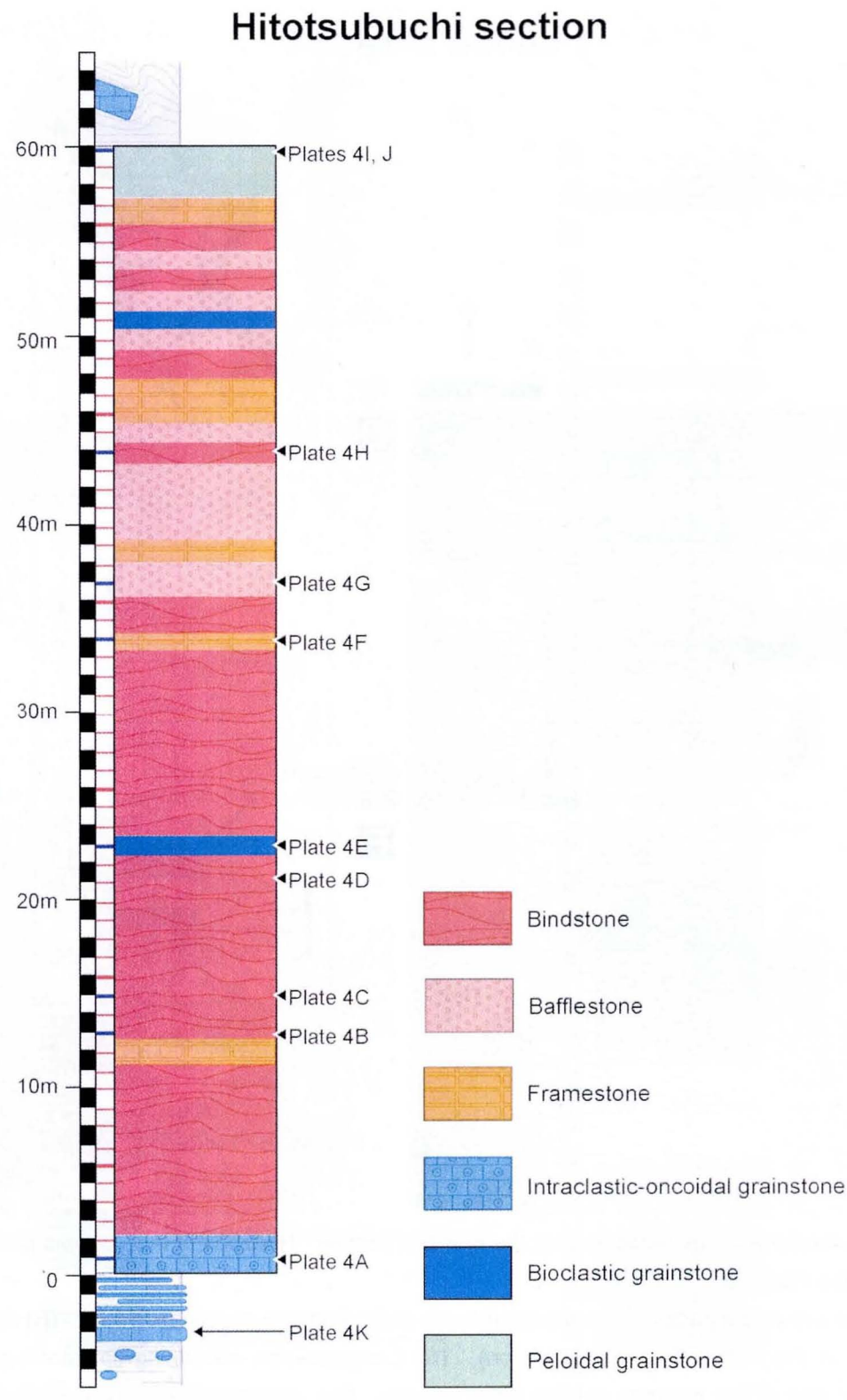

Plate 3. Columnar section of the Hitotsubuchi section (Torinosu Group) in Kochi Prefecture. Locality of this section is shown in Figure 3C.

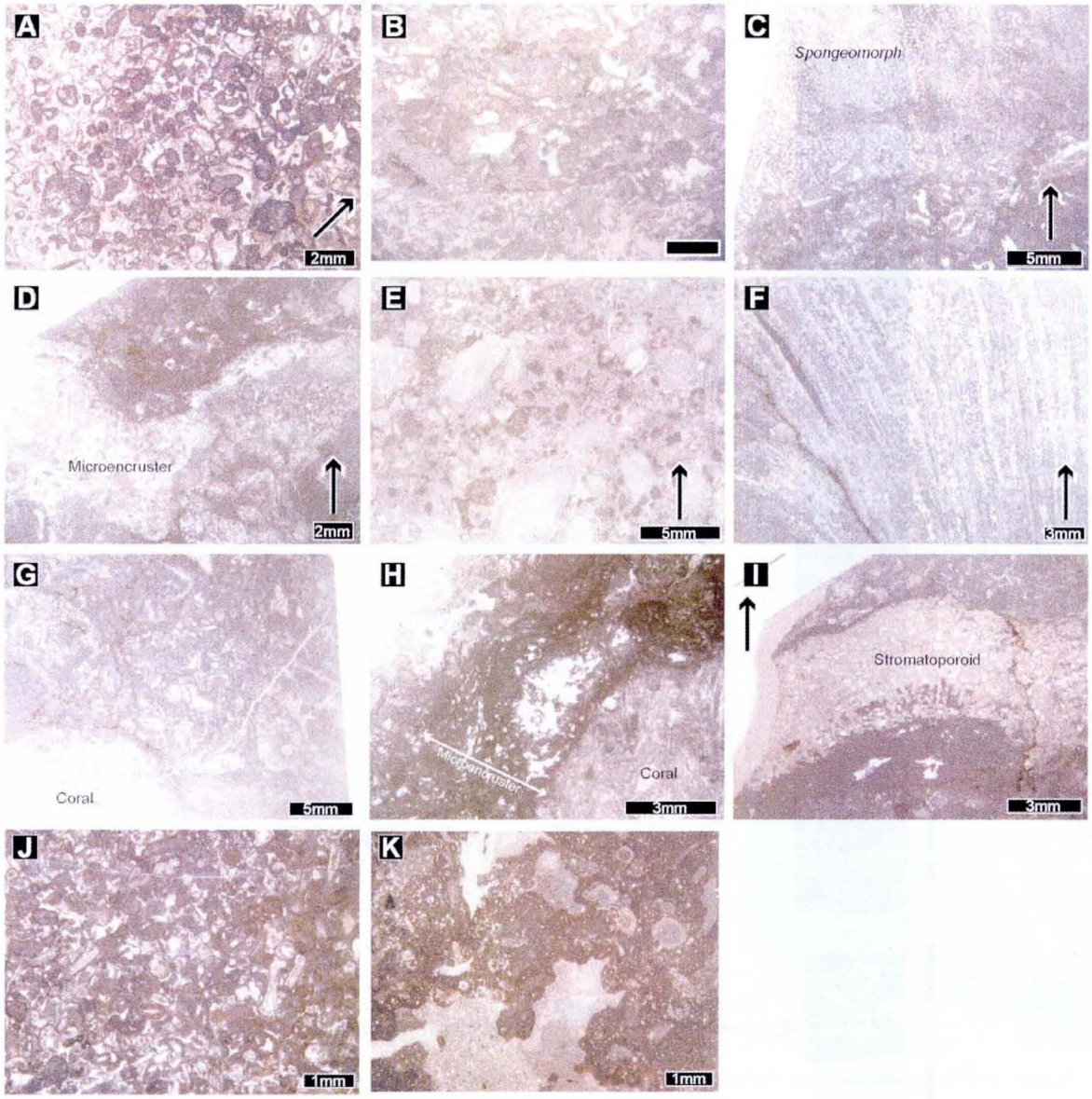

Plate 4. Limestone facies in the Hitotsubuchi section. Sample horizons are shown in the Plate 3. **(A)** Intraclastic-oncoidal grainstone characterizing the lowermost part of the section (HIT-06, 2m horizon). **(B)** Bindstone (HIT-17, 13m horizon). **(C)** Bindstone (HIT-19, 15m horizon) containing *Spongeomorph* sp. **(D)** Bindstone (HIT-25, 21m horizon) containing microencrusters. **(E)** Bioclastic grainstone (HIT-27, 23m horizon). **(F)** Framestone (HIT-38, 34m horizon). **(G)** Bafflestone (HIT-41, 37m horizon). **(H)** Bindstone (HIT-48, 44m horizon) by corals and microencrusters. **(I)** Skeleton of stromatporoid (*Parastromatopora* sp.) in paloidal wackestone (HIT-54, 60m horizon). **(J)** Peloidal wackestone (HIT-64, 60m horizon). **(K)** *Tubiphytes* sp. in the lowermost section (HIT-01, -3m horizon).

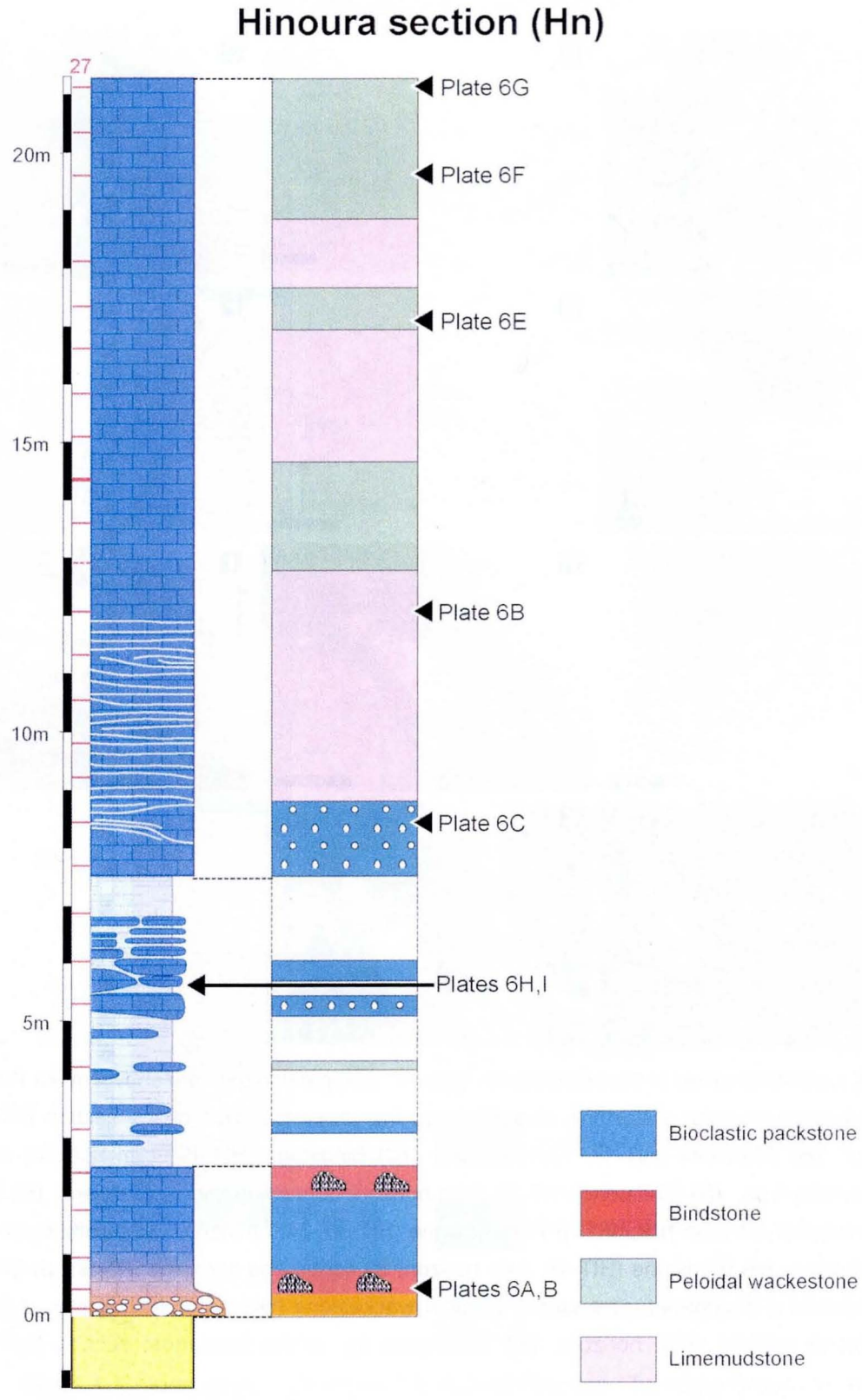

Plate 5. Columnar section of the Hinoura section (Imaidani Group), Ehime Prefecture. Locality of this section is shown in Figure 3D.

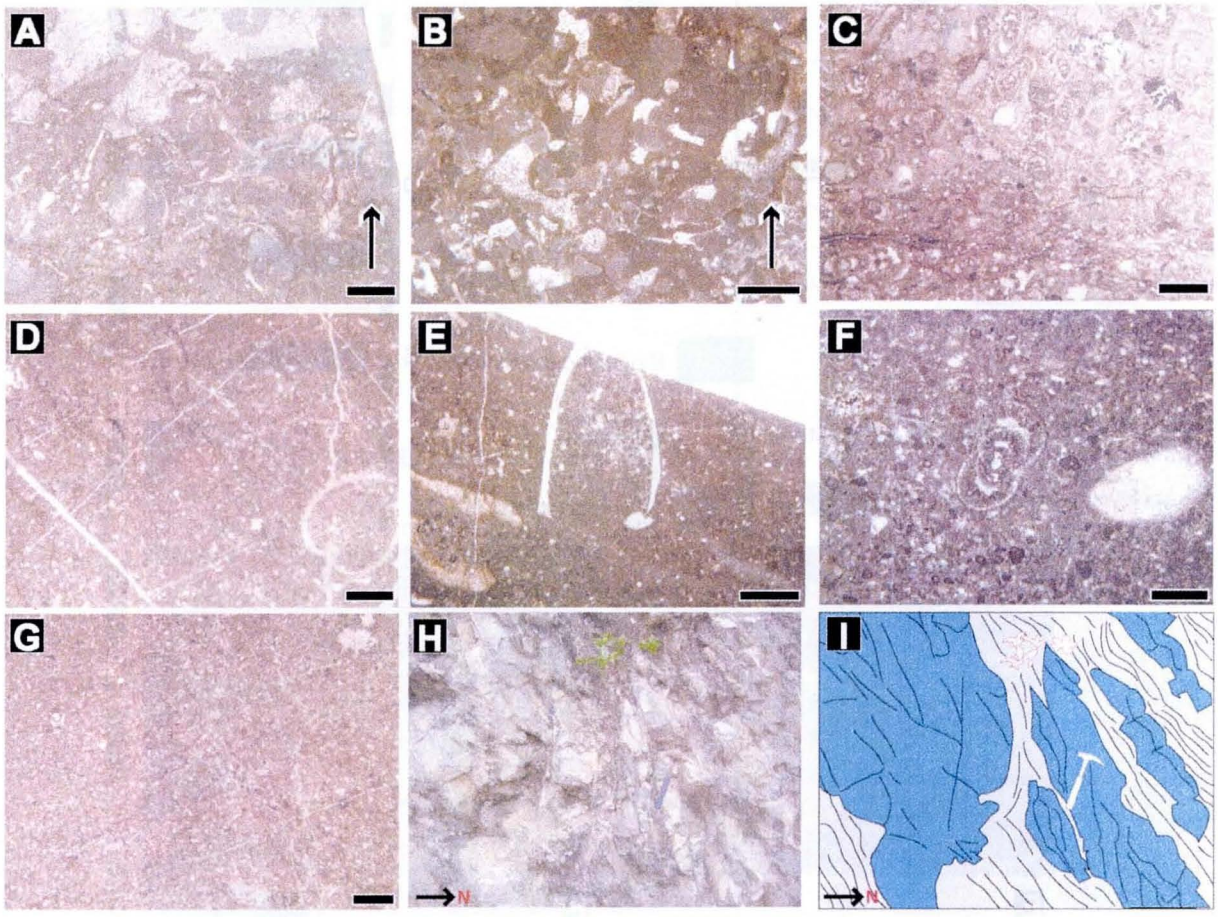

Plate 6. Limestone facies in the Hinoura section. Horizons of samples and an outcrop are shown in the Plate 5.

(A)-(B) Bindstone yielding microencrusters and bioclasts (Hn-u09, 0.5m horizon). **(C)** Bioclastic packstone containing litulinids (Hn-02, 8.5m horizon). **(D)** Limemudstone (Hn-07, 12m horizon). **(E)** Longitudal section of a possible calpionerid observed in upper part of the section (Hn-12, 17m horizon). **(F)** Longitudal section of a lituolinid. (Hn-17, 19.5 m horizon) **(G)** Peloidal wackestone (Hn-21, 21m horizon). **(H)** An outcrop showing an irregular alternation of mudstone and limestone (near 6m horizon). **(I)** Sketch of the outcrop in Plate 6H. Limestone is shown in blue, and mudstone is shown in gray.

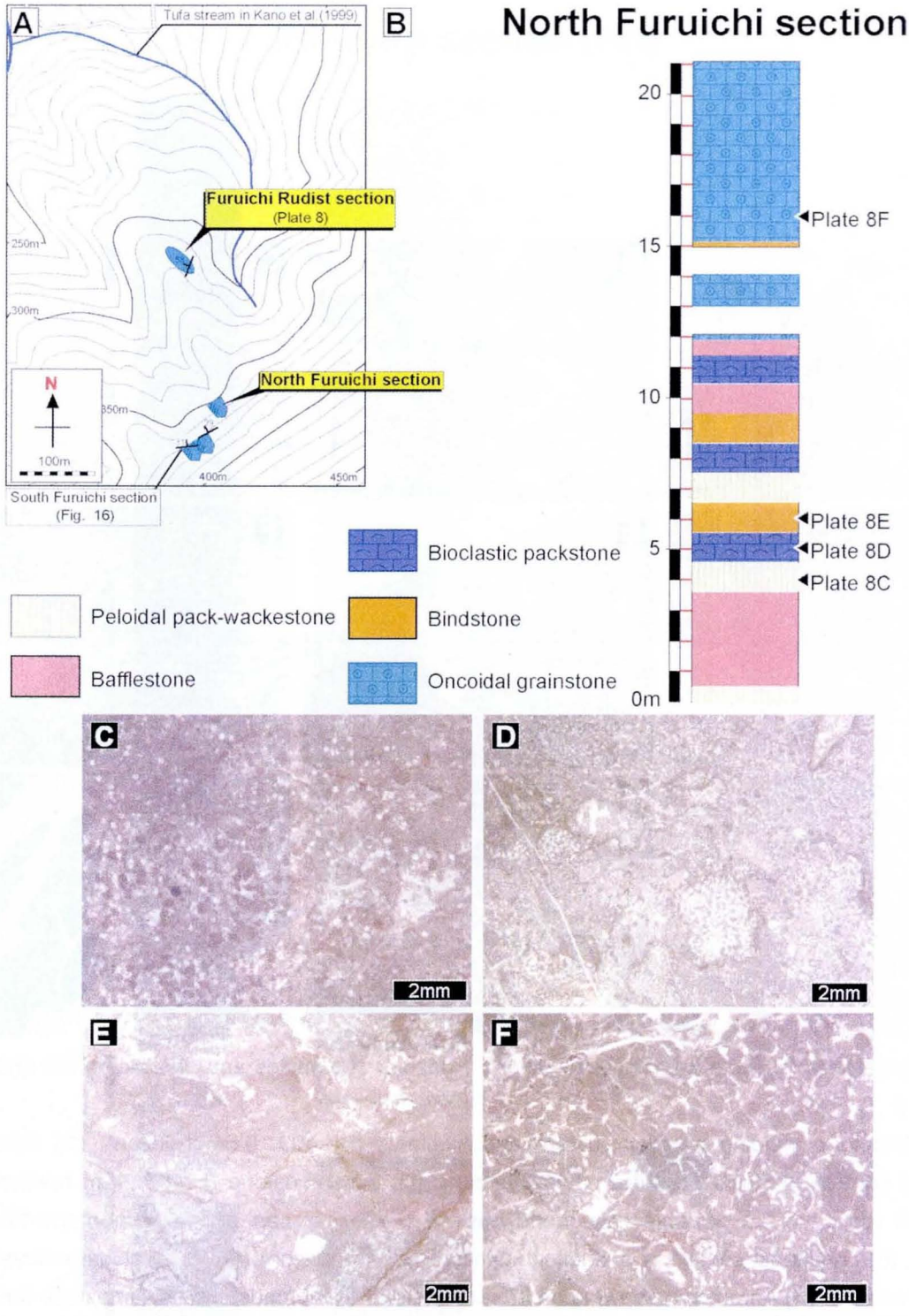

Plate 7. Columnar section and limestone facies of the North Furuichi section (Imaidani Group), Ehime Prefecture. **(A)** Detailed locality map of three localities around Nakatsugawa, Seiyo City. **(B)** Columnar section of the North Furuichi section. **(C)** - **(F)** Microscopic views of limestone facies. **(C)** Peloidal pack-wackestone (Fur-N-05, 4m horizon). **(D)** Bioclastic packstone (Fur-N-06, 5m horizon). **(E)** Bindstone consisting of microbial crusts (Fur-N-07, 6m horizon). **(F)** Oncoidal grainstone (Fur-N-17, 16m horizon).

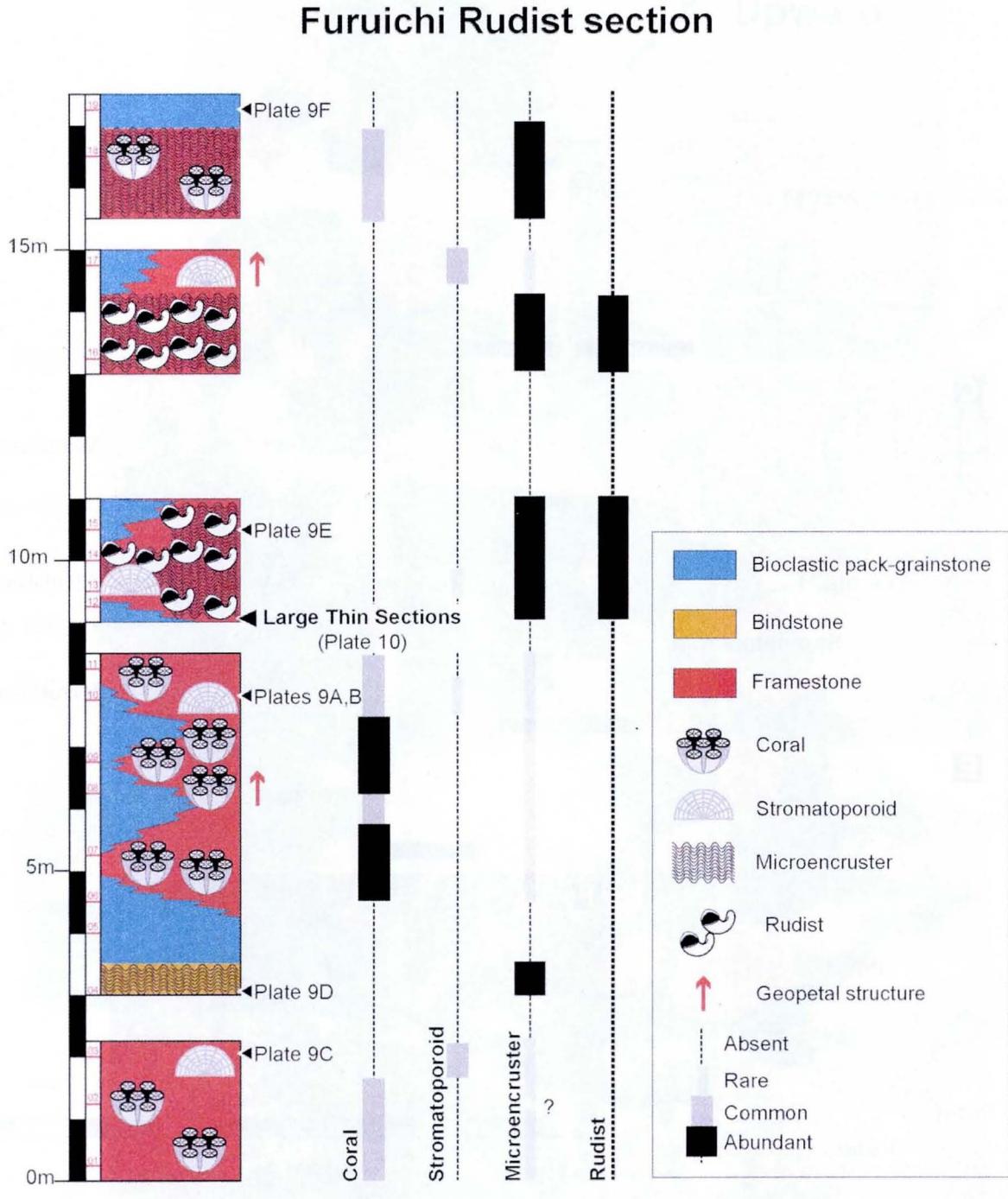

Plate 8. Columnar section of the Furuichi Rudist section (Imaidani Group), Ehime Prefecture. The location is shown in Plate 7A.

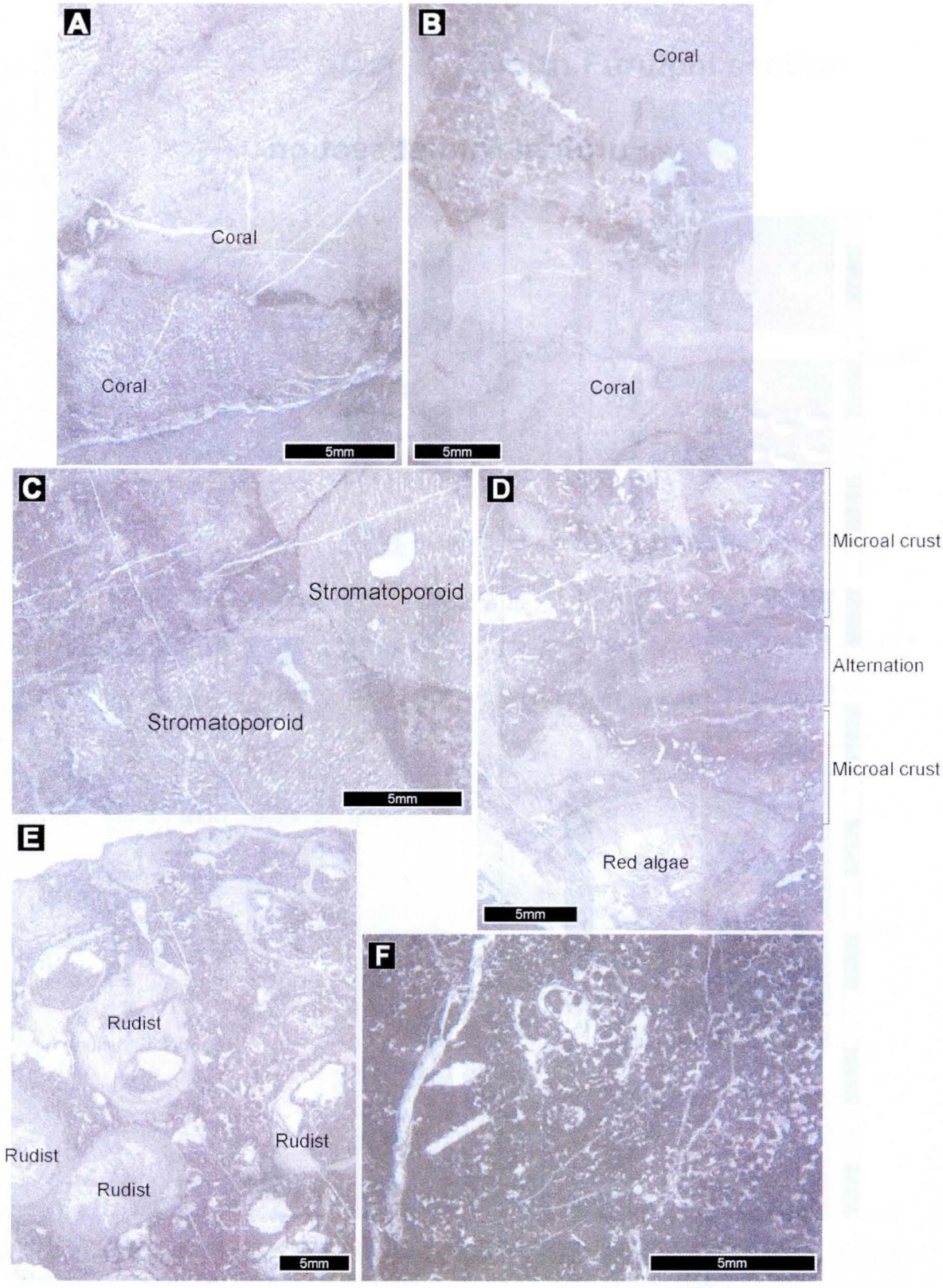

Plate 9. Limestone facies of the Furuichi Rudist section.

(A) and **(B)** Framestone consisting a coral robst framework (Fur-Rudist 10, 11). **(C)** Framestone yielding branching stromatoporoids (Fur-Rudist 03). **(D)** Red algae and bindstone showing alternation of microbial film and fine peloids (Fur-Rudist 04). **(E)** A typical appearance of rudist-microencrusters bindstone (Fur-Rudist 14). **(F)** Bioclastic pack-grainstone in the uppermost part of the section.

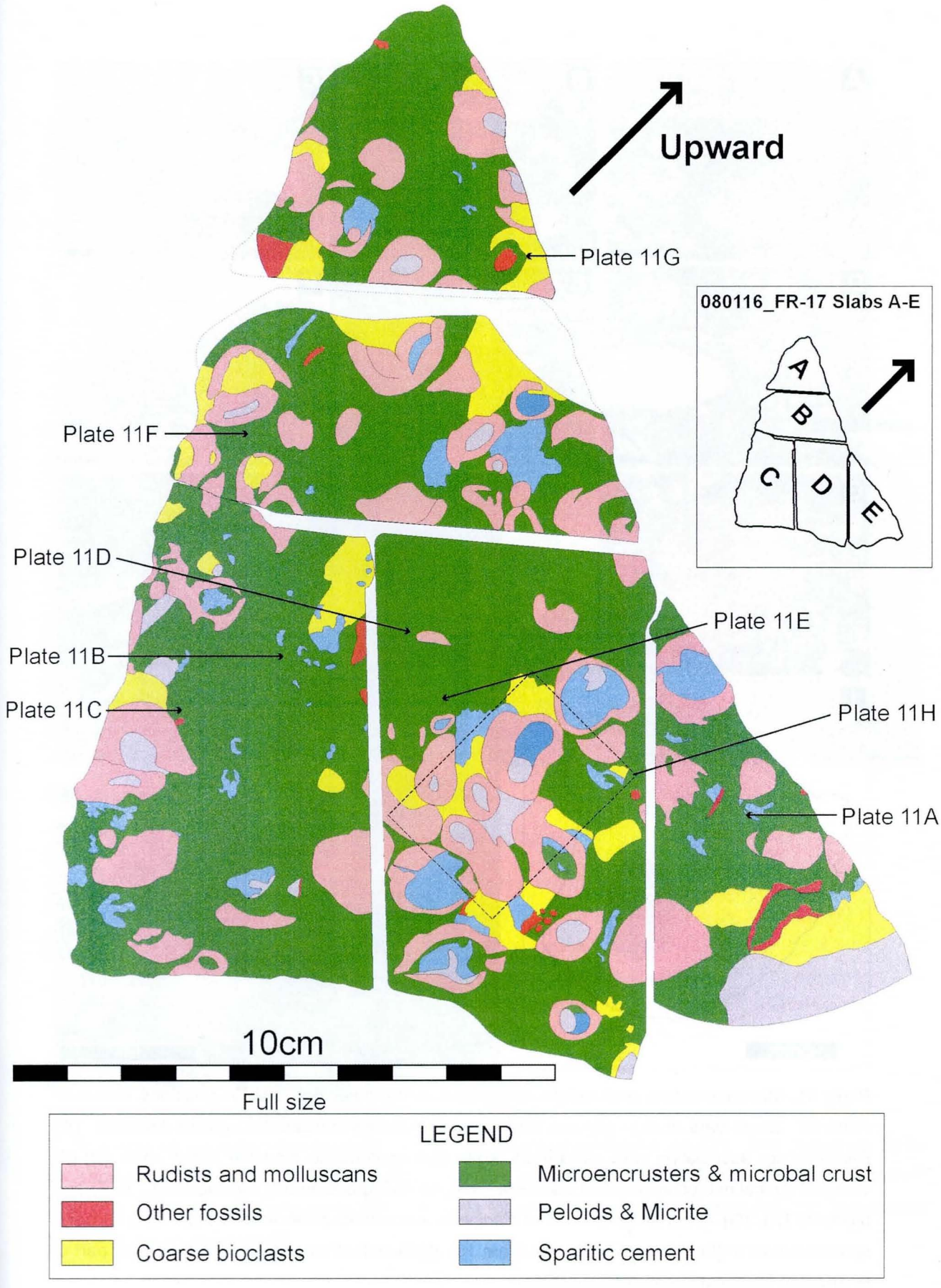

Plate 10. A sketch of a limestone slab showing rudist-microencruster bindstone of the Furuichi Rudist section, based on the observation of thin sections.

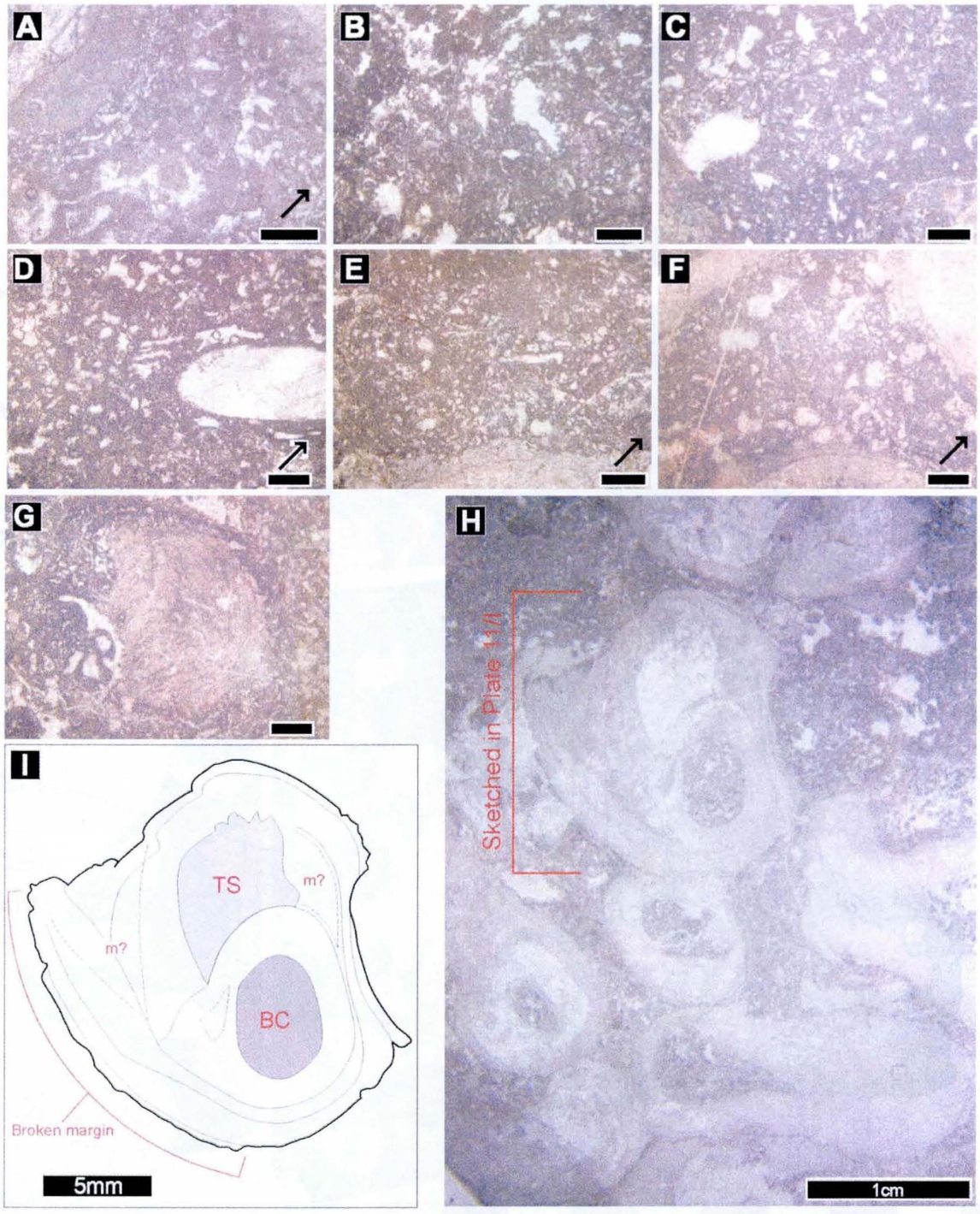

Plate 11. Microencrusters and rudists recognized in the limestone slab in positions shown in Plate 10. Scale bars of (A) - (G) are 1mm long, and arrows indicate the upward direction. **(A)** *Bacinella* sp. associating with calcareous algae that contriute to bind the rudist shell. **(B)-(F)** Views of typical microbial crusts of *Bacinella*. They fill the space among the rudists **(C, E, F)** and bioclasts **(D)**. **(G)** A ball-shaped crust of *Bacinella*, encrusting a calcareous alga. **(H)** Closely-spaced rudists in the thin section D (see Plate 10). **(I)** Sketch of the individual in the upper part of H, showing diagnostic features for rudists.

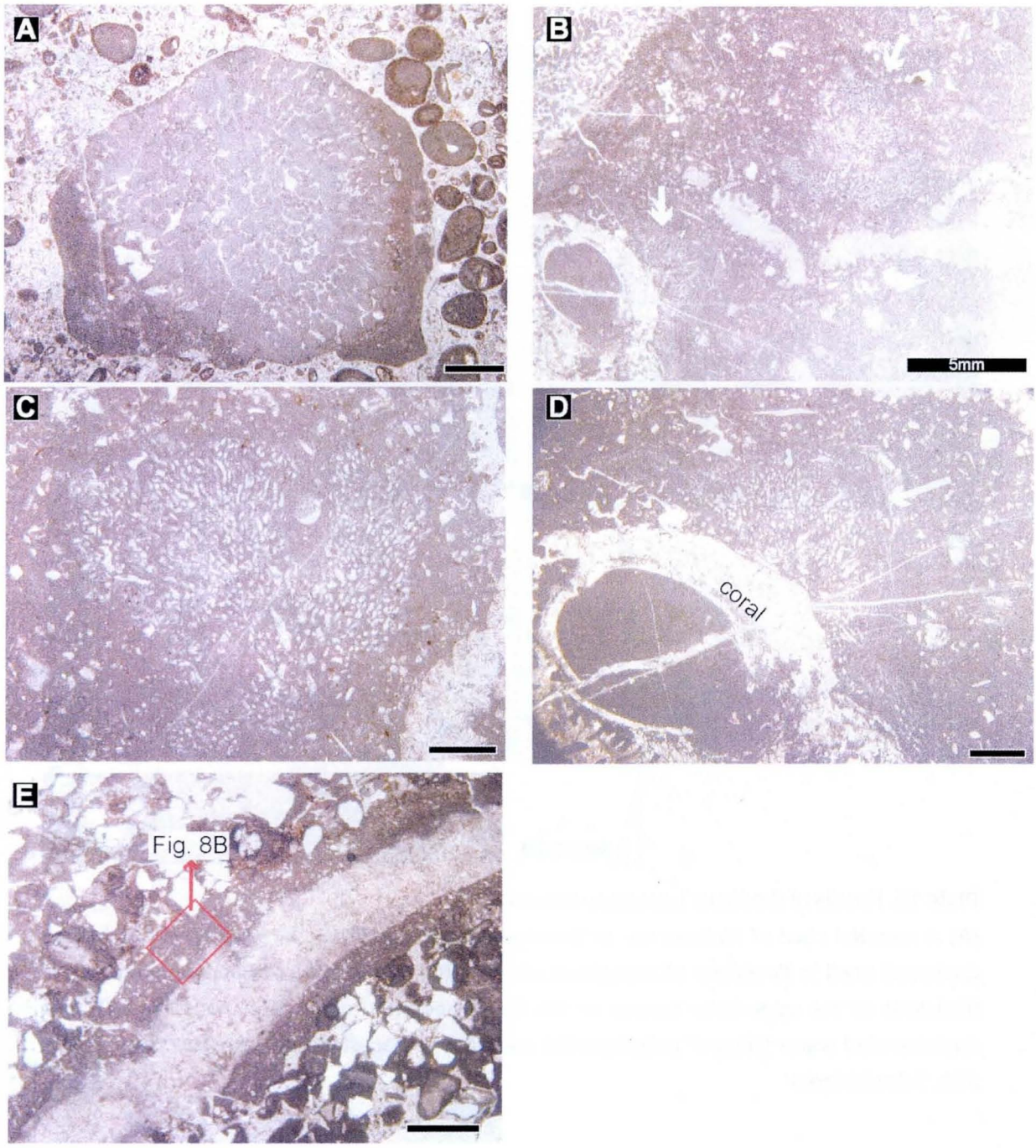

Plate12. Microencrusters from the Koike Limestone Member.

(A) *Marinella* sp. as a rounded bioclast (Kk-20). **(B)** Microbial bindstone (Nk-O'). The closed-up views are shown in Plate 12D. **(C)** *Pycnoporidium lobatum* growing in a radial form. **(D)** *Pycnoporidium lobatum* encrusting a stromatoporoid. **(E)** *Girvanella tosaensis* encrusting a bivalve (Koi-01). The closed up view is shown in Figure 8B.

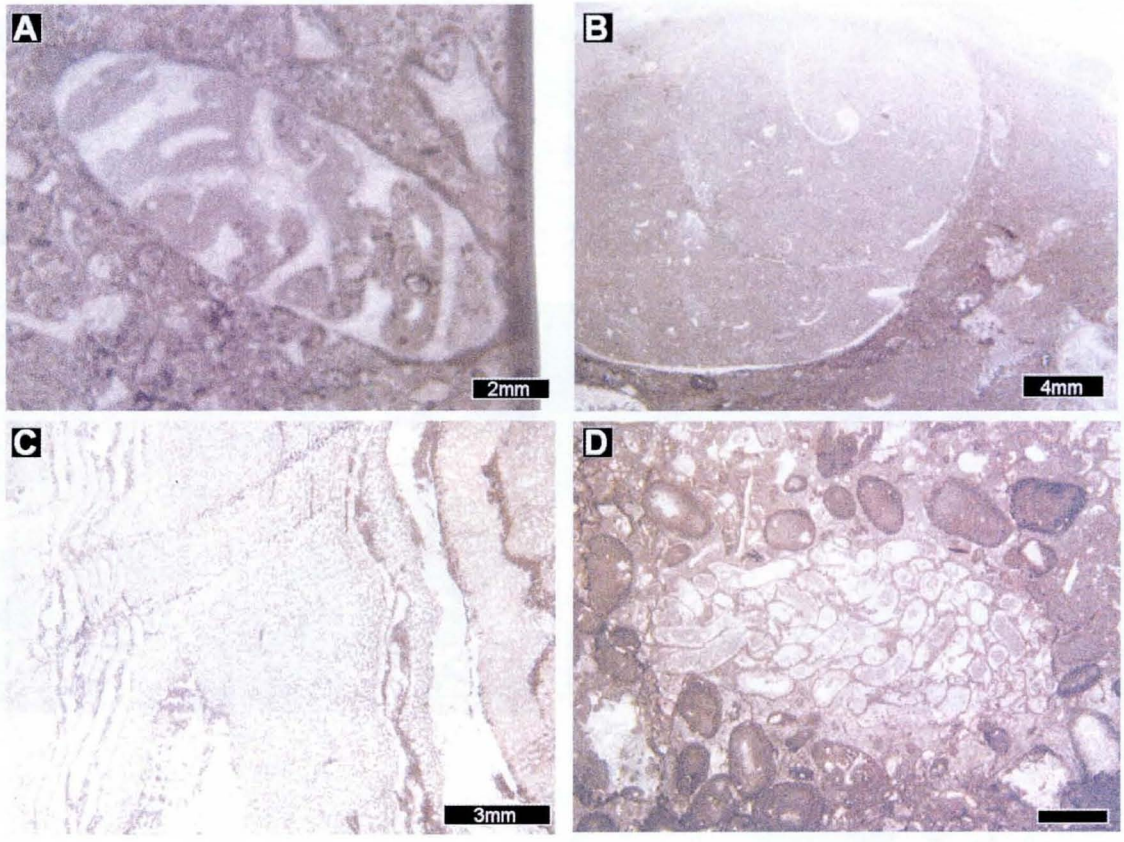

Plate 13. Fossils of the Koike Limestone Member

(A) A rounded clast of Nerinea sp. in Tatenosawa section (Tt-10, 10m horizon). **(B)** A large gastropod shell in floatstone of Kakusawa section. **(C)** The skelton of Spongeomorph sp. in bindstone of the uppermost horizon in the Koike section (Koi-52, 52m horizon). **(D)** The agglomerated warm tubes of polychaetetes (serpulid) in packstone in Kakusawa section (Kk-25A, 7-9m horizon).

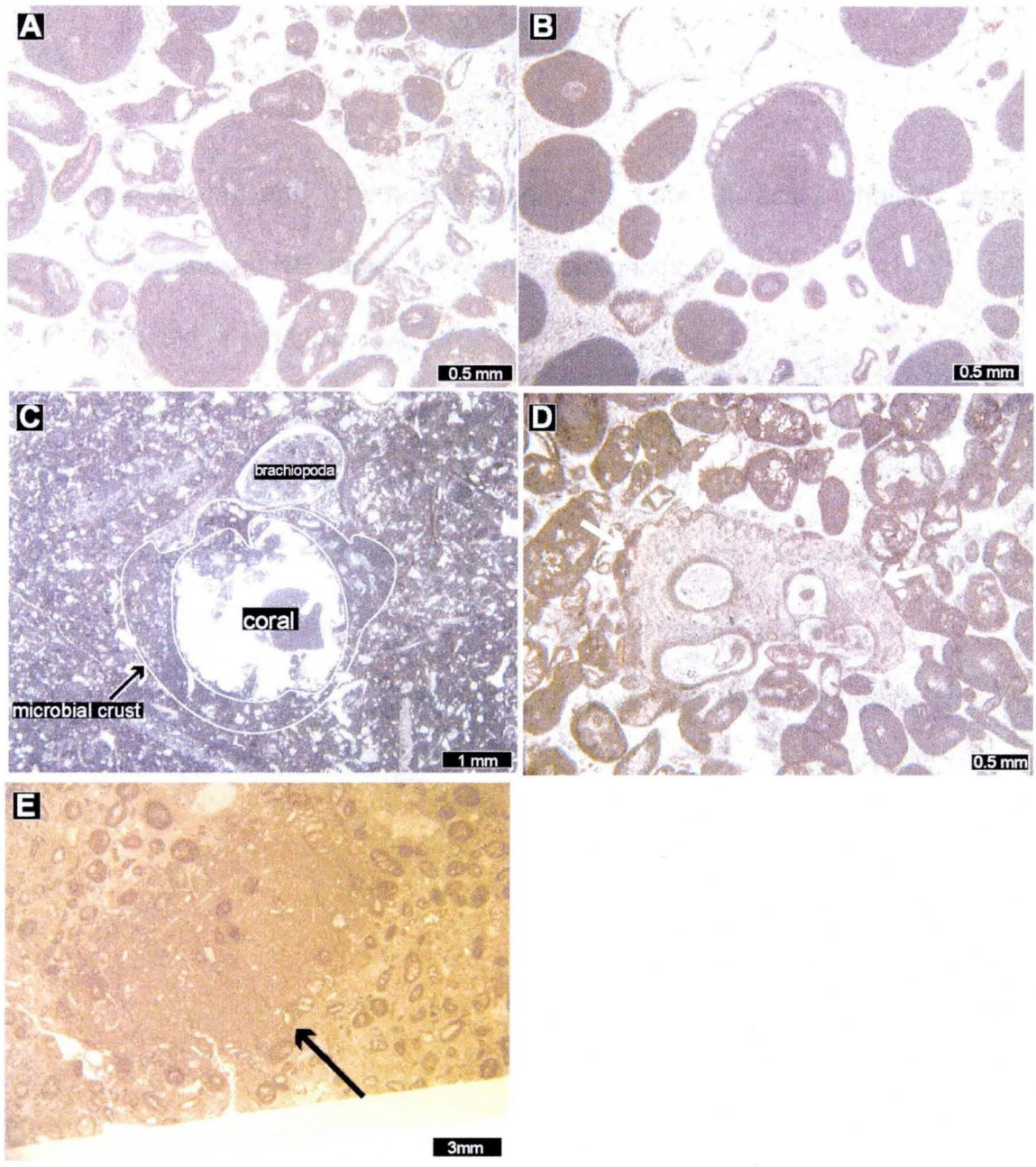

Plate 14 Microscopic photographs of oncoids.

(A) Typical oncoidal grains, showing irregular lamination in cortex (Koi-11). **(B)** An oncoid encrusted by foraminifera (Koi-38). **(C)** An oncoid consisting of a nucleus of coral and cortex including microbial filaments (white arrow). It attaches with a brachiopod shell (Koi-44). **(D)** An oncoidal grain, with a thick cortex including microbial filaments (white arrow) (Nk-7). **(E)** A large oncoid encasing smaller oncoids (arrow) (Nk-19).

公表論文

(1) Architecture and chemostratigraphy of Late Jurassic shallow marine carbonates in NE Japan, western Paleo-pacific.

Kakizaki, Y. and Kano, A.

Sedimentary Geology, 214, (2009) 49-61.

(2) Facies and depositional environment of the uppermost Jurassic stromatoporoid biostromes in the Zagros Mountains of Iran.

Kano, A., Kakizaki, Y., Takashima, C., Wang, W. and Matsumoto, R.

GFF, 128, (2007) 107-122.